Article

Tumour extracellular vesicles and particles induce liver metabolic dysfunction

https://doi.org/10.1038/s41586-023-06114-4

Received: 22 April 2022

Accepted: 21 April 2023

Published online: 24 May 2023

Check for updates

Gang Wang[1,26], Jianlong Li[1,2,26], Linda Bojmar[1,3], Haiyan Chen[1,4,5], Zhong Li[6], Gabriel C. Tobias[1], Mengying Hu[1], Edwin A. Homan[7], Serena Lucotti[1], Fengbo Zhao[1,8], Valentina Posada[9], Peter R. Oxley[10], Michele Cioffi[1], Han Sang Kim[1,11], Huajuan Wang[1], Pernille Lauritzen[1], Nancy Boudreau[1], Zhanjun Shi[2], Christin E. Burd[9], Jonathan H. Zippin[12], James C. Lo[7], Geoffrey S. Pitt[7], Jonathan Hernandez[13,14], Constantinos P. Zambirinis[13,15], Michael A. Hollingsworth[16], Paul M. Grandgenett[16], Maneesh Jain[16], Surinder K. Batra[16], Dominick J. DiMaio[17], Jean L. Grem[18], Kelsey A. Klute[18], Tanya M. Trippett[19], Mikala Egeblad[20], Doru Paul[21], Jacqueline Bromberg[22], David Kelsen[23], Vinagolu K. Rajasekhar[24], John H. Healey[24], Irina R. Matei[1], William R. Jarnagin[13], Robert E. Schwartz[25] ✉, Haiying Zhang[1] ✉ & David Lyden[1] ✉

Cancer alters the function of multiple organs beyond those targeted by metastasis[1,2]. Here we show that inflammation, fatty liver and dysregulated metabolism are hallmarks of systemically affected livers in mouse models and in patients with extrahepatic metastasis. We identified tumour-derived extracellular vesicles and particles (EVPs) as crucial mediators of cancer-induced hepatic reprogramming, which could be reversed by reducing tumour EVP secretion via depletion of *Rab27a*. All EVP subpopulations, exosomes and principally exomeres, could dysregulate hepatic function. The fatty acid cargo of tumour EVPs—particularly palmitic acid—induced secretion of tumour necrosis factor (TNF) by Kupffer cells, generating a pro-inflammatory microenvironment, suppressing fatty acid metabolism and oxidative phosphorylation, and promoting fatty liver formation. Notably, Kupffer cell ablation or TNF blockade markedly decreased tumour-induced fatty liver generation. Tumour implantation or pre-treatment with tumour EVPs diminished cytochrome P450 gene expression and attenuated drug metabolism in a TNF-dependent manner. We also observed fatty liver and decreased cytochrome P450 expression at diagnosis in tumour-free livers of patients with pancreatic cancer who later developed extrahepatic metastasis, highlighting the clinical relevance of our findings. Notably, tumour EVP education enhanced side effects of chemotherapy, including bone marrow suppression and cardiotoxicity, suggesting that metabolic reprogramming of the liver by tumour-derived EVPs may limit chemotherapy tolerance in patients with cancer. Our results reveal how tumour-derived EVPs dysregulate hepatic function and their targetable potential, alongside TNF inhibition, for preventing fatty liver formation and enhancing the efficacy of chemotherapy.

Cancer is a systemic disease that is mediated by the release of soluble factors, including EVPs[1,3]. Tumour-derived EVPs establish pre-metastatic niches (PMNs) and reprogramme cell function in multiple metastasis-free organs[3,4]. Liver functional reprogramming in the absence of metastasis during cancer progression has not been widely studied. However, the liver has been identified as one of the primary organs targeted by tumour-derived EVPs[5–9], prompting us to investigate the roles of EVPs in altering liver function. Here, by applying multi-omic analyses to multiple mouse tumour models and liver tissues from patients with cancer, we demonstrate that saturated fatty acids packaged in tumour EVPs induce metabolic dysregulation, which, in turn, promotes fatty liver formation and diminishes the drug-metabolizing capacity of the liver.

Remote tumours alter liver metabolism

To investigate how cancer affects the liver, we orthotopically implanted mouse B16F10 melanoma or K7M2 osteosarcoma cells, which preferentially metastasize to the lung[10,11]. Three to four weeks after implantation, we observed no liver metastasis in either model, but detected lung metastases in the K7M2 model by histology (Extended Data Fig. 1a–c). Furthermore, melanoma-specific *Trpm1* and mCherry mRNA were detected by quantitative reverse transcription PCR (RT–qPCR) in the lungs but not in the livers of B16F10 and K7M2-mCherry tumour-bearing mice, respectively (Extended Data Fig. 1d), ruling out liver micrometastases.

A list of affiliations appears at the end of the paper.

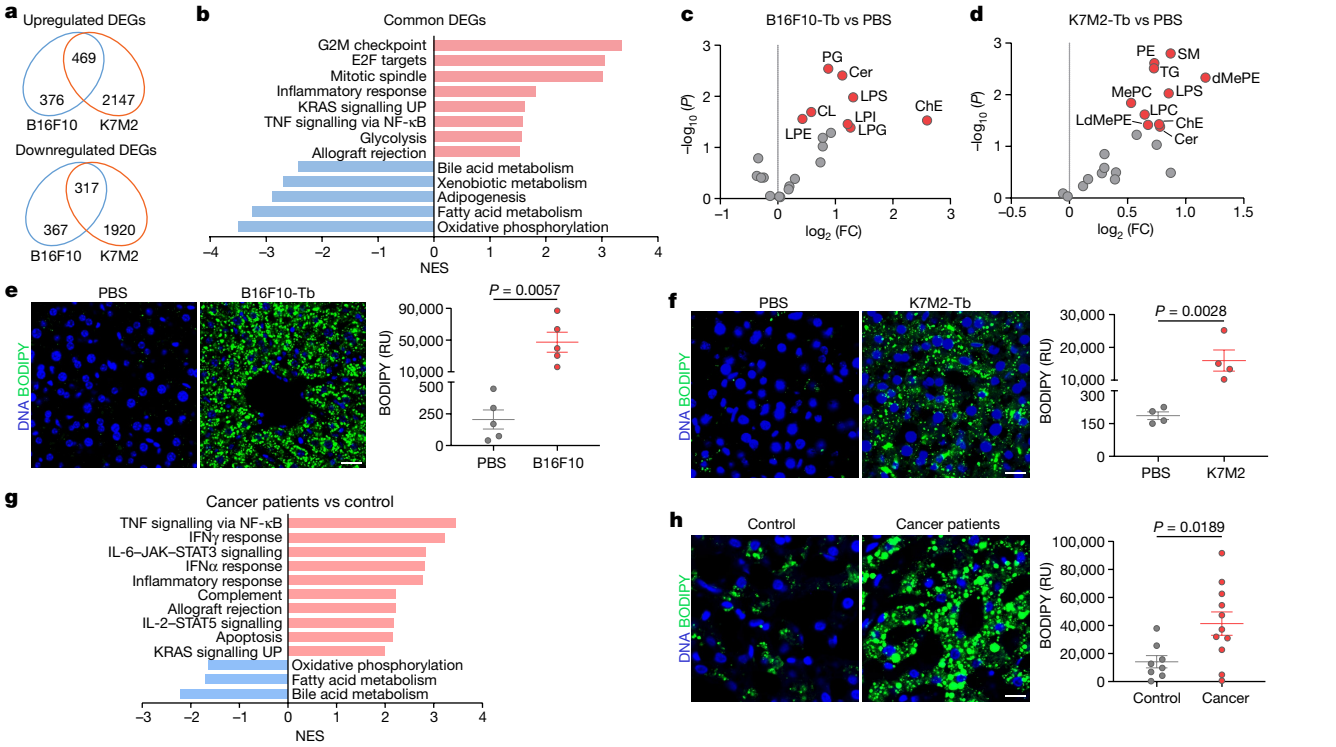

Fig. 1 | Remote primary tumours induce metabolic dysfunction in the liver. **a**, Venn diagram for differentially expressed genes (DEGs) ($q < 0.05$) in livers from mice bearing B16F10 ($n = 3$) and K7M2 ($n = 5$) compared to the respective PBS-injected control mice. **b**, GSEA of the common DEGs in **a** using Hallmark gene sets, showing significantly changed signalling pathways with false discovery rate (FDR) < 0.1. Gene lists for signalling pathways are shown in Supplementary Table 6. NES, normalized enrichment score. **c**,**d**, Volcano plots showing lipid classes (labelled in red, $P < 0.05$) that are significantly enriched in the livers of mice bearing B16F10 (**c**) and K7M2 (**d**) tumours, compared to the respective PBS-injected control mice ($n = 5$ each). Cer, ceramide; ChE, cholesterol ester; CL, cardiolipin; LPC, lysophosphatidylcholine; LPE, lysophosphatidylethanolamine; LPG, lysophosphatidylglycerol; LPI, lysophosphatidylinositol; LPS, lysophosphatidylserine; PE, phosphatidylethanolamine; PG, phosphatidylglycerol; SM, sphingomyelin; TG, triglyceride; MePC, methyl phosphatidylcholine; dMePE, dimethylphosphatidylethanolamine; LdMePE, lysodimethylphosphatidylethanolamine. FC, fold change. **e**,**f**, Representative images (left) and associated statistical analysis (right) of BODIPY staining of livers from mice bearing B16F10 ($n = 5$) (**e**) and K7M2 ($n = 4$) (**f**) tumours, and the respective PBS-injected control mice. RU, relative units. **g**, GSEA using normalized gene expression values of tumour-free livers from patients with PDAC ($n = 5$) compared with control subjects ($n = 8$) with benign lesions, using Hallmark gene sets. Downregulated signalling pathways with FDR < 0.05 and top 10 upregulated signalling pathways with FDR < 0.05 are shown. Gene lists for signalling pathways are shown in Supplementary Table 7. **h**, Representative images (left) and associated statistical analysis (right) of BODIPY staining of livers from patients with PDAC ($n = 11$) and control subjects ($n = 8$) with benign lesions. Scale bars, 20 µm. **c**–**f**,**h**, Two-tailed, unpaired Student's *t*-test. Data are mean ± s.e.m. Tb, tumour-bearing.

Notably, RNA sequencing (RNA-seq) of metastasis-free livers of control and tumour-bearing mice revealed concordant transcriptional changes with 469 upregulated and 317 downregulated genes ($q < 0.05$) in both models (Fig. 1a and Extended Data Fig. 1e). Gene set enrichment analysis (GSEA) revealed dysregulated immune homeostasis and metabolism, including links to inflammation and TNF signalling via NF-κB and decreased oxidative phosphorylation (OXPHOS) and fatty acid metabolism (Fig. 1b).

Additional orthotopic low-metastatic melanoma B16F1 and non-metastatic (67NR) and highly metastatic[12] (lung-tropic 4T1) breast cancer models resulted in similar alterations in pathways associated with immune response and metabolism in metastasis-free livers (Extended Data Fig. 1a,b,e–h), indicating that multiple cancer types systemically and uniformly reprogramme liver function.

To evaluate liver metabolic dysfunction, we performed metabolomic mass spectrometry (Supplementary Tables 1 and 2) and partial least squares–discriminant analysis (PLS-DA) which showed segregated metabolite profiles with amino acids, carbohydrates, cofactors and vitamins, citric acid cycle, lipids and nucleotides being significantly elevated in metastasis-free livers of mice bearing B16F10 or K7M2 tumours compared with their respective controls (Extended Data Fig. 2a–d). Furthermore, metabolite set enrichment analysis identified lipid- and amino acid-associated metabolite sets, including phosphatidylethanolamine biosynthesis, phosphatidylcholine biosynthesis, glycine and serine metabolism, urea cycle and arginine and proline metabolism pathways, suggesting metabolic rewiring of metastasis-free livers in both models (Extended Data Fig. 2e,f).

As lipid-associated metabolic pathways were affected, we conducted lipidomic mass spectrometry (Supplementary Tables 3 and 4). PLS-DA revealed distinct liver lipid profiles in mice bearing B16F10 or K7M2 tumours relative to their respective controls (Extended Data Fig. 3a,b). Multiple lipid classes, including phospholipids (cardiolipin, lysophosphatidylethanolamine, lysophosphatidylglycerol, lysophosphatidylinositol, lysophosphatidylserine and phosphatidylglycerol for B16F10; lysophosphatidylcholine, lysophosphatidylserine and phosphatidylethanolamine for K7M2), sphingolipids (ceramide for B16F10; ceramide and sphingomyelin for K7M2) and neutral lipids (cholesterol ester for B16F10; cholesterol ester and triglyceride for K7M2), as well as multiple cholesterol ester and triglyceride species (for B16F10 and K7M2) were significantly elevated in the livers of tumour-bearing mice (Fig. 1c,d and Extended Data Fig. 3c,d).

Liver accumulation of cholesterol, triglycerides, and ceramides is linked to non-alcoholic fatty liver disease[13] (NAFLD). We performed BODIPY staining to quantify lipid droplet formation in the livers of

B16F10, K7M2, B16F1, 67NR and 4T1 allograft tumour models and a genetic model of spontaneous melanoma[14] (Extended Data Fig. 1a), none of which develop liver metastasis. We found increased lipid droplet accumulation in the livers of tumour-bearing mice compared with controls (Fig. 1e,f and Extended Data Fig. 3e), showing that fatty liver formation is common in multiple cancer models.

We also used a genetic mouse model of pancreatic ductal adenocarcinoma[15] (PDAC) to determine whether fatty liver disease co-exists with liver PMN formation. Livers of 14-week-old tumour-bearing mice, before tumour cells appear in the liver at 20 weeks of age, represent the PMN (Extended Data Fig. 3f). Lipid droplets did not accumulate in PMN livers (Extended Data Fig. 3g), suggesting that PMN formation precludes fatty liver generation. Thus, tumours with extrahepatic metastatic tropism, but not those with liver metastatic propensity, induce fatty liver generation.

To determine the clinical relevance of our findings, we analysed metastasis-free livers of mice implanted with human SK-MEL-192 melanoma or seven patient-derived osteosarcoma xenografts (PDXs) (Extended Data Fig. 3h–j and Supplementary Table 5a). All of these models displayed fatty livers (Extended Data Fig. 3k). Concordant with mouse studies, RNA-seq analysis of liver biopsies from newly diagnosed patients with localized PDAC, who later developed extrahepatic (peritoneal or lung, but not liver) metastasis versus controls with non-cancerous lesions (Supplementary Table 5b) revealed that immune homeostasis (that is, TNF signalling via NF-κB) and metabolic function (that is, fatty acid metabolism and OXPHOS) were significantly altered in these patients compared with controls (Fig. 1g). Fatty liver disease was noted in both biopsied and autopsied patients with PDAC who presented with extrahepatic metastases (Fig. 1h and Supplementary Table 5b), despite similar body mass index in the patients with cancer and controls (Extended Data Fig. 3l). Thus, in the absence of liver metastasis, remote tumours can disrupt liver metabolism and induce fatty liver formation in patients with cancer.

Tumour EVPs reprogramme liver metabolism

Liver is a primary organ targeted by tumour EVPs[5–9]. We investigated whether tumour-secreted factors, specifically EVPs, targeted the liver to initiate metabolic dysfunction and fatty liver formation. We isolated a heterogeneous population of vesicles[5] (small exosomes (Exo-S), 60–80 nm; large exosomes (Exo-L), 90–120 nm) and particles (exomeres, <50nm), from B16F10 and K7M2 tumour explants by ultracentrifugation[16,17] and characterized them by transmission electron microscopy and nanoparticle tracking analysis (Extended Data Fig. 4a). Whole-organ imaging confirmed liver uptake of EVPs 24 h after intravenous injection of B16F10 and K7M2 tumour explant-derived EVPs (TE-EVPs) labelled with near-infrared dye into naive mice (Fig. 2a,b).

To investigate the role of TE-EVPs in liver metabolic 'education', we intravenously injected 10 μg of B16F10-TE-EVPs or K7M2-TE-EVPs—equivalent to physiological concentrations—into mice[10], every other day for 4 weeks (Extended Data Fig. 4b,c). The livers of mice educated with TE-EVPs or PBS control were anlayed by RNA-seq and metabolomic and lipidomic mass spectrometry (Fig. 2c–h and Supplementary Tables 8–11). Transcriptomic analysis revealed increased inflammatory responses and decreased metabolism (that is, OXPHOS and fatty acid metabolism) in TE-EVP-educated livers (Fig. 2c,d and Extended Data Fig. 4d). Metabolomic mass spectrometry identified similar dysregulated metabolites in TE-EVP-educated and tumour-bearing mouse livers (Fig. 2e,f and Extended Data Fig. 4e–h). Lipids (such as *O*-phosphoethanolamine, cholesterol and sitosterol) and lipid metabolism-associated pathways (such as phosphatidylethanolamine, phosphatidylcholine and steroid biosynthesis pathways) were enriched in B16F10-TE-EVP-educated livers (Fig. 2e and Extended Data Fig. 4g). Groups of amino acids (β-alanine for the B16F10 model, glutarate and mimosine for the K7M2 model) and carbohydrates (glucose-6-phosphate and lactose for the B16F10 model, and sedoheptulose, 2-ketogluconic acid and ribose 5-phosphate for the K7M2 model) were also enriched in TE-EVP-educated livers (Fig. 2e,f). Lipidomic mass spectrometry further revealed that ceramide and cholesterol ester were upregulated in B16F10-TE-EVP-educated livers and triglyceride was upregulated in both B16F10-TE-EVP- and K7M2-TE-EVP-educated livers (Fig. 2g,h and Extended Data Fig. 4i–l). Consistently, lipid droplets accumulated in TE-EVP-educated livers compared with controls, although to a lesser extent than in livers of tumour-bearing mice (Fig. 2i,j and Extended Data Fig. 4m,n). Together, these data show that TE-EVPs recapitulate tumour function in systemically disrupting liver metabolism and inducing fatty liver formation.

Distinct tumour EVP subsets induce fatty livers

Upon examining whether tumour cell-specific EVPs were responsible for liver dysfunction, we observed that cell line-derived EVPs (CL-EVPs) isolated from B16F10 and K7M2 cells primarily targeted the liver (Extended Data Fig. 5a–d) and—similar to TE-EVPs—they activated immune response pathways and suppressed metabolic pathways, resulting in enrichment of amino acids, carbohydrates and lipids and accumulation of lipid droplets in the liver (Extended Data Fig. 5e–p). These data suggest that tumour CL-EVPs are sufficient to dysregulate liver metabolism and induce fatty liver formation. We therefore used these tumour CL-EVPs for further studies.

To determine whether non-EVP soluble factors could contribute to fatty liver generation, we injected mice intraperitoneally with control medium or EVP-depleted conditioned medium from B16F10 or K7M2 cells (concentrated from the same volume required to isolate 10 μg of EVPs) every other day for four weeks, but did not observe fatty liver formation (Extended Data Fig. 5q). Furthermore, simultaneous education with EVP-depleted conditioned medium and B16F10-CL-EVPs did not enhance B16F10-CL-EVP-induced fatty liver formation (Extended Data Fig. 5r), suggesting that tumour-derived EVPs, but not soluble factors, are sufficient to promote fatty liver generation.

To examine whether tumour CL-EVPs are essential for cancer-induced fatty liver formation, we targeted *Rab27a* expression, a key regulator of EVP secretion[10,18], in B16F10 and K7M2 cells via knockout and knockdown, respectively. Consistent with previous results[10], *Rab27a* ablation suppressed EVP secretion by tumour cells without altering their morphology (Extended Data Fig. 6a–h). *Rab27a* loss reduced primary tumour growth in both models, despite unaltered proliferation in vitro (Extended Data Fig. 6i–l). BODIPY staining showed significantly decreased fatty liver induction in mice bearing *Rab27a*-knockout or *Rab27a*-knockdown tumours compared with their respective controls with similar tumour burdens (Extended Data Fig. 6m–p), indicating that tumour-derived EVPs are crucial for metabolic reprogramming of liver.

As EVPs are heterogeneous, we evaluated which EVP subpopulations[5] from B16F10 cells (among exomeres, Exo-S and Exo-L; isolated by asymmetric-flow field-flow fractionation (AF4); Fig. 2k) could induce hepatic lipid droplet accumulation after four weeks of education. All three subpopulations induced inflammation and altered liver metabolism (Extended Data Fig. 6q–t) and induced fatty liver formation, although fatty liver was induced by exomeres and Exo-S to a greater extent than by Exo-L (Fig. 2l). Notably, *Rab27a* loss reduced the production of exomeres, Exo-S (to a lesser extent) and Exo-L (to the least extent) from B16F10 cells and decreased B16F10 tumour-induced fatty liver generation (Extended Data Fig. 6o,p,u), suggesting that exomeres are a major contributor to fatty liver induction, consistent with previous findings of exomere uptake by the liver[5].

Kupffer cells drive lipid accumulation

To identify the liver cells that are targeted by tumour EVPs, we intravenously injected fluorescently labelled B16F10-CL-EVPs or K7M2-CL-EVPs into mice. Flow cytometry analysis of livers 24 h after injection revealed

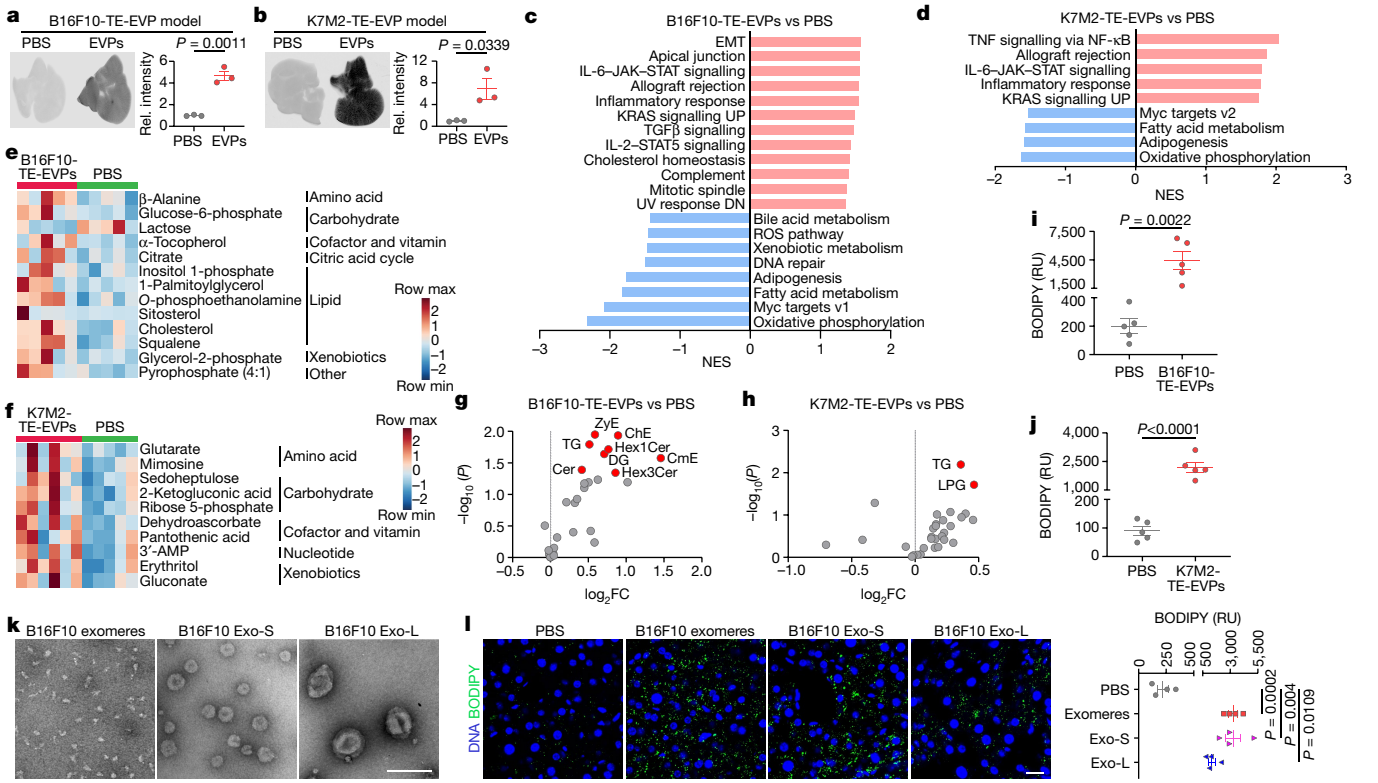

Fig. 2 | Tumour-derived EVPs induce liver metabolic dysfunction. **a**,**b**, Representative LI-COR Odyssey images (left) and associated quantification of relative (rel.) signal intensity (right) of livers from mice 24 h after intravenous injection of 10 μg CellVue NIR815-labelled B16F10-TE-EVPs (**a**) and K7M2-TE-EVPs (**b**), and PBS controls. $n = 3$ each. **c**,**d**, GSEA of gene profiles ranked on the basis of the sign of $\log_2FC \times (-\log_{10}(P\text{-value}))$ for livers from mice educated for 4 weeks with B16F10-TE-EVPs ($n = 5$) (**c**) or K7M2-TE-EVPs ($n = 3$) (**d**), compared with PBS-educated controls, using Hallmark gene sets. Significantly changed signalling pathways with FDR<0.05 are shown. Gene lists for signalling pathways are shown in Supplementary Tables 12 and 13. DN, down. **e**,**f**, Heat maps showing metabolites that are significantly changed in livers from B16F10-TE-EVP- (**e**) and K7M2-TE-EVP- (**f**) educated mice compared to PBS-educated controls. $n = 5$ B16F10-TE-EVP-educated mice and controls; $n = 6$ K7M2-TE-EVP-educated mice and $n = 5$ controls. **g**,**h**, Volcano plots showing the significantly enriched lipid classes (labelled in red, $P < 0.05$) in the livers from B16F10-TE-EVP- (**g**) and K7M2-TE-EVP- (**h**) educated mice, compared to PBS-educated controls. $n = 7$ B16F10-TE-EVP-educated mice and $n = 5$ controls; $n = 5$ K7M2-TE-EVP-educated mice and controls. ZyE, zymosterol ester; Hex1Cer, hexosylceramide; Hex3Cer, trihexosylceramide; CmE, campesterol ester. **i**,**j**, Quantification of BODIPY staining of the livers from B16F10-TE-EVP- (**i**) and K7M2-TE-EVP- (**j**) educated mice and PBS-educated controls. $n = 5$ each. **k**, Representative transmission electron microscopy (TEM) images of exomeres, Exo-S and Exo-L produced by B16F10 cells. This experiment was repeated three times independently with similar results. **l**, Representative images (left) and associated quantification (right) of BODIPY staining of the livers from mice educated with PBS, B16F10 exomeres, B16F10 Exo-S or B16F10 Exo-L for 4 weeks. $n = 4$ each. Scale bars: 200 nm (**k**), 20 μm (**l**). **a**,**b**,**g**–**j**,**l**, Two-tailed, unpaired Student's *t*-test. Data are mean ± s.e.m. EMT, epithelial mesenchymal transition. ROS, reactive oxygen species.

that EVPs from both models were taken up predominantly by $CD45^+$ immune cells and $CD31^+$ vascular endothelial cells, but not by $desmin^+$ stellate cells, $albumin^+$ hepatocytes or $LYVE1^+$ lymphatic and sinusoidal endothelial cells (Extended Data Fig. 7a–d). Specifically, more than 90% of $CD45^+$ immune cells taking up EVPs were $Cd11b^+F4/80^+$ Kupffer cells, a finding confirmed by immunofluorescence microscopy (Fig. 3a,b and Extended Data Fig. 7e).

We hypothesized that Kupffer cells, which promote NAFLD development[19], are key for fatty liver induction by tumour-derived EVPs. We therefore depleted Kupffer cells in mice bearing B16F10 and K7M2 tumours by intravenous injection of clodronate from day 12 or day 15 after tumour implantation. The efficiency of Kupffer cell depletion was confirmed by flow cytometry and immunofluorescence analyses (Fig. 3c and Extended Data Fig. 8a–d). Hepatic lipid droplet deposition was markedly reduced by Kupffer cell depletion in both models compared with liposome-injected controls, without affecting primary tumour growth (Fig. 3d and Extended Data Fig. 8e,f). Next, we depleted Kupffer cells in naive mice via clodronate treatment and generated viable precision-cut liver slices (PCLS) for ex vivo EVP treatment. Neither CL-EVPs nor TE-EVPs from B16F10 or K7M2 models could induce lipid droplet formation in Kupffer cell-ablated liver slices (Fig. 3e,f and Extended Data Fig. 8g–j). Collectively, these findings indicate that Kupffer cells are necessary for tumour EVP-induced fatty liver formation.

Tumour EVP-educated Kupffer cells upregulate TNF

To investigate whether tumour EVPs induce Kupffer cells to release specific factors that mediate fatty liver formation, after validating the functional integrity of isolated Kupffer cells, we showed that multiple cytokines and chemokines, including IL-1α, TNF, CCL2, CCL3, CXCL1, CXCL2 and CXCL13, were enriched in Kupffer cells isolated from mice bearing B16F10 or K7M2 tumours (Extended Data Fig. 9a–d), indicating an inflammatory liver microenvironment. We then isolated Kupffer cells from naive mice and treated them ex vivo with 10 μg ml^{-1} of B16F10-CL-EVPs, K7M2-CL-EVPs or PBS every 24 h for 3 days. Cytokine array analysis of Kupffer cell-conditioned media showed increased secretion of TNF, CCL2, CCL3, CXCL1 and CXCL2 from CL-EVP-treated Kupffer cells compared with control PBS-treated Kupffer cells (Extended Data Fig. 9e,f).

Kupffer cells treated with B16F10-CL-EVPs released 100 times more TNF than control Kupffer cells, as confirmed by enzyme-linked

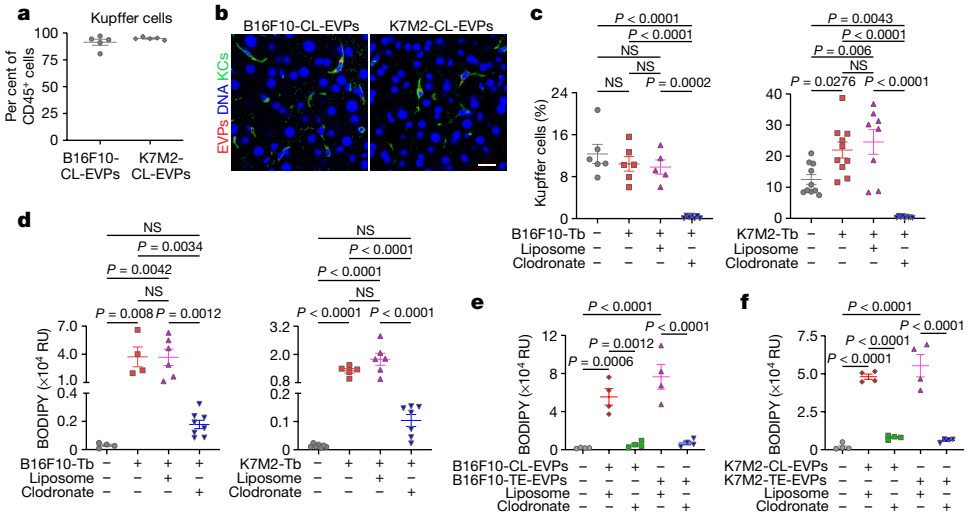

Fig. 3 | Uptake of tumour-derived EVPs by Kupffer cells induces fatty liver formation. a, Flow cytometry analysis of Kupffer cells among CD45$^+$ immune cells in mice. $n = 5$ each. **b**, Representative immunofluorescence images showing co-localization of Kupffer cells (KCs) and B16F10-CL-EVPs (left) or K7M2-CL-EVPs (right). DNA in blue. Scale bar, 20 µm. This experiment was repeated three times independently with similar results. **c**,**d**, Flow cytometry analysis of Kupffer cells (**c**) and quantification of BODIPY staining (**d**) in livers from PBS-injected control mice, mice bearing B16F10 or K7M2 tumours, and tumour-bearing mice treated with liposome or clodronate, as illustrated in Extended Data Fig. 8a. **c**, B16F10 tumour model: $n = 6$ controls and tumour-bearing mice, $n = 5$ tumour-bearing mice treated with liposomes and $n = 7$ tumour-bearing mice treated with clodronate; K7M2 tumour model: $n = 10$ controls and tumour-bearing mice, $n = 8$ tumour-bearing mice treated with liposomes and $n = 9$ tumour-bearing mice treated with clodronate. **d**, B16F10 tumour model: $n = 4$ controls and tumour-bearing mice, $n = 6$ tumour-bearing mice treated with liposomes and $n = 8$ tumour-bearing mice treated with clodronate; K7M2 tumour model: $n = 7$ controls, $n = 5$ tumour-bearing mice, $n = 6$ tumour-bearing mice treated with liposomes and $n = 7$ tumour-bearing mice treated with clodronate. **e**,**f**, Quantification of BODIPY staining of PCLS from mice treated with liposomes or clodronate after treatment with B16F10-CL-EVPs or B16F10-TE-EVPs (**e**) or K7M2-CL-EVPs or K7M2-TE-EVPs (**f**), following the procedure illustrated in Extended Data Fig. 8h. $n = 4$ each. **c**–**f**, One-way ANOVA with Tukey's test. Data are mean ± s.e.m. NS, not significant.

immunosorbent assay (ELISA) (Extended Data Fig. 9e,g). Furthermore, for both B16F10 and K7M2 models, plasma TNF levels were significantly higher in tumour-bearing mice and CL-EVP- or TE-EVP-educated mice than in control mice (Fig. 4a,b). *Tnf* gene expression was also upregulated in Kupffer cells isolated from tumour-bearing mice and naive mice after CL-EVP or TE-EVP treatment in vitro (Extended Data Fig. 9h,i). Since TNF was not detected in EVP-depleted B16F10- or K7M2-conditioned medium, we ruled out the tumour as the source of the TNF (Extended Data Fig. 9j).

As TNF promotes NAFLD development[20], we speculated that TNF drives liver dysregulation. We treated primary hepatocytes with recombinant TNF, which induced lipid droplet formation (Fig. 4c). Transcriptomic profiling revealed significant downregulation of lipid and fatty acid catabolic signatures in TNF-treated primary hepatocytes (Extended Data Fig. 9k). We administered a pan-TNF-blocking antibody intraperitoneally in mice bearing B16F10 or K7M2 tumours and observed reduced hepatic lipid droplet accumulation without affecting tumour growth (Fig. 4d and Extended Data Fig. 9l–n). Similar results were obtained in B16F10-EVP- or K7M2-CL-EVP-educated mice treated with anti-TNF antibody (Fig. 4e and Extended Data Fig. 9l,o), indicating that TNF secreted by Kupffer cells is required for tumour EVP-induced fatty liver formation.

Tumour EVP palmitic acid activates Kupffer cells

To identify the EVP cargo responsible for Kupffer cell activation, we performed metabolomic mass spectrometry on B16F10-TE-EVPs and control skin tissue explant-derived EVPs. Long-chain saturated fatty acids, especially palmitic acid and stearic acid, were significantly enriched in the B16F10-TE-EVPs (Extended Data Fig. 10a and Supplementary Table 14). Quantitative mass spectrometry of free fatty acids confirmed the enrichment of multiple saturated (with palmitic acid displaying the highest concentration) and unsaturated fatty acids in B16F10-TE-EVPs, B16F10-CL-EVPs and K7M2-CL-EVPs compared with their respective controls (EVPs isolated from mouse skin tissue explants, melan-A melanocytes and primary osteoblasts) (Fig. 4f,g, Extended Data Fig. 10b and Supplementary Tables 15–17).

As palmitic acid induces the secretion of pro-inflammatory cytokines—including TNF—by Kupffer cells during NAFLD progression[21,22], we tested whether palmitic acid packaged in tumour EVPs stimulated TNF secretion in Kupffer cells. We first showed that palmitic acid treatment induced *Tnf* expression in Kupffer cells compared with controls (Extended Data Fig. 10c). Treatment with the fatty acid synthase inhibitor C75[23] significantly reduced the amount of free fatty acids, including palmitic acid and longer chain fatty acids, in tumour cell EVPs (Extended Data Fig. 10d), which impaired EVP-induced *Tnf* expression in Kupffer cells (Fig. 4h). Moreover, EVPs secreted by primary osteoblasts (osteoblast-EVPs), which package less palmitic acid, did not induce *Tnf* expression in Kupffer cells or lipid droplet accumulation ex vivo or in vivo, despite efficient osteoblast-EVP uptake in the liver (Extended Data Fig. 10e–g). Neither skin (for B16F10) nor bone (for K7M2) normal tissue explant-derived EVP controls could induce *Tnf* expression in Kupffer cells or promote lipid droplet accumulation in liver slices (Extended Data Fig. 10e,h). However, EVPs secreted by melan-A melanocytes (melan-A-EVPs) induced *Tnf* expression in Kupffer cells despite low palmitic acid levels owing to 12-*O*-tetradecanoylphorbol-13-acetate in the culture medium (Extended Data Fig. 10e,i,j). Together, these data support a critical role for palmitic acid packaged in tumour EVPs in inducing TNF secretion by Kupffer cells.

Previous studies have shown that saturated fatty acids promote Toll-like receptor 4 (TLR4)-dependent signalling[24,25]; we therefore assessed whether TLR4 was required for *Tnf* expression in Kupffer cells induced by EVP-packaged palmitic acid. We pretreated Kupffer cells with the TLR4 inhibitor TAK for 1 h followed by palmitic acid treatment in the presence of TAK or DMSO control for another 4 h. Inhibition of TLR4 diminished palmitic acid-induced *Tnf*

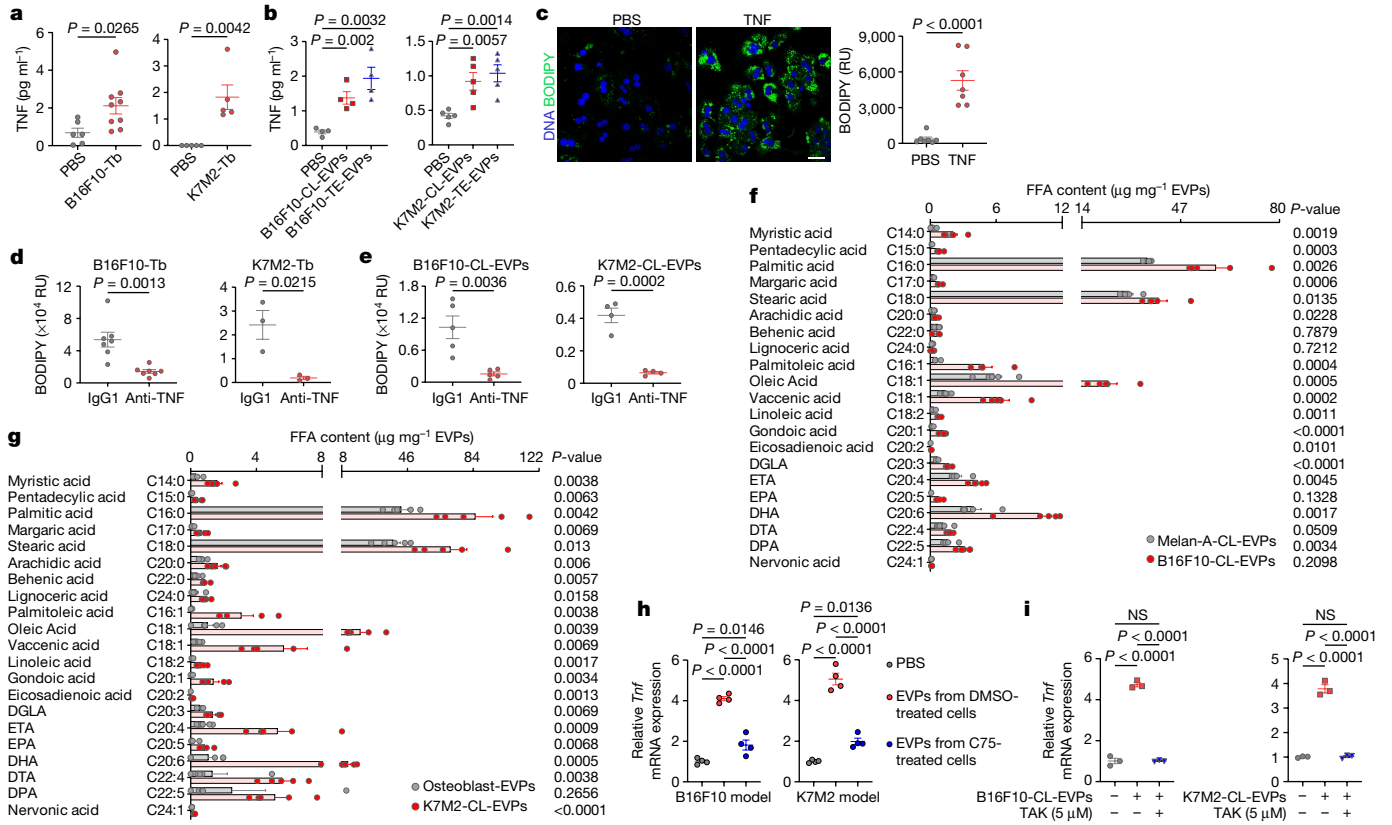

Fig. 4 | Palmitic acid in tumour EVPs induces TNF secretion from Kupffer cells and promotes fatty liver generation. a, TNF concentration in plasma from mice bearing B16F10 (left) and K7M2 (right) tumours and PBS-injected control mice, determined by ELISA. B16F10 tumour model: $n = 6$ controls, $n = 9$ tumour-bearing mice; K7M2 tumour model: $n = 5$. **b**, TNF concentration in the plasma of B16F10-CL-EVP- and B16F10-TE-EVP-educated mice ($n = 4$ each) (left), K7M2-CL-EVP- and K7M2-TE-EVP-educated mice ($n = 5$ each) (right) and PBS-educated controls. **c**, Representative images (left) and associated quantification (right) of BODIPY staining of primary hepatocytes 48 h after treatment with recombinant mouse TNF (25 ng ml^{-1}) or PBS control. $n = 7$ independent experiments. Scale bar, 20 μm. **d**,**e**, BODIPY staining of livers from mice bearing B16F10 and K7M2 tumours (**d**) and B16F10-CL-EVP- and K7M2-CL-EVP-educated mice (**e**), treated with anti-TNF antibody or IgG1 isotype control. B16F10 tumour model: $n = 7$; K7M2 tumour model: $n = 3$; B16F10-CL-EVP model: $n = 5$; K7M2-CL-EVP model: $n = 4$. **f**,**g**, Quantitative analysis of long-chain free fatty acids in EVPs derived from B16F10 and melan-A-expressing cells (**f**) and K7M2 cells and primary mouse osteoblasts (**g**). $n = 5$ per group. DGLA, dihomo-γ-linolenic acid; ETA, eicosatetraenoic acid; EPA, eicosapentaenoic acid; DHA, docosahexaenoic acid; DTA, docosatetraenoic acid; DPA, docosapentaenoic acid. **h**, RT–qPCR analysis of *Tnf* expression in Kupffer cells 4 h after treatment with PBS or 10 μg EVPs derived from B16F10 (left) or K7M2 (right) cells treated with DMSO or C75 (40 μM). $n = 4$ independent experiments. **i**, RT–qPCR analysis of *Tnf* expression in Kupffer cells pretreated with DMSO or TAK (5 μM) for 1 h and subsequently treated with PBS, 10 μg B16F10-CL-EVPs (left) or 10 μg K7M2-CL-EVPs (right) with or without TAK (5 μM) for 4 h. $n = 3$ independent experiments. Two-tailed, unpaired Student's *t*-test (**a**–**g**) or one-way ANOVA with Tukey's test (**h**,**i**). Data are mean ± s.e.m.

expression in Kupffer cells (Extended Data Fig. 10c). Notably, TLR4 inhibition also suppressed *Tnf* induction mediated by B16F10-CL-EVPs, K7M2-CL-EVPs, B16F10-TE-EVPs or K7M2-TE-EVPs (Fig. 4i and Extended Data Fig. 10k), suggesting that the activation of inflammatory pathways in Kupffer cells by EVP-packaged palmitic acid requires TLR4 activity.

Tumour EVPs suppress liver drug metabolism

Low tolerance for standard chemotherapy is often observed in patients with advanced cancers, probably owing to impaired detoxification by the liver[26,27]. We hypothesized that tumour EVP-induced fatty liver and inflammation could suppress drug metabolism by the liver. Indeed, recombinant TNF downregulated core Cyp genes corresponding to human cytochrome P450 homologues—*Cyp1a2*, *Cyp2b10*, *Cyp2c38*, *Cyp2d9*, *Cyp2d10* and *Cyp3a11*—in mouse hepatocytes (Fig. 5a and Supplementary Table 18). These genes were also downregulated in hepatocytes isolated from mice bearing B16F10 tumours or from B16F10-CL-EVP-educated mice compared with controls (Fig. 5b,c). Notably, CYP enzymes metabolize 70–80% of prescribed drugs[28], and GSEA revealed downregulation of the drug-metabolizing cytochrome P450 signalling pathway in primary hepatocytes after TNF treatment and in the livers of B16F10 tumour-bearing mice and patients with pancreatic cancer without liver metastasis (but who later developed extrahepatic metastasis) (Fig. 5d).

Next, we showed that the capacity of each Cyp enzyme to metabolize specific substrates was indeed decreased in liver slices from tumour-bearing mice compared with controls by measuring the levels of metabolized products (Extended Data Fig. 11a,b). Using methoxsalen (a CYP1A2 inhibitor) and phenobarbital (a CYP2B10 inducer) as negative and positive controls, respectively, we further showed that ex vivo B16F10-CL-EVP treatment was sufficient to suppress drug metabolism in liver slices from naive mice (Extended Data Fig. 11c,d). Notably, TNF blockade rescued hepatocyte expression of Cyp genes in mice bearing B16F10 tumours and in B16F10-CL-EVP-educated mice (Fig. 5b,c) and reversed the impaired drug metabolism in liver slices from mice bearing B16F10 tumours and in B16F10-CL-EVP-treated liver slices from naive mice (Extended Data Fig. 11b,d). These results suggest that tumour EVP-induced secretion of TNF by Kupffer cells impairs liver drug metabolism via Cyp enzyme suppression.

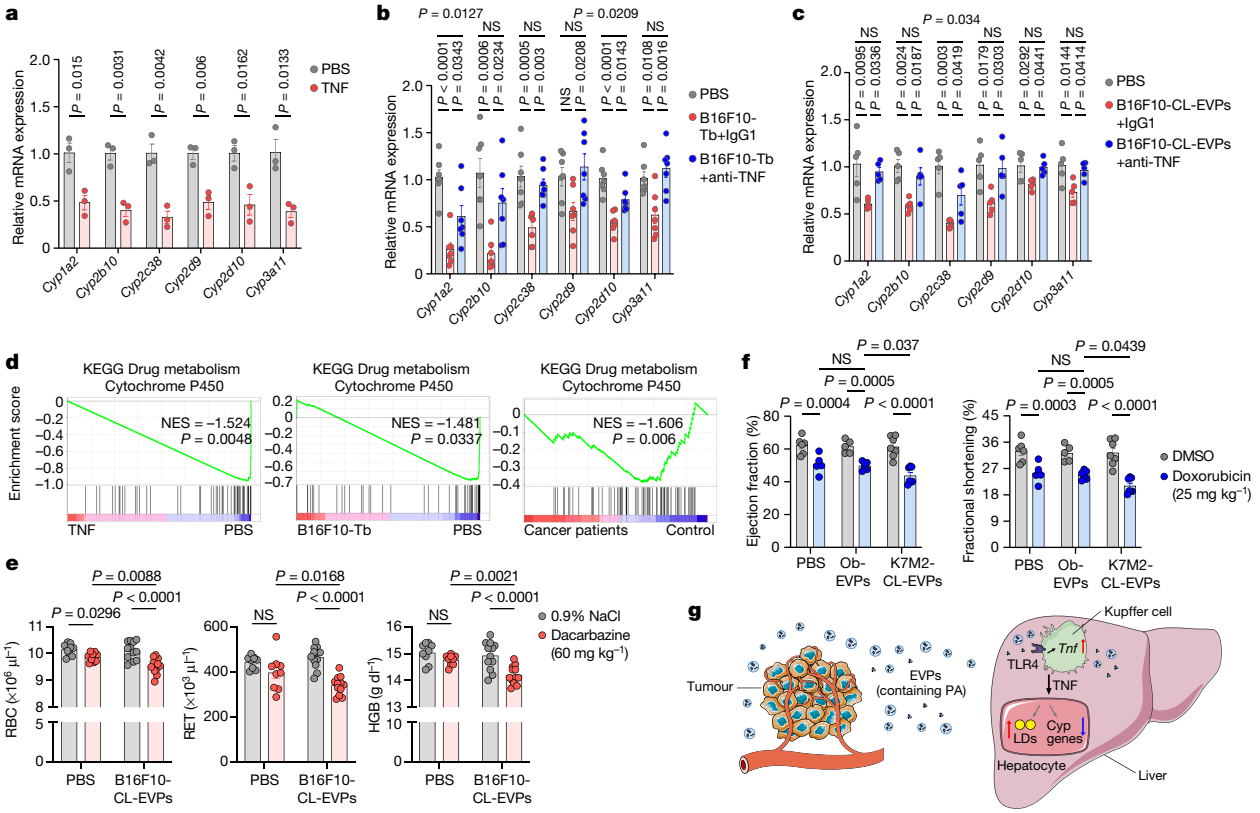

Fig. 5 | Tumour EVPs suppress liver drug metabolism and enhance chemotoxicity. a, RT–qPCR analysis of *Cyp* expression in primary hepatocytes treated with PBS or recombinant mouse TNF (25 ng ml^{-1}) for 24 h. $n = 3$ independent experiments. **b**,**c**, RT–qPCR analysis of *Cyp* expression in hepatocytes isolated from mice bearing B16F10 tumours ($n = 7$) (**b**) or B16F10-CL-EVP-educated mice ($n = 5$) (**c**) treated with anti-TNF antibody or IgG1 isotype control, compared to the respective PBS-injected controls. **d**, GSEA of gene expression profiles of TNF-treated mouse primary hepatocytes (top) in livers from mice bearing B16F10 tumours (middle) and human patients with cancer (bottom), compared to the respective controls. $n = 3$ per group for TNF treatment, B16F10 tumour mice and PBS controls; $n = 5$ cancer patients and $n = 8$ control subjects. **e**, Analysis of red blood cell (RBC), reticulocyte (RET) and haemoglobin (HGB) counts in PBS- ($n = 9$) or B16F10-CL-EVP- ($n = 12$) educated mice after treatment with dacarbazine (60 mg kg^{-1}) or 0.9% NaCl. **f**, Left ventricular ejection fraction and fractional shortening (M-mode) in PBS-, osteoblast (Ob)-EVP- or K7M2-CL-EVP-educated mice after treatment with doxorubicin (cumulative dose of 25 mg kg^{-1}) or DMSO. PBS groups: $n = 6$; K7M2-CL-EVP groups: $n = 7$; Ob-EVP group: $n = 5$ DMSO and $n = 6$ doxorubicin. **g**, Schematic of the working model for EVP-mediated dysregulation of liver metabolism. Tumour-derived EVPs specifically target Kupffer cells in the liver. EVP-packaged saturated fatty acids, such as palmitic acid (PA), stimulate the secretion of TNF from Kupffer cells in a TLR4-dependent manner. This produces a pro-inflammatory microenvironment in the liver, thereby systemically inducing fatty liver formation and suppressing the drug-metabolizing activity of the liver. LDs, lipid droplets. Two-tailed, unpaired *t*-test (**a**), one-way ANOVA with Tukey's test (**b**,**c**) and two-way ANOVA with Fisher's least significant difference test (**e**,**f**). Data are mean ± s.e.m.

Tumour EVPs enhance chemotherapy toxicity

As impaired drug metabolism induced by tumour EVPs may affect chemotherapy toxicity, we evaluated the toxicity of dacarbazine and doxorubicin, two drugs metabolized by Cyp enzymes that are used to treat melanoma and osteosarcoma, respectively[29–31]. We injected dacarbazine (60 mg kg^{-1}) or 0.9% NaCl intraperitoneally into mice pre-educated with PBS or B16F10-CL-EVPs every other day for one week while continuing B16F10-CL-EVP or PBS education (Extended Data Fig. 11e). One day after the last injection, we observed a 2.8% decrease in red blood cells and no significant decrease in reticulocyte numbers or haemoglobin levels in PBS-educated mice; however, dacarbazine toxicity was significantly enhanced, with a 5.6% reduction in red blood cells, a 26.9% reduction in reticulocytes and a 4.9% reduction in haemoglobin in EVP-educated mice versus controls (Fig. 5e).

Next, we injected doxorubicin (1 mg kg^{-1}) or DMSO intraperitoneally into mice pre-educated with PBS, primary osteoblast-EVPs or K7M2-CL-EVPs every 24 h for 25 days while continuing PBS or EVP education. One day after the last injection, echocardiography revealed that doxorubicin decreased the left ventricular ejection fraction from 62.1% and 61.5% to 50.8% and 49.7% (an 18.2% and 19.2% reduction) in PBS and osteoblast-EVP-educated mice, respectively, with a further decrease, from 61.3% to 43.7% (a 28.7% reduction) in K7M2-CL-EVP-educated mice (Fig. 5f, Extended Data Fig. 11e–g and Supplementary Videos 1–6), into a range approaching that observed in heart failure (ejection fraction of 40% or less versus above 55% for normal cardiac function[32]). Doxorubicin also decreased left ventricular fractional shortening from 32.9% and 32.2% to 25.4% and 24.8% (a reduction of 22.8% and 23%, respectively) in PBS- and osteoblast-EVP-educated mice, with a further decrease from 32.3% to 21% (a 35% reduction) in K7M2-CL-EVP-educated mice (Fig. 5f and Extended Data Fig. 11f,g). Thus, tumour EVPs enhance chemotherapy toxicity by impairing liver drug metabolism, consequently reducing chemotherapy tolerance in patients with cancer.

Discussion

Cancer cells secrete EVPs, systemically reprogramming local and remote organ function[1,3,6,7,10]. EVPs promote PMN formation as well as pathological events in other organs that are not destined for metastasis[3,4,6,33]. Here we show that EVPs derived from remote tumours induce

inflammation and downregulate lipid catabolism in tumour-free livers, reprogramming metabolism in mice and in patients with cancer (Fig. 5g). Mechanistically, palmitic acid in tumour EVPs elicits TNF secretion in Kupffer cells, thus driving fatty liver formation. Blocking EVP secretion by ablating Rab27a in cancer cells, depleting Kupffer cells or blocking TNF rescues these phenotypes. Notably, we show that exomeres, the predominant EVP targeting the liver[5], are the primary contributor to fatty liver formation.

We observed an inverse relationship between fatty liver generation and liver PMN formation, as liver-tropic tumour EVPs stimulate TGFβ secretion by Kupffer cells to activate stellate cells and produce a fibrotic PMN[6,7], whereas tumours with extrahepatic metastatic tropism induce fatty liver via EVP-mediated TNF secretion by Kupffer cells. Furthermore, we observed that exosome subpopulations target PMN organs[7], whereas exomeres predominantly target the liver[5], driving fatty liver formation. Further dissection of EVP cargo and functional heterogeneity within each subpopulation will be critical to decipher the mechanisms promoting PMN formation and metastasis versus the paraneoplastic effects of cancer. Our study also highlights a novel mechanism whereby EVP-packaged palmitic acid alters non-metastatic liver function, distinct from the effects of palmitic acid in PMNs[34].

EVP-induced fatty liver may provide energy to support tumour growth systemically at other sites, consistent with reports that NAFLD increases the risk of extrahepatic cancers[35,36]. Beyond tumour support, liver metabolic dysregulation could have multi-organ systemic effects, promoting cardiovascular disease through increased cholesterol and triglyceride production as seen here; impairing immune functions, such as T cell function; or promoting cachexia.

Our work highlights the need to take into account for cancer treatments the systemic effects of cancers. Strategies that restore liver function are critical to minimize side effects and enhance treatment responses to chemotherapeutic drugs metabolized by the liver. As we have shown that tumour EVP-induced TNF secretion downregulates Cyp genes and compromises liver drug metabolism, integrating chemotherapy with TNF inhibitors may restore liver function in patients being treated for cancer. Strategies to reduce tumour EVP production should also be considered, since they would prevent liver metabolic dysfunction as well as inhibit PMN formation. Finally, restoration of normal liver function may also prevent further systemic pathologies (such as cardiovascular disease) associated with cancer.

Online content

Any methods, additional references, Nature Portfolio reporting summaries, source data, extended data, supplementary information, acknowledgements, peer review information; details of author contributions and competing interests; and statements of data and code availability are available at https://doi.org/10.1038/s41586-023-06114-4.

1. McAllister, S. S. & Weinberg, R. A. The tumour-induced systemic environment as a critical regulator of cancer progression and metastasis. *Nat. Cell Biol.* **16**, 717–727 (2014).
2. Wang, G. et al. Metastatic cancers promote cachexia through ZIP14 upregulation in skeletal muscle. *Nat. Med.* **24**, 770–781 (2018).
3. Lucotti, S., Kenific, C. M., Zhang, H. & Lyden, D. Extracellular vesicles and particles impact the systemic landscape of cancer. *EMBO J.* **41**, e109288 (2022).
4. Zhang, G. et al. Tumor induces muscle wasting in mice through releasing extracellular Hsp70 and Hsp90. *Nat. Commun.* **8**, 589 (2017).
5. Zhang, H. et al. Identification of distinct nanoparticles and subsets of extracellular vesicles by asymmetric flow field-flow fractionation. *Nat. Cell Biol.* **20**, 332–343 (2018).
6. Costa-Silva, B. et al. Pancreatic cancer exosomes initiate pre-metastatic niche formation in the liver. *Nat. Cell Biol.* **17**, 816–826 (2015).
7. Hoshino, A. et al. Tumour exosome integrins determine organotropic metastasis. *Nature* **527**, 329–335 (2015).
8. Zhang, H. et al. Exosome-delivered EGFR regulates liver microenvironment to promote gastric cancer liver metastasis. *Nat. Commun.* **8**, 15016 (2017).
9. Xie, Z. et al. Exosome-delivered CD44v6/C1QBP complex drives pancreatic cancer liver metastasis by promoting fibrotic liver microenvironment. *Gut* **71**, 568–579 (2022).
10. Peinado, H. et al. Melanoma exosomes educate bone marrow progenitor cells toward a pro-metastatic phenotype through MET. *Nat. Med.* **18**, 883–891 (2012).
11. Khanna, C. et al. Metastasis-associated differences in gene expression in a murine model of osteosarcoma. *Cancer Res.* **61**, 3750–3759 (2001).
12. Aslakson, C. J. & Miller, F. R. Selective events in the metastatic process defined by analysis of the sequential dissemination of subpopulations of a mouse mammary tumor. *Cancer Res.* **52**, 1399–1405 (1992).
13. Tilg, H., Adolph, T. E., Dudek, M. & Knolle, P. Non-alcoholic fatty liver disease: the interplay between metabolism, microbes and immunity. *Nat. Metab.* **3**, 1596–1607 (2021).
14. Burd, C. E. et al. Mutation-specific RAS oncogenicity explains NRAS codon 61 selection in melanoma. *Cancer Discov.* **4**, 1418–1429 (2014).
15. Maddipati, R. & Stanger, B. Z. Pancreatic cancer metastases harbor evidence of polyclonality. *Cancer Discov.* **5**, 1086–1097 (2015).
16. Hoshino, A. et al. Extracellular vesicle and particle biomarkers define multiple human cancers. *Cell* **182**, 1044–1061.e1018 (2020).
17. Bojmar, L. et al. Extracellular vesicle and particle isolation from human and murine cell lines, tissues, and bodily fluids. *STAR Protoc.* **2**, 100225 (2021).
18. Ostrowski, M. et al. Rab27a and Rab27b control different steps of the exosome secretion pathway. *Nat. Cell Biol.* **12**, 19–30 (2010).
19. Stienstra, R. et al. Kupffer cells promote hepatic steatosis via interleukin-1beta-dependent suppression of peroxisome proliferator-activated receptor alpha activity. *Hepatology* **51**, 511–522 (2010).
20. De Taeye, B. M. et al. Macrophage TNF-α contributes to insulin resistance and hepatic steatosis in diet-induced obesity. *Am. J. Physiol.* **293**, E713–E725 (2007).
21. Feldstein, A. E. et al. Free fatty acids promote hepatic lipotoxicity by stimulating TNF-α expression via a lysosomal pathway. *Hepatology* **40**, 185–194 (2004).
22. Korbecki, J. & Bajdak-Rusinek, K. The effect of palmitic acid on inflammatory response in macrophages: an overview of molecular mechanisms. *Inflamm. Res.* **68**, 915–932 (2019).
23. Kuhajda, F. P. et al. Synthesis and antitumor activity of an inhibitor of fatty acid synthase. *Proc. Natl Acad. Sci. USA* **97**, 3450–3454 (2000).
24. Rocha, D. M., Caldas, A. P., Oliveira, L. L., Bressan, J. & Hermsdorff, H. H. Saturated fatty acids trigger TLR4-mediated inflammatory response. *Atherosclerosis* **244**, 211–215 (2016).
25. Milanski, M. et al. Saturated fatty acids produce an inflammatory response predominantly through the activation of TLR4 signaling in hypothalamus: implications for the pathogenesis of obesity. *J. Neurosci.* **29**, 359–370 (2009).
26. Fearon, K. C., Glass, D. J. & Guttridge, D. C. Cancer cachexia: mediators, signaling, and metabolic pathways. *Cell Metab.* **16**, 153–166 (2012).
27. Vasilogianni, A. M. et al. Proteomics of colorectal cancer liver metastasis: A quantitative focus on drug elimination and pharmacodynamics effects. *Br. J. Clin. Pharmacol.* **88**, 1811–1823 (2021).
28. Jamwal, R. & Barlock, B. J. Nonalcoholic fatty liver disease (NAFLD) and hepatic cytochrome P450 (CYP) enzymes. *Pharmaceuticals* **13**, 222 (2020).
29. Reid, J. M., Kuffel, M. J., Miller, J. K., Rios, R. & Ames, M. M. Metabolic activation of dacarbazine by human cytochromes P450: the role of CYP1A1, CYP1A2, and CYP2E1. *Clin. Cancer Res.* **5**, 2192–2197 (1999).
30. Lewis, I. J. et al. Improvement in histologic response but not survival in osteosarcoma patients treated with intensified chemotherapy: a randomized phase III trial of the European Osteosarcoma Intergroup. *J. Natl Cancer Inst.* **99**, 112–128 (2007).
31. Bagdasaryan, A. A. et al. Pharmacogenetics of drug metabolism: the role of gene polymorphism in the regulation of doxorubicin safety and efficacy. *Cancers* **14**, 5436 (2022).
32. Savarese, G., Stolfo, D., Sinagra, G. & Lund, L. H. Heart failure with mid-range or mildly reduced ejection fraction. *Nat. Rev. Cardiol.* **19**, 100–116 (2022).
33. Peinado, H. et al. Pre-metastatic niches: organ-specific homes for metastases. *Nat. Rev. Cancer* **17**, 302–317 (2017).
34. Altea-Manzano, P. et al. A palmitate-rich metastatic niche enables metastasis growth via p65 acetylation resulting in pro-metastatic NF-κB signaling. *Nat. Cancer* **4**, 344–364 (2023).
35. Allen, A. M., Hicks, S. B., Mara, K. C., Larson, J. J. & Therneau, T. M. The risk of incident extrahepatic cancers is higher in non-alcoholic fatty liver disease than obesity—a longitudinal cohort study. *J. Hepatol.* **71**, 1229–1236 (2019).
36. Mantovani, A. et al. Non-alcoholic fatty liver disease and increased risk of incident extrahepatic cancers: a meta-analysis of observational cohort studies. *Gut* **71**, 778–788 (2022).

[1]Children's Cancer and Blood Foundation Laboratories, Departments of Pediatrics, and Cell and Developmental Biology, Drukier Institute for Children's Health, Meyer Cancer Center, Weill Cornell Medicine, New York, NY, USA. [2]Department of Orthopedic Surgery, Nanfang Hospital, Southern Medical University, Guangzhou, China. [3]Department of Biomedical and Clinical Sciences, Linköping University, Linköping, Sweden. [4]Department of Radiation Oncology, The Second Affiliated Hospital, Zhejiang University School of Medicine, Hangzhou, China. [5]Key Laboratory of Cancer Prevention and Intervention, China National Ministry of Education, Key Laboratory of Molecular Biology in Medical Sciences, Hangzhou, China. [6]Duke Proteomics and Metabolomics Shared Resource, Duke University School of Medicine, Durham, NC, USA. [7]Cardiovascular Research Institute and Department of Medicine,

Weill Cornell Medicine, New York, NY, USA. [8]Basic Medical Research Center, Medical School of Nantong University, Nantong, China. [9]Departments of Molecular Genetics, Cancer Biology and Genetics, The Ohio State University, Columbus, OH, USA. [10]Samuel J. Wood Library, Weill Cornell Medicine, New York, NY, USA. [11]Yonsei Cancer Center, Division of Medical Oncology, Department of Internal Medicine, Brain Korea 21 FOUR Project for Medical Science, Severance Biomedical Science Institute, Yonsei University College of Medicine, Seoul, Korea. [12]Department of Dermatology, Weill Cornell Medical College of Cornell University, New York, NY, USA. [13]Hepatopancreatobiliary Service, Department of Surgery, Memorial Sloan Kettering Cancer Center, New York, NY, USA. [14]Thoracic and Gastrointestinal Oncology Branch, National Cancer Institute, National Institutes of Health, Bethesda, MD, USA. [15]Division of Surgical Oncology, Rutgers Cancer Institute of New Jersey, New Brunswick, NJ, USA. [16]Fred and Pamela Buffett Cancer Center, University of Nebraska Medical Center, Omaha, NE, USA. [17]Department of Pathology and Microbiology, College of Medicine, University of Nebraska Medical Center, Omaha, NE, USA. [18]Department of Internal Medicine, University of Nebraska Medical Center, Omaha, NE, USA. [19]Department of Pediatrics, Memorial Sloan Kettering Cancer Center, New York, NY, USA. [20]Cold Spring Harbor Laboratory, Cold Spring Harbor, NY, USA. [21]Division of Hematology and Medical Oncology, Department of Medicine, Weill Cornell Medicine, New York, NY, USA. [22]Department of Medicine, Memorial Sloan Kettering Cancer Center, New York, NY, USA. [23]Gastrointestinal Oncology Service, Memorial Sloan Kettering Cancer Center, New York, NY, USA. [24]Orthopedic Service, Department of Surgery, Memorial Sloan Kettering Cancer Center, New York, NY, USA. [25]Division of Gastroenterology and Hepatology, Department of Medicine, Weill Cornell Medicine, New York, NY, USA. [26]These authors contributed equally: Gang Wang, Jianlong Li. ✉e-mail: res2025@med.cornell.edu; haz2005@med.cornell.edu; dcl2001@med.cornell.edu

Methods

Cell lines and cell culture

B16F10, K7M2, B16F1, 4T1 and 293T cells were purchased from American Type Culture Collection (ATCC); the SK-MEL-192 cell line was obtained from Memorial Sloan Kettering Cancer Center (MSKCC). These cells were cultured in DMEM (Corning, 10-013-CV) supplemented with 10% FBS (Gibco, 10438-026) and 1× penicillin/streptomycin (100 U ml^{-1} of penicillin and 100 μg ml^{-1} of streptomycin, Thermo Fisher Scientific, 15070-063).

The 67NR cell line was obtained from F. Miller[12], and cultured in RPMI (Corning, 10-040-CV) supplemented with 10% FBS and 1× penicillin/streptomycin. The mouse melanocyte melan-A line was obtained from The Wellcome Trust Functional Genomics Cell Bank and cultured in RPMI supplemented with 10% FBS, 1× penicillin/streptomycin and 0.2 μM 12-*O*-tetradecanoylphorbol-13-acetate (TPA) (Sigma, P1585). Primary osteoblasts were isolated from mouse bones, and primary hepatocytes and Kupffer cells were isolated from mouse livers as described below. When collecting conditioned media for EVP isolation, FBS was first depleted of EVPs by ultracentrifugation at 100,000*g* for 4 h. Cells were cultured in EVP-depleted media for 3 days and supernatant was collected before cells reached confluency for EVP isolation. Cells were maintained in a humidified 37 °C incubator with 5% CO_2, and cell lines routinely tested and confirmed to be negative for mycoplasma.

Generation of *Rab27a*-knockout B16F10, *Rab27a*-knockdown K7M2 and mCherry-expressing K7M2 cell lines

Rab27a knockout in B16F10 cells was achieved by infecting cells using lentivirus (lentiCRISPR vector (Addgene, #52961) carrying guide RNA targeting mouse *Rab27a* at 5′-CCTGAAATCAATGCCCACTG-3′). The single guide RNA targeting sequence was chosen using GPP sgRNA Designer (https://portals.broadinstitute.org/gpp/public/analysis-tools/sgrna-design). Lentivirus-infected cells were single-cell-sorted into a 96-well plate for clonal growth. RAB27A depletion was confirmed by western blotting analysis and *Rab27a* gene knockout was verified by Sanger sequencing. As a control, B16F10 cells were infected with lentiCRISPR empty-vector virus. *Rab27a* knockdown in K7M2 cells was achieved by infecting cells using lentivirus (pLKO.1 sh*Rab27a*, TRCN0000381753, Sigma). Knockdown efficiency of RAB27A in K7M2 cells was confirmed by western blotting analysis. As a control, K7M2 cells were infected with pLKO.1 shRNA empty-vector virus. mCherry-expressing K7M2 (K7M2-mCherry) cell line was generated by infecting cells using lentivirus (LeGO-C, Addgene, #27348).

Lentivirus was produced by co-transfection of the lentiviral expression vector and viral packaging/envelope plasmids, including pRRE (Addgene, #12251), pMD2g (Addgene, #12259) and pRSV-REV (Addgene, #12253) into 293T cells using Lipofectamine LTX/PLUS (Invitrogen, 15338030).

Cell proliferation assay

Cell proliferation was assessed according to the manufacturer's instructions (Cell Counting Kit-8, CCK-8). In brief, cells were plated in a 96-well plate at a concentration of 5,000 cells per well. After cells attached to the plate (time point set as 0 h), 10 μl of CCK-8 (Dojindo, CK04) was added into the cell culture medium (100 μl) and incubated at 37 °C for 30 min. The absorbance at 450 nm was measured using a microplate reader (accuSkan GO, Thermo Fisher Scientific). Cell proliferation assay was also performed at time point of 24 h, 48 h, 72 h and 96 h, respectively.

Western blotting

Western blotting was done as previously described[2]. In brief, cells were lysed in RIPA buffer (Millipore, Sigma, R0278) supplemented with Halt Protease Inhibitor Cocktail (Thermo Fisher Scientific, 87786). Proteins were separated by SDS–PAGE (Invitrogen, XP00100BOX) and transferred onto a polyvinylidene difluoride (PVDF) membrane (Bio-Rad, 1620177). After membranes were blocked with 5% BSA (EMD, Millipore, 12659) for 30 min, they were probed with primary antibodies, including anti-RAB27A (Cell Signaling, 69295) and anti-β-actin (Cell Signaling, 4970) overnight at 4 °C, followed by incubation with HRP-conjugated secondary antibodies for 1 h at room temperature. The membranes were then developed using ECL substrate (Bio-Rad) and visualized using the Bio-Rad ChemiDoc Touch Imaging System.

Isolation of primary hepatocytes and Kupffer cells from mouse livers

Plates were coated with collagen I (30 μg ml^{-1} in sterile water, Thermo Fisher Scientific, A10483-01) overnight prior to seeding cells. Mice were anaesthetized using 2% isoflurane/1.5% oxygen inhalation, and the livers were first perfused with 30 ml of HBSS (Ca^{2+} and Mg^{2+} free, Thermo Fisher Scientific, 14175-095) containing 0.5 mM of EGTA (Sigma, E8145) and 25 mM of HEPES (Gibco, 15630-080), and then digested with 50 ml of collagenase solution (DMEM containing 100 U ml^{-1} of collagenase type 2 (Worthington Biochemical, LS004176), 15 mM of HEPES, 1× penicillin/streptomycin). After collagenase digestion, livers were removed and whole liver cells were released into DMEM containing 1× non-essential amino acids solution (Thermo Fisher Scientific, 11140-050), 1× penicillin/streptomycin and 1× L-glutamine (Gibco, 25030-081) by rupturing the Glisson's capsule, and filtered through a 70 μm cell strainer (Thermo Fisher Scientific, 08-771-2) to remove undigested tissues. The flow-through cells were subjected to centrifugation at 50*g* for 3 min at 4 °C, and the pellet was collected for primary hepatocyte isolation and the supernatant was collected for Kupffer cell isolation, respectively. For primary hepatocyte isolation, the pellet was washed twice in 30 ml of Hepatocyte Wash Medium (Thermo Fisher Scientific, 17704-024) by centrifugation at 50*g* for 2 min at 4 °C, and the hepatocytes were pelleted down at 50*g* for 2 min at 4 °C and resuspended in Hepatocyte Culture Medium (Lonza, CC-3198) and cultured in collagen I-coated plates in a humidified 37 °C incubator with 5% CO_2. For Kupffer cell isolation, the supernatant was subjected to centrifugation at 300*g* for 10 min at 4 °C to pellet non-parenchymal cells, which were resuspended in 450 μl of MACS buffer (PBS containing 2% FBS). Fifty microlitres of anti-F4/80 microbeads (Miltenyi Biotec, 130-110-443) was added to the cell suspension, which was gently rocked at 4 °C for 15 min in the dark, and then the cells were washed twice with MACS buffer and pelleted by centrifugation at 300*g* for 10 min at 4 °C. Cells were then resuspended in 0.5 ml of MACS buffer and applied onto an LS column (Miltenyi Biotec, 130-042-401). After washing with MACS buffer, the Kupffer cells retained in the LS column were collected according to the manufacturer's protocol. Kupffer cells were resuspended in DMEM containing 1× non-essential amino acids solution, 1× penicillin/streptomycin, 1× L-glutamine and 10% EVP-depleted FBS, and cultured in the collagen I-coated 6-well plates in a humidified 37 °C incubator with 5% CO_2. Cells were washed with PBS 1-2 h after plating to remove dead cells and either collected for RNA extraction or cultured in fresh medium overnight for downstream experiments. RT–qPCR analysis of the expression of Cyp genes (in hepatocytes) and *Tnf* (in Kupffer cells) was performed as described below.

TNF treatment of primary hepatocytes

Primary hepatocytes cultured in the collagen I-coated 6-well plates or 8-well chamber slides (Millipore, Sigma) were treated with PBS or 25 ng ml^{-1} of recombinant mouse TNF (aa 80–235) protein (R&D system, 410-MT-025/CF) for 24 h or 48 h, followed by RT–qPCR analysis of the Cyp gene expression or BODIPY staining, respectively.

Treatment of Kupffer cells

For EVP treatment, Kupffer cells were treated with PBS or 10 μg ml^{-1} of EVPs derived from cell lines or tissue explants for 4 h; or pretreated with DMSO or 5 μM of TAK (MedChemExpress, HY-11109) for 1 h, followed

by treatment with EVPs (10 μg ml^{-1}) in the presence or absence of TAK (5 μM) for 4 h. Kupffer cells were then collected for RNA extraction and RT–qPCR analysis.

For TPA treatment, Kupffer cells were treated with DMSO or 0.2 μM of TPA for 4h, followed by RNA extraction and RT–qPCR analysis.

For palmitic acid treatment, stock palmitic acid (Millipore Sigma, P5585) was made up in 100% ethanol at 200 mM and diluted into 0.2-μm-filter sterilized PA-carrier medium (DMEM containing 5% EVP-depleted FBS, 5% fatty acid-free BSA (Sigma Aldrich, A3803), 1× non-essential amino acids solution, 1× penicillin/streptomycin and 1× L-glutamine) at a final concentration of 200 μM. As a control, 100% ethanol was diluted into PA-carrier medium at 1:1,000 dilution. To facilitate the conjugation of palmitic acid to BSA, the mixture was incubated at 37 °C for 30 min with gentle shaking. Kupffer cells were pretreated with DMSO or 5 μM of TAK for 1 h, washed once with PBS and then incubated in medium carrying 200 μM of palmitic acid or control ethanol with or without TAK (5 μM) for 4 h. Kupffer cells were then collected for RNA extraction and RT–qPCR analysis.

RNA extraction and RT–qPCR analysis

Total RNA was extracted using TRIzol reagent (Thermo Fisher Scientific, 15596018) as previously described[2], and RNA was further purified using RNeasy Mini kit including a DNase digest following the manufacturer's instructions (Qiagen, 74014). Total RNA was then subjected to RT–qPCR analysis and RNA-seq as described below.

For RT–qPCR analysis, 100–500 ng of total RNA was used for cDNA synthesis using the high-capacity cDNA reverse transcription kit with RNase inhibitor (Thermo Fisher Scientific, 4374966) following the manufacturer's instructions. Ten nanograms of cDNA were used for RT–qPCR reactions using SYBR Green Supermix (Bio-Rad, 1725271) and gene-specific primers. The *18S* rRNA was used as an internal control. RT–qPCR was performed on a CFX384 Touch Real-Time PCR System (Bio-Rad), and data were analysed by CFX Manager (version 3.1, Bio-Rad). The relative gene expression was quantified by $2^{-\Delta\Delta Ct}$ method[37]. Primers used in RT–qPCR analysis are listed in Supplementary Table 27.

Primary osteoblast isolation and culture

Primary mouse osteoblasts were isolated from BALB/c mouse bones as previously described[38]. In brief, 7-week-old female mice were euthanized and bone tissues including tibia, femur and humerus were collected. Bone marrow was removed by flushing with basal medium (10 g l^{-1} of αMEM (BioConcept, 1-23P10-M) containing 2.2 g l^{-1} of $NaHCO_3$, 1× penicillin/streptomycin, 2 mM of L-glutamine, 0.375× MEM amino acids (BioConcept, 5-12K01-H) and 10% EVP-depleted FBS). Bone tissues were then cut into small pieces and seeded into a 10-mm dish with 10 ml of digestion medium (basal medium containing 1 mg ml^{-1} of collagenase II (Sigma, C6885)). After incubation at 37 °C for 90 min, the digestion medium was replaced by basal medium to allow the cells to migrate from bone pieces and attach to the dish. Three days later, cells were detached with collagenase I (Thermo Fisher Scientific, 17100-017) solution (1 mg ml^{-1} in 0.9% NaCl) followed by TrypLE Express Enzyme (Thermo Fisher Scientific, 12604013). When cells reached passage 3 to 5, the isolation of osteoblasts was confirmed by measuring of mineralization using Alizarin Red-S staining, and >97% of cultured cells were osteoblasts (data not shown). The supernatant from passage 3 to 5 osteoblasts was collected for EVP isolation.

EVP purification, characterization and labelling

To isolate EVPs from cultured cell lines, the cell culture and preparation of conditioned media were described above. For tissue explant culture, primary tumours (B16F10 or K7M2) and mouse skin were cut into millimetre-sized pieces and cultured overnight in RPMI supplemented with 1× penicillin/streptomycin, and the supernatant was collected and filtered using a 70-μm cell strainer to remove tissue debris. To purify EVPs from DMSO or C75 (MedChemExpress, HY-12364) treated cells, B16F10 or K7M2 cells were cultured in EVP-depleted media for 48 h, and then washed three times with PBS and cultured in EVP-depleted media containing DMSO or C75 (40 μM) for 48 h. Conditioned media was then collected for EVP purification. For EVP isolation from the circulation, 200 μl of mouse plasma was diluted into 800 μl of PBS to a total volume of 1 ml before centrifugation as described below.

EVP purification was performed as previously described[16,17]. In brief, the conditioned media of the cultured cells or tumour explants, or PBS-diluted mouse plasma, was sequentially centrifuged at 500*g* for 10 min, at 3,000*g* for 20 min and then at 12,000*g* for 20 min. EVPs were pelleted by ultracentrifugation of this supernatant at 100,000*g* for 70 min and washed with PBS once. EVPs were then collected by ultracentrifugation at 100,000*g* for 70 min and resuspended in PBS. The protein concentration of EVPs in PBS was measured by BCA Protein Assay Kit (Thermo Fisher Scientific, 23225). EVP size and particle number were analysed using the LM10 nanoparticle characterization system (NanoSight, Malvern Instruments). EVPs were imaged by negative-stain transmission electron microscopy.

For EVP labelling, 10 μg of EVPs, or an equivalent volume of mock PBS, were first gently mixed with 0.4 μl of CellVue dye (NIR815 or Burgundy, LI-COR) diluted in 50 μl of Diluent C and incubated in the dark for 5 min; 25 μl of 35% BSA (Sigma, A7979) was added to the mixture to quench the labelling reaction and incubated for 1 min. The mixture was washed with PBS and EVPs were pelleted by ultracentrifugation at 100,000*g* for 70 min, and then resuspended in PBS for downstream experiments.

Transmission electron microscopy

TEM was performed as previously described[5,16]. For negative staining TEM analysis, 5 μl of EVPs in PBS (0.1 μg μl^{-1}) were placed on a formvar/carbon-coated grid and allowed to settle for 1 min. The sample was blotted and negatively stained with four successive drops of aqueous uranyl acetate (1.5%), blotting between each drop. Following the last drop of stain, the grid was blotted and air-dried. Grids were imaged with a JEOL JSM 1400 (JEOL) transmission electron microscope operating at 100 kV. Images were captured on a Veleta 2k × 2k charge-coupled device camera (Olympus-SIS).

Asymmetric-flow field-flow fractionation

EVP subpopulations (exomeres, <50 nm with an average of 35 nm in diameter; Exo-S, 60–80 nm in diameter; Exo-L, 90–120 nm in diameter) were separated using AF4 as previously described[5,39]. In brief, EVP samples were separated in a short channel (144 mm length, Wyatt Technology) with a 10 kDa molecular weight cutoff (MWCO) Regenerated Cellulose membrane (Millipore) on the accumulation bottom wall and a 490 μm spacer (channel thickness). The fractionation was operated by the Eclipse AF4 system (Wyatt Technology). EVP samples were spun at 12,000*g* for 5 min to remove aggregates before loading onto the AF4 system, and 100 μg of EVPs (1 μg μl^{-1}, and 100 μl in total) was injected using the autosampler (Agilent Technologies). Chemstation software (Agilent Technologies) with an integrated Eclipse module (Wyatt Technology) was used to operate the AF4 flow and Astra 6 (Wyatt Technology) was used for data acquisition and analysis.

Flow cytometry

Flow cytometry analyses were performed as previously described[40]. To identify the liver cells taking up tumour-derived EVPs, mice were intravenously injected with 10 μg of CellVue Burgundy-labelled EVPs in 100 μl of PBS, or an equivalent volume of mock reaction mixture. At 24 h post injection, mice were sacrificed and a small lobe of mouse liver was dissected and digested with dispase/collagenase/DNase (Roche; 1.5 mg ml^{-1} of dispase II (4942078001) and collagenase A (10103586001), 0.1 mg ml^{-1} of DNase I (10104159001)) for 30 min at 37 °C with gentle shaking (40 rpm). Single-cell suspensions were obtained by pipetting and filtering through a 70 μm cell strainer. Cells were washed with flow cytometry buffer (PBS (Ca^{2+}/Mg^{2+}-free) containing 2% BSA and 2 mM

of EDTA) and collected by centrifugation at 300*g* for 5 min. Cell pellets were incubated with ACK Lysing buffer (Gibco, A10492-01) at room temperature for 5 min to remove red blood cells. Cells were resuspended in flow cytometry buffer and one million cells were incubated with TruStain FcX PLUS (anti-mouse CD16/32) antibody (Biolegend, clone S17011E) for 10 min on ice. Subsequently, the cell suspensions were incubated with antibodies (see Supplementary Table 28) for 25 min on ice. For intracellular staining, cell suspensions were treated with 0.01% paraformaldehyde (PFA) for 10 min and 0.5% Tween-20 for 15 min before incubating with antibodies. After antibody labelling, cells were washed with flow cytometry buffer and stained with 0.1 ng ml^{-1} DAPI solution (Thermo Scientific, 62248). Flow cytometry was performed on a Cytek Aurora. Single cells were gated according to forward and side scatter to exclude doublets. Different cell populations were analysed by gating live cells (DAPI-negative) and then measuring the expression of CD45, CD11b, F4/80, CD31, albumin, LYVE1 and desmin. FlowJo Software was used for data analysis. To analyse the abundance of Kupffer cells in the livers of mice treated with liposome (Liposoma BV) or clodronate (Liposoma BV), livers were subjected to flow cytometry analyses of CD45, Cd11b and F4/80-expressing cells following the method described above.

Tissue processing and immunofluorescence staining

Liver tissues were collected and fixed in 4% PFA overnight at 4 °C, immersed in 30% sucrose in PBS overnight at 4 °C, followed by 30% sucrose: OCT (1:1, v/v) incubation for overnight at 4 °C, and then embedded in OCT compound (Sakura, 4583) and frozen on dry ice. OCT-embedded liver tissues were sectioned at 10-µm thickness using LEICA CM3050 S, and slides were stored in −80 °C freezer or used immediately.

For IF staining, slides were dried and cryosections were blocked with universal Fc receptor blocker (Innovex, NB309-15) for 0.5 h, incubated in normal blocking and penetrating buffer (PBS containing 2% BSA and 0.1% Triton X-100), and then incubated with primary antibodies (see Supplementary Table 28) overnight at 4 °C. Slides were then washed with PBS for 5 min, incubated with secondary antibodies (see Supplementary Table 28) for 1.5 h, stained with DAPI (1 µg ml^{-1}), and mounted with ProLong Diamond Antifade Mountant (Thermo Fisher Scientific, P36970). Images were captured using Confocal Microscope (Zeiss LSM 880).

For precision-cut liver slices (PCLS), immunofluorescence staining was performed on free-floating slices using the same protocol as for liver tissue cryosections.

For histological analysis of livers with H&E staining, liver tissues were fixed in 4% PFA overnight at 4 °C and subjected to paraffin embedding. Paraffin-embedded liver tissues were sectioned at 7-µm thickness, and sections were processed for H&E staining and mounted with Vecta-Mount medium (Vector Laboratories, H-5000).

Precision-cut liver slices

Preparation and incubation of the mouse PCLS were modified from the previously described protocols[40–42]. In brief, 6–8 weeks aged C57BL/6 or BALB/c mice (Jackson Laboratories) were anaesthetized using 2% isoflurane/1.5% oxygen inhalation, and livers were dissected in Krebs-Henseleit buffer (KHB, pH 7.4, Sigma, K3753). Fresh liver was cored using an 8-mm biopsy punch (Acuderm). Cores were embedded in microwave-preheated 4% low-melting agarose (Lonza, 50101) in KHB once the agarose cooled to 37 °C. Once solidified, the agarose-embedded liver tissues were superglued to the specimen plate, submersed in the buffer tray containing ice-cold KHB, and cut into slices (250 µm of thickness) using a VT1200s vibratome (Leica) at the speed of 0.08 mm s^{-1} and amplitude of 2 mm. Groups of two PCLS were transferred onto the 0.4 µm pore polycarbonate membrane cell culture insert (Sigma, Z353086) in 6-well plate with 1.5 ml of medium (William's E Medium (Thermo Fisher Scientific, 32551020) containing 2% EVP-free FBS, 1× penicillin/streptomycin, 1× L-glutamine and 2g l^{-1} glucose (Gibco, A24940-01)) per well, and cultured in a humidified 37 °C incubator with 5% CO_2 with agitation (50 rpm).

To visualize the EVP-induced lipid droplet accumulation, the PCLS from naive mice were cultured overnight, and then treated with PBS or 10 µg ml^{-1} of EVPs for 48 h, followed by BODIPY staining as described below.

To measure drug metabolism after EVP administration, the PCLS from naive mice were cultured overnight, followed by treatment with PBS or 10 µg ml^{-1} of B16F10-EVPs in the presence of anti-TNF antibody (20 µg ml^{-1}, BP0058, Clone: XT3.11 from BioXCell) or IgG1 isotype control (20 µg ml^{-1}, BP0290 from BioXCell) for 24 h. Then, the PCLS were cultured in media containing substrates for the core Cyp enzymes in the presence of PBS or 10 µg ml^{-1} of B16F10-EVPs and co-treated with anti-TNF antibody (20 µg ml^{-1}) or IgG1 isotype control (20 µg ml^{-1}) for another 24 h. One millilitre of media was collected to measure drug-metabolizing activity using liquid chromatography–tandem mass spectrometry (LC–MS/MS) as described below, and PCLS were weighed for normalization.

To measure drug metabolism in the livers of PBS-injected control and B16F10 tumour-bearing mice treated with anti-TNF antibody or IgG1 isotype control (described below), the PCLS from PBS-injected control and anti-TNF antibody or IgG1 isotype control treated B16F10 tumour-bearing mice were cultured overnight, and then cultured in the media containing substrates for the core Cyp enzymes for 24 h. Then, 1 ml of media was collected for drug-metabolizing activity assay using LC–MS/MS and PCLS were weighed for normalization. The substrates for Cyp enzymes and their concentrations are shown in Supplementary Table 18.

Lipid droplet staining

For liver tissues, the cryosections were dried and rinsed first with Milli-Q water, followed by PBS. The cryosections were then incubated with autofluorescence quenching reagents (Vector Laboratories, SP-8400-15) for 10 min, and washed thoroughly with PBS for 5 min. Subsequently, the cryosections were stained with 2 µM of BODIPY 493/503 (Thermo Fisher Scientific, D3922) at 37 °C for 15 min and then washed with PBS for 5 min. For primary hepatocytes cultured on chamber slides, the culture media were removed, and hepatocytes were rinsed in PBS three times and stained with 2 µM of BODIPY 493/503 at 37 °C for 15 min, and then washed with PBS for 5 min. For PCLS, the culture media were removed, and PCLS were rinsed in PBS three times and incubated with autofluorescence quenching reagents for 10 min, and washed thoroughly with PBS for 5 min. PCLS were then stained with 2 µM of BODIPY 493/503 at 37 °C for 15 min and washed with PBS for 5 min, followed by 4% PFA fixation for 30 min and PBS washing for 5 min. All samples, including cryosections, hepatocytes and PCLS, were then counter-stained with DAPI (1 µg ml^{-1}) for 5 min, washed with PBS for 5 min and mounted with ProLong Diamond Antifade Mountant. Lipid droplets were imaged by Confocal Microscope (Zeiss LSM 880) and BODIPY fluorescence intensities were quantified using ImageJ.

Cytokine array

For tumour-bearing mouse models, Kupffer cells isolated from control and tumour-bearing mice were first cultured for 2 h. Dead (unattached) cells were removed and viable cells were lysed in RIPA buffer (Sigma) for cytokine array analysis. For EVP education model, Kupffer cells isolated from naive mice were cultured overnight, followed by treatment with PBS or 10 µg ml^{-1} of EVPs for 3 d. The conditioned media were then collected for cytokine array analysis. Cytokine array analysis was carried out using the Proteome Profiler Mouse Cytokine Array Kit, Panel A (R&D, ARY006) according to manufacturer's instructions. Multiple exposure times (1–30 min) of the membranes to X-ray film were applied, and the pixel densities on the developed X-ray film was quantified using ImageJ.

Enzyme-linked immunosorbent assay

To measure Kupffer cell-secreted IL-6 after treatment with lipopolysaccharide (LPS) in vitro, Kupffer cells isolated from naive mice were cultured overnight, followed by treatment with LPS (1 μg ml^{-1}) for 0 h, 1 h, 2 h, 4 h, and 16 h, respectively. The culture media were then collected for IL-6 measurement using the mouse IL-6 ELISA kit (Thermo Fisher, KMC0061) according to the manufacturer's instructions.

To measure Kupffer cell-secreted TNF after treatment with EVPs in vitro, Kupffer cells isolated from naive mice were cultured overnight, followed by treatment with 10 μg ml^{-1} of EVPs or an equivalent volume of PBS for 3 d. The conditioned media was then collected for TNF measurement using the mouse TNF ELISA kit (R&D, MHSTA50) according to the manufacturer's instructions.

To determine whether TNF is secreted by cancer cells, 1 ml of EVP-depleted conditioned media obtained after EVP isolation (that is, after first spin of 100,000*g* for 70 min as described above) from cultured B16F10 and K7M2 cells was subjected to TNF measurement using the mouse TNF ELISA kit according to the manufacturer's instructions.

To measure TNF in the circulation, the retroorbital blood samples were collected from tumour-bearing mice and EVP-educated mice, and their respective controls, using K2EDTA plasma collection tubes (BD, 365974). Plasma TNF was then measured using the mouse TNF ELISA kit according to the manufacturer's instructions.

Mouse studies

Treatment of mice was performed in accordance with institutional, IACUC and AAALAS guidelines. All the mouse studies were performed according to Weill Cornell Medicine animal protocols 0709-666A and 2016-0057, except for studies using the genetic melanoma mouse model, which were performed at The Ohio State University according to animal protocol 2012A00000134. In addition, PDX models of primary osteosarcoma were generated in compliance with MSKCC animal protocol 14-02-002. All animal experiments were conducted in compliance with relevant ethical regulations regarding animal research. Animals were monitored for stress, illness or abnormal tissue growth, and euthanized if health deteriorated. Mice that died before the experimental endpoint were excluded from the analysis. Female C57BL/6, BALB/c, Nude (outbred) and NOD/SCID/IL2Rγ^{null} (NSG) mice aged 6–8 weeks were obtained from The Jackson Laboratory. BALB/c mice aged 6–8 weeks were used for the implantation of mouse breast cancer cell lines (67NR and 4T1) and mouse osteosarcoma cell line (K7M2), as well as treatment with osteoblast-EVPs, K7M2-CL-EVPs, K7M2-TE-EVPs, bone-TE-EVPs; C57BL/6 mice aged 6–8 weeks were used for the implantation of mouse melanoma cell lines (B16F1 and B16F10), and treatment with B16F10-CL-EVPs, B16F10-TE-EVPs and skin-TE-EVPs. Nude (outbred) mice aged 6–8 weeks were used for implantation of human melanoma cell line SK-MEL-192. NSG mice aged 6–8 weeks were used for PDX models. Mice were housed in the animal facility under conventional conditions with a light (12 h dark/light circle)-, humidity (30%–70%)- and temperature (21–23 °C)-controlled environment. No statistical method was used to pre-determine the sample size and no method of randomization was used to allocate animals to experimental groups.

For tumour cell implantation, 1×10^5 of 67NR or 4T1 cells in 50 μl of PBS were injected into the mammary fat pad of BALB/c mice; 5×10^5 of B16F1 or B16F10 cells in 100 μl of PBS were subcutaneously injected into C57BL/6 mice; 1×10^6 of K7M2 cells in 10 μl of PBS were injected into the tibias of BALB/c mice; 5×10^5 of SK-MEL-192 cells in 100 μl of PBS were subcutaneously injected into nude (outbred) mice. Tumour growth was monitored by measuring the tumour size with a digital calliper using the formula: tumour volume (mm^3) = width (in mm)^2 × length (in mm)/2. Mice were euthanized 3 weeks (for B16F1-, B16F10-, 67NR-, 4T1- and SK-MEL-192-tumour-bearing models), or 4 weeks (for K7M2 tumour-bearing model) after tumour cell implantation for tissue collection. The maximal tumour size in mice that was permitted by Weill Cornell Medicine IACUC is 2 cm in any one dimension, and this limit was not exceeded in any of the experiments. Mice injected with an equivalent volume of PBS following the same procedure were used as the control group.

For the genetic melanoma mouse model, C57BL/6 TN mice[43], carrying a Cre-inducible *Nras*^{Q61R} oncogene, were treated topically with 20 mM of 4-hydroxytamoxifen (4-OHT) on postnatal days 1 and 2 to activate melanocyte-specific Cre recombination from the Tyr-CRE-ER(T2) transgene[44]. On postnatal day 3, pups received 1.5 SED (standard erythemal dose) of solar radiation as described[45]. Animals were monitored for spontaneous tumour formation and euthanized upon reaching exclusion criteria (tumour length ≥1.6cm or ulceration ≥2 mm) and this limit was not exceeded in any of the experiments. Non-tumour-bearing control mice carried the *Nras*^{Q61R}, *p16*$^{fl/f}$ and Tyr-CRE-ER (T2) alleles but were not treated to induce Cre activity or tumour formation. To increase melanoma susceptibility, eight of the tumour-bearing mice were functionally null *Mc1r*, a gene important for eumelanin production.

To generate PDX models of human primary osteosarcoma, freshly surgically excised tumour specimens obtained from patients at MSKCC were transplanted into female NOD/SCID/IL2Rγ^{null} (NSG) mice. All patients provided informed consent for tissue donation according to the IRB approved protocol (MSKCC IRB 06-107 and 17-067), and de-identified patient information was described in Supplementary Table 5a. In brief, freshly obtained tumour tissue specimens were rinsed with PBS (EDTA-free), minced into 2–4 mm-sized pieces, and then transplanted subcutaneously into mice. Typically, PDX tumour growth became evident during the first 1–2 weeks after engraftment and mice were euthanized for tissue collection within a total of 4–8 weeks after engraftment. Primary tumour growth and metastases were followed carefully by small animal magnetic resonance imaging (MRI). Mouse MRI was carried out on a 400 MHz Bruker 9.4T Biospec scanner equipped with a 530 mT/m ID 114 mm gradient (Bruker Biospin MRI). Radio frequency excitation and acquisition was achieved by a Bruker 40 mm quadrature birdcage resonator. The mice were immobilized with 2% isoflurane (Baxter Healthcare) gas in oxygen. Animal respiration was monitored with a small animal physiological monitoring system (SA Instruments). Scout images along three orthogonal orientations were first acquired for animal positioning. Mouse thoracic imaging was performed using a respiratory gated gradient-echo sequence with the time of repetition 170 ms, time of echo 1.6 ms, 10 average, a slice thickness of 0.5 mm and an in-plane resolution of 198 μm × 146 μm. For mouse liver imaging, axial T2-weighted images using fast spin-echo rapid acquisition with relaxation enhancement (RARE) sequence was acquired with time of repetition 3.1 s, time of echo 11 ms, RARE factor of 8, slice thickness of 0.7 mm, 3 averages and in-plane resolution of 113 μm × 168 μm. The maximal tumour size in mice that was permitted by MSKCC IACUC is 2 cm in any one dimension, and this limit was not exceeded in any of the experiments.

For the mouse model of spontaneous PDAC, tamoxifen-inducible KPC mice (*Kras*^{tm4Tyj} *Trp53*^{tm1Brn} Tg[Pdx1-cre/Esr1*]#Dam/J, The Jackson Laboratory, JAX 032429) were used, as previously described[15]. In brief, *Trp53* excision was induced in pups via lactation upon administration of tamoxifen (6 mg per mouse) via oral gavage to the dam. Mice carrying the *Kras*^{G12D} mutation in one allele (*Kras*$^{WT/G12D}$) developed pancreatic intraepithelial neoplasia (PanIN) lesions at 8–10 weeks of age, which progressed into local PDAC at 10–14 weeks and invasive PDAC at 15–18 weeks, associated with distant metastasis to several sites including lymph nodes, liver, lungs, diaphragm and spleen. *Kras*$^{WT/WT}$ mice from the same litter were used as healthy controls. For PDAC tumour-bearing mice, the tumour volume cannot be appreciated as tumours grow internally, but the mice will be euthanized in cases of discomfort, including loss of appetite, inactivity, difficulty breathing, hunched posture and withdrawal from other mice. The exclusion criteria were not exceeded in any of the experiments.

For in vivo EVP biodistribution assessment, CellVue NIR815-labelled EVPs (10 μg) resuspended in 100 μl of PBS, or an equivalent volume of mock reaction mixture, were intravenously injected into naive mice. At 24 h post injection, livers were collected and imaged using Odyssey CLx (LI-COR). Data quantification was performed using Image Studio (version 5.2).

For in vivo EVP education, 10 μg of EVPs, exomeres, Exo-S, or Exo-L, resuspended in 100 μl of PBS, were intravenously injected into mice every other day for 4 weeks, mimicking continuous and systemic EVP release from primary tumours[7,10]. Mice injected with 10 μg of control cell-derived EVPs or an equivalent volume of PBS following the same procedure served as the control group. One day post the last injection, the EVP-educated mice and control mice were euthanized, and tissues were collected for downstream analysis.

For in vivo conditioned medium education, EVP-depleted conditioned medium obtained after EVP isolation (that is, the media supernatant after first spin of 100,000*g* for 70 min as described above) from cultured cancer cells was concentrated using Amicon Ultra-15 centrifugal filters with 10 kDa cutoff (Millipore, UFC901024) at 4,000*g* at 4 °C. In general, 5 ml of conditioned medium from cell culture yields approximately 10 μg of EVPs. The same volume of EVP-depleted conditioned medium was further concentrated to a volume of 200 μl and used for each injection. Blank media (DMEM supplemented with 10% EVP-depleted FBS and 1× penicillin/streptomycin) was also concentrated to obtain control conditioned medium. Two-hundred microlitres of concentrated EVP-depleted conditioned medium, equivalent to 10 μg of EVPs, were intraperitoneally injected into mice every other day for 4 weeks. Mice injected with 200 μl of control conditioned medium according to the same procedure served as the control group. One day after the last injection, conditioned medium-educated and control mice were euthanized, and tissues were collected for downstream analysis.

For in vivo education with both EVPs and conditioned medium, 10 μg of EVPs in 100 μl of PBS and 200 μl of concentrated conditioned medium were simultaneously injected into mice via intravenous injection and intraperitoneal injection, respectively, every other day for 4 weeks. One day post the last injection, the educated mice were euthanized, and tissues were collected for downstream analysis.

For Kupffer cell depletion in naive mice, liposome or clodronate was intravenously injected into mice at a dosage of 100 μl of suspension per 10 g of mouse weight. The concentration of clodronate in the suspension is 5 mg ml^{-1}. At 24 h post injection, mice were euthanized and livers were sectioned into PCLS using a VT 1200s vibratome. PCLS were then subjected to immunofluorescence staining to confirm the efficiency of Kupffer cell depletion, or cultured for EVP treatment and subsequent BODIPY staining as described above.

For Kupffer cell depletion in tumour-bearing mice, liposome or clodronate (100 μl of suspension per 10 g of mouse weight) was intravenously injected into mice bearing B16F10 tumours on day 12, day 15, and day 19; or into mice bearing K7M2 tumours on day 15, day 18, day 22 and day 25 post tumour cell implantation (see Extended Data Fig. 8a). Mice were euthanized at the endpoint, and liver tissues were collected for flow cytometry, immunofluorescence and BODIPY staining.

For in vivo neutralization assays, InVivoPlus anti-TNF (BP0058, Clone: XT3.11) or InVivoPlus IgG1 Isotype control (BP0290) from BioXCell were intraperitoneally injected into the mice at a dosage of 200 μg per mouse every other day starting on day 12 post injection of B16F10 tumour cells; or on day 15 post injection of K7M2 tumour cells; or on day 15 post education of B16F10-CL-EVPs or K7M2-CL-EVPs (see Extended Data Fig. 9l). One day after the last injection, mice were euthanized and tissues were collected for downstream analysis.

Chemotoxicity analysis were performed on B16F10-CL-EVP and K7M2-CL-EVP education models. For the B16F10-CL-EVP education model, mice were intravenously injected with PBS or 10 μg of B16F10-CL-EVPs every other day for 4 weeks, and then intraperitoneally injected with dacarbazine (60 mg kg^{-1}) or 0.9% NaCl together with intravenous injection of PBS or 10 μg of B16F10-CL-EVPs every other day, for a total of 4 injections. One day after the last injection, retroorbital blood was collected for complete blood count by the Laboratory of Comparative Pathology at MSKCC. For the K7M2-CL-EVP education model, mice were intravenously injected with PBS, 10 μg of osteoblast-EVPs or K7M2-CL-EVPs every other day for 4 weeks, and then intraperitoneally injected with doxorubicin (1 mg kg^{-1}) or DMSO every 24 h together with intravenous injection of PBS, 10 μg of osteoblast- or K7M2-CL-EVPs every other day for 25 days. The cumulative dose of doxorubicin was 25 mg kg^{-1}. One day after the last injection, mice were subjected to echocardiography. Dacarbazine (MedChemExpress, HY-B0078) was dissolved in 0.2-μm-filter sterilized 0.9% NaCl solution with sonication to prepare the dacarbazine suspension. Doxorubicin hydrochloride (MedChemExpress, HY-15142) was dissolved in DMSO to prepare the doxorubicin hydrochloride solution.

Echocardiography

Transthoracic echocardiography was performed using a VisualSonics Vevo 3100 system equipped with MX400 transducer (VisualSonics). Measurements were performed on anaesthetized mice under body-temperature-controlled conditions. The echocardiographer was blinded to treatment conditions. Anaesthesia was induced by 3% isoflurane and confirmed by lack of response to firm pressure on one of the hind paws.

During echocardiogram acquisition, isoflurane was reduced to 1.0–1.5% and adjusted to maintain a heart rate in the range of 400–500 beats per minute. Left ventricular ejection fraction, fractional shortening, and left ventricular end-diastolic diameter were obtained from parasternal long-axis M-mode scans at the basal-to-mid ventricular level. Following echocardiography, all mice recovered from anaesthesia without difficulty. All parameters were measured on three separate heartbeats, and means were presented.

Percent fractional shortening was calculated by the formula (LVIDd − LVIDs)/LVIDd × 100%. Left ventricular ejection fraction (LVEF) was calculated automatically with VisualSonics Vevo LAB image analysis software from calculated LV volumes (LVOL) using the formula LVEF = (LVOLd − LVOLs)/LVOLd, where LVOLd or LVOLs were calculated by the cubed sphere formula $LVOL = (7/(2.4 + LVID) \times LVID^3)$ at end diastole or end systole, respectively. LVID, left ventricular internal diameter; LVIDd, left ventricular internal diameter at end diastole; LVIDs, left ventricular internal diameter at end systole; LVOLd, left ventricular volume at end diastole; LVOLs, left ventricular volume at end systole.

Human studies

Fresh human liver tissues were obtained intraoperatively at MSKCC (IRB 15-015) from patients undergoing pancreatectomy for either localized resectable pancreatic cancer or non-cancerous pancreatic or peri-pancreatic lesions (details of included pathologies are shown in Supplementary Table 5b). None of the patients had any evidence of distant metastasis at the time of surgery. Patients with pancreatic cancer were followed for at least 21 months after surgery and site(s) of initial recurrence was identified. In addition, fresh, grossly normal liver tissues were obtained from patients undergoing hepatectomy for hepatic adenomas at MSKCC (IRB 06-107). Intraoperative liver biopsies were collected from patients with germline *CDH1* mutations undergoing risk-reducing gastrectomy at the NIH (IRB 13-C-0076). Although these patients had very early-stage incidental gastric cancer in the stomach specimens, none had evidence of metastasis on imaging or by pathologic examination of sampled tissues (lymph nodes, skin, spleen, liver and jejunum). Finally, unaffected liver specimens from decedents who have previously been diagnosed with PDAC were obtained from the University of Nebraska Medical Center (UNMC) Tissue Bank through the Rapid Autopsy Program (RAP) in compliance with IRB 091-01, and de-identified patient information was described in Supplementary Table 5b. To ensure specimen quality, organs were

harvested within 3 h post-mortem. All individuals provided informed consent for tissue donation according to protocols approved by the Institutional Review Boards of MSKCC, NIH and UNMC. All patient liver tissue-associated experiments were performed according to the protocol approved by the Institutional Review Boards of Weill Cornell Medicine (IRB 0604008488). The study is compliant with all relevant ethical regulations regarding research involving human participants.

Gas chromatography–mass spectrometry metabolomics and data analysis

Approximately 150 mg of liver tissues, or 150–500 µg of EVPs, were homogenized in 1 ml or 200 µl of methanol:chloroform (1:2, v/v) using Bead Rupture 24 (OMNI), respectively. The homogenized liver tissues or EVPs were then subjected to metabolite-profiling mass spectrometry at the Metabolomics Laboratory of the Roy J. Carver Biotechnology Center, University of Illinois at Urbana-Champaign. In brief, samples were dried in a vacuum and derivatized with 50 µl of methoxyamine hydrochloride (Sigma) (40 mg ml^{-1} in pyridine) at 50 °C for 1.5 h, then with 50 µl of *N*-methyl-*N*-trimethylsilyl-trifluoroacetamide (MSTFA) + 1% trimethylchlorosilane (TMCS) (Thermo) at 70 °C for 2 h, followed by incubation at room temperature for 2 h. 30 µl of 1 mg ml^{-1} hentriacontanoic acid was added to each sample prior to derivatization to serve as an internal standard. Metabolite profiles were acquired using a gas chromatography–mass spectrometry system (Agilent) consisting of an Agilent 7890 gas chromatograph, an Agilent 5975 MSD and 7683B autosampler as previously described[46]. Gas chromatography was carried out on a ZB-5MS (60 m × 0.32 mm internal diameter and 0.25 µm film thickness) capillary column (Phenomenex). The inlet and mass spectrometry interface temperatures were 250 °C, and the ion source temperature was adjusted to 230 °C. An aliquot of 2 µl was injected with the split ratio of 10:1. The helium carrier gas was kept at a constant flow rate of 2.4 ml min^{-1}. The temperature program was: isothermal heating at 70 °C for 5 min, followed by an oven temperature increase of 5 °C min^{-1} to 310 °C after which a final 10 min incubation at 310 °C. The mass spectrometer was operated in positive electron impact mode (EI) at 69.9 eV ionization energy at *m*/*z* 30–800 scan range. The spectra of all chromatogram peaks were evaluated using the AMDIS 2.71 (NIST) using a custom-built mass spectrometry database (460 unique metabolites). Throughout the sample preparation, data acquisition and data preprocessing, samples were compared to the QCs to evaluate potential variation that may have arisen in the dataset throughout the analytical study. All known artificial peaks were identified and removed prior to data mining. To allow comparison between samples, all data were normalized to the internal standard in each chromatogram and sample volume. The instrument variability was within the standard acceptance limit (5%).

Data derived from the metabolomic mass spectrometry were analysed using MetaboAnalyst 4.0[47]. In brief, following imputation of missing values—that is, removing features with >25% missing values and estimating the remaining missing values using a *k*-nearest neighbors algorithm (feature-wise), data were normalized by auto scaling (mean-centred and divided by standard deviation of each variable). PLS-DA was performed to visualize the discrimination of groups. Significantly changed metabolites ($P < 0.05$ for tumour-bearing models and $P < 0.1$ for EVP-education models) identified by *t*-test were utilized for generating heat map and subsequent metabolite set enrichment analysis (MSEA) based on the Small Molecule Pathway Database (SMPDB).

Lipidomic mass spectrometry and data analysis

Approximately 150 mg of liver tissues were homogenized in 1 ml of methanol: chloroform (1:2, v/v) using Bead Rupture 24, and then subjected to lipidomic mass spectrometry as previously described[5]. In brief, samples were first sonicated with a Model Q700 QSonica sonicator equipped with an Oasis 180 Chiller (4 °C; amplitude, 95; process, 5 min; pulse on 30 s; plus off 55 s), centrifuged at 14,800 rpm for 10 min at 4 °C, then 50 µl of the extract supernatant was spiked with 2 µl, 50 µg ml^{-1}, of internal standard mixture (ceramide 18:1/12:0; phosphatidylcholine 12:0/12:0; phosphatidylethanolamine 14:0/14:0; phosphatidylglycerol 14:0/14:0; phosphatidylserine 14:0/14:0). Subsequently, the samples were analysed using the Thermo Q-Exactive mass spectrometry system at the Metabolomics Laboratory of the Roy J. Carver Biotechnology Center, University of Illinois at Urbana-Champaign. Xcalibur 3.0.63 was used for data acquisition and analysis. A Dionex Ultimate 3000 series HPLC system (Thermo) was used, and liquid chromatography separation was performed on a Thermo Accucore C30 column (2.1 × 150 mm, 2.6 µm) with mobile phase A (60% acetonitrile: 40% H_2O with 10 mM ammonium formate and 0.1% formic acid) and mobile phase B (90% isopropanol: 10% acetonitrile with 10 mM ammonium formate and 0.1% formic acid) and a flow rate of 0.3 ml min^{-1}. The linear gradient was as follows: 0–2 min, 80% A; 4 min, 55% A; 12 min, 35% A; 18 min, 15% A; 20–28 min, 0% A; 28.1–36 min, 80% A. The autosampler was set to 15 °C and the column was kept at 45 °C. The injection volume was 10 µl. Mass spectra were acquired under both positive (sheath gas flow rate, 50; auxiliary gas flow rate, 13; sweep gas flow rate, 3; spray voltage, 3.5 kV; capillary temperature, 263 °C; auxiliary gas heater temperature, 425 °C) and negative (sheath gas flow rate, 50; auxiliary gas flow rate, 13; sweep gas flow rate, 3; spray voltage, −2.5 kV; capillary temperature, 263 °C; auxiliary gas heater temperature, 425 °C) electrospray ionization. The full scan mass spectrum resolution was set to 70,000 with a scan range of *m*/*z* 230–1,600 and the automatic gain control (AGC) target was 10^6 with a maximum injection time of 200 ms. For MS/MS scans, the mass spectrum resolution was set to 17,500 and the AGC target was 5×10^4 with a maximum injection time of 50 ms. The loop count was ten. The isolation window was 1.0 *m*/*z* with normalized collision energy of 25 and 30 eV. For data analysis, LipidSearch (v.4.1.30, Thermo) was used for lipid identification. The lipid signal responses were normalized to the corresponding internal standard signal response. For those lipid classes without corresponding internal standard, positive lipid ion signals were normalized with the signal of internal standard ceramide 18:1/12:0 and negative ion signals were normalized with the signal of internal standard phosphatidylglycerol 14:0/14:0.

The amount of lipid classes within a sample was calculated by adding that of each of the individual molecular species quantified within a specific lipid class as previously described[5]. For lipid species, following imputation of missing values—that is, removing features with >25% missing values and estimating the remaining missing values using a *k*-nearest neighbors algorithm (feature-wise), data were normalized by auto scaling (mean-centred and divided by standard deviation of each variable). PLS-DA was performed to visualize the discrimination of groups using MetaboAnalyst 4.0. Statistical significance was determined by *t*-test and *P*-value < 0.05 was considered statistically significant. Volcano plots were generated using Prism 9 software (GraphPad).

Free fatty acid analysis

Approximately 300 µg of EVPs were dissolved in 600 µl of methanol: chloroform (1:2, v/v) for free fatty acids (FFA) analysis at the Metabolomics Laboratory of the Roy J. Carver Biotechnology Center, University of Illinois at Urbana-Champaign. Raw samples were converted to fatty acid methyl esters using (trimethylsilyl)diazomethane hexanes with a 1 h incubation at room temperature. Derivatized samples were subjected to gas chromatography–mass spectrometry analysis using the Agilent 7890B GC with 5977A/Extractor XL mass spectrometry system. The gas chromatography separation was performed on a ZB-5MS (60 m × 0.32 mm internal diameter and 0.25 µm film thickness) capillary column (Phenomenex). The inlet and MSD interface temperatures were both at 250 °C, with the ion source temperature adjusted to 230 °C. The helium carrier gas was kept at a constant flow rate of 2 ml min^{-1}. The temperature program was as follows: initial 5-min isothermal heating at 150 °C, followed by an oven temperature increase of 5 °C min^{-1}

to 310 °C (3 min isothermal). Mass spectra were recorded in the *m/z* 50–800 scanning range. Data analysis was performed using Prism 9 software (GraphPad), and statistical significance (*P*-value < 0.05) was determined by multiple unpaired *t*-test.

FFA content in the EVPs isolated from DMSO or C75-treated cells was determined using Free Fatty Acid Quantitation Kit (Sigma, MAK044). In brief, 50 µg of EVPs were homogenized in 250 µl of a 1% (w/v) Triton X-100 in chloroform solution. Samples were spun at 13,000*g* for 10 min to remove insoluble material, and the organic phase (lower phase) was collected and air dried at 50 °C to remove chloroform. Samples were vacuum-dried for 30 min to remove trace chloroform and dissolved in 200 µl of fatty acid assay buffer by vortexing extensively for 5 min. Fifty microliters of the solution were subjected to FFA quantification following the manufacturer's instructions.

Drug-metabolizing activity analysis

Drug-metabolizing activity analysis was performed at the Metabolomics Laboratory of the Roy J. Carver Biotechnology Center, University of Illinois at Urbana-Champaign. The collected media were analysed using the Triple 6500+ LC–MS/MS system (Sciex). Software Analyst 1.7.1 was used for data acquisition and analysis. The 1260 Infinity II HPLC system (Agilent Technologies) includes a degasser, an autosampler, and a binary pump. The liquid chromatography separation was performed on an Agilent SB-Aq (4.6 × 50 mm, 5 µm) with mobile phase A (0.1% formic acid in water) and mobile phase B (0.1% formic acid in acetonitrile). The flow rate was 0.3 ml min^{-1}. The linear gradient was as follows: 0-1 min, 95% A; 10–14 min, 2% A; 14.1–20 min, 95% A. The autosampler was set at 10 °C and the injection volume was 10 µl. Mass spectra were acquired positive electrospray ionization with an ion spray voltage of 5,500 V. The source temperature was 400 °C. The curtain gas, ion source gas 1, and ion source gas 2 were 35, 50 and 65 psi, respectively. Multiple reaction monitoring was used for quantification: acetaminophen *m/z* 152.0 → *m/z* 43.0; 4-hydroxytolbutamide *m/z* 287.0 → *m/z* 188.0; dextrorphan *m/z* 258.1 → *m/z* 115.0; 1-hydroxymidazolam *m/z* 342.2 → *m/z* 168.1; hydroxybupropion *m/z* 256.1 → *m/z* 167.0.

LC–MS/MS analysis of 12-*O*-tetradecanoylphorbol-13-acetate in EVP samples

LC–MS/MS analysis of TPA in EVP samples was performed at the Duke Proteomics and Metabolomics Core Facility. Approximately 100 µg of EVPs resuspended in PBS were vortexed for 2 min, and subjected to ultrasonication for 20 min. The ultrasonicated EVPs were then centrifuged at 10,000 rpm for 10 min at 4 °C, and the supernatants were collected for LC–MS/MS injection. Samples were analysed using the 6500+ QTRAP LC–MS/MS system (Sciex). Software Analyst 1.7.1 was used for data acquisition and analysis. The Sciex ExionLC UPLC system includes a degasser, an AD autosampler, an AD column oven, a controller, and an AD pump. The liquid chromatography separation was performed on an Agilent Zorbax Eclipse plus C18 (2.1 × 50 mm, 1.8 µm) with mobile phase A (0.2% formic acid in water) and mobile phase B (0.2% formic acid in acetonitrile). The flow rate was 0.4 ml min^{-1}. The linear gradient was as follows: 0–1 min, 60% A; 5–7 min, 0% A; 7.1–8.5 min, 60% A. The autosampler was set at 10 °C and the column was kept at 40 °C. The injection volume was 15 µl. Mass spectra were acquired under negative electrospray ionization with the ion spray voltage of −4,500 V. The source temperature was 500 °C. The curtain gas, ion source gas 1, and ion source gas 2 were 32, 60 and 60 psi, respectively. Multiple reaction monitoring was used for quantification: *m/z* 615.2 → *m/z* 227.1.

RNA-seq and computational analysis

For RNA-seq of mouse livers, total RNA was quantified using Nanodrop 2000c (Thermo Scientific), and RNA quality was assessed by Agilent 2100 Bioanalyzer (Agilent Technologies). TruSeq stranded mRNA library preparation and RNA-seq using Illumina HiSeq 4000 or Illumina NovaSeq 6000 were performed in the Genomics Resources Core Facility at Weill Cornell Medicine. The raw sequencing reads in BCL format were processed through bcl2fastq 2.19 (Illumina) for FASTQ conversion and demultiplexing. RNA reads were aligned and mapped to the mm9 mouse reference genome by TopHat2 (version 2.0.11) (http://ccb.jhu.edu/software/tophat/index.shtml), and transcriptome reconstruction was performed by Cufflinks (version 2.1.1) (http://cole-trapnell-lab.github.io/cufflinks/). The abundance of transcripts was measured with Cufflinks in fragments per kilobase of exon model per million mapped reads (FPKM). Gene expression profiles were constructed for differential expression, clustering, and principal component analyses using the DESeq2 package (https://bioconductor.org/packages/release/bioc/html/DESeq2.html). For differential expression analysis, pairwise comparisons between two or more groups were performed using parametric tests where read counts follow a negative binomial distribution with a gene-specific dispersion parameter. Corrected *P*-values were calculated based on the Benjamini–Hochberg method to adjust for multiple testing.

RNA-seq of human liver biopsies was performed at Integrated Genomics Operation (IGO), MSKCC. In brief, total RNA from 5 mg of frozen liver tissue was extracted using the RNeasy Mini Kit (QIAGEN, 74104) according to the manufacturer's instructions. After RiboGreen quantification and QC analysis of 1 µg of RNA using Total RNA Nano chip on Agilent Bioanalyzer 2100, samples were subjected to ribosomal RNA depletion and library preparation using the TruSeq Stranded Total RNA LT Kit (Illumina, RS-122-1202) according to the manufacturer's instructions with 6–8 cycles of PCR. Samples were barcoded and run on a HiSeq 2500 in Rapid or High Output Mode or a HiSeq 4000 in a 50 bp–50 bp paired end run, using the HiSeq Rapid SBS Kit v2, TruSeq SBS Kit v4, or HiSeq 3000/4000 SBS Kit, respectively (Illumina). Alignment metrics were calculated by GATK's CollectRnaSeqMetrics and AlignmentSummaryMetrics to obtain raw STAR alignments and htseq count files. On average, 88 million paired reads were generated per sample and 32% of the data mapped to the human GENECODE 18 transcriptome. Standard pipeline analyses were performed by IGO and subsequent comparisons were performed using DESeq2, R software.

For B16F10 and K7M2 tumour-bearing models, a pre-ranked gene list was created with shared DEGs ($q < 0.05$) in livers from both B16F10 and K7M2 models, where $\log_2$FC values were used for ranking. Gene set enrichment analysis was then conducted for those pre-ranked gene lists. For all the other models, except RNA-seq data from human liver biopsies, genes were ranked based on the sign of $\log_2\text{FC} \times (-\log_{10}(P\text{-value}))$ and subjected to gene set enrichment analysis. For RNA-seq data from human liver biopsies, the normalized gene expression values were utilized for gene set enrichment analysis using weighted enrichment statistic and Signal2Noise method (metric for ranking genes). Gene set enrichment analysis was performed using standalone GSEA software (v4.1.0 & v4.3.2) (downloaded from http://www.gsea-msigdb.org/gsea/downloads.jsp) against the Hallmark or KEGG gene sets[48,49].

Statistical analysis

Statistical significance was determined by two-tailed, unpaired Student's *t*-test, one-way ANOVA with post hoc Tukey's test, two-way ANOVA followed with Bonferroni's multiple comparisons test, two-way ANOVA followed with Fisher's least significant difference test, or multiple unpaired *t*-test using Prism 9 software (GraphPad). The *P*-value and FDR *q*-value were determined by Kolmogorov–Smirnov test for GSEA[48]. *P*-value < 0.05 was considered statistically significant. All values are mean ± s.e.m. The number of independent biological replicates for each experiment and the sample size of each experimental group or condition are provided in the figure legends. ImageJ (version 1.53i) was used for image processing and analysis.

Reporting summary

Further information on research design is available in the Nature Portfolio Reporting Summary linked to this article.

Data availability

RNA-seq raw data and associated processed data files that support the findings of this study have been deposited in the Gene Expression Omnibus under accession codes GSE199863 and GSE220446. Metabolomics data derived from livers of PBS-injected control and B16F10 tumour-bearing mice (Supplementary Table 1) have been deposited at Figshare (https://doi.org/10.6084/m9.figshare.22233187). Metabolomics data derived from livers of PBS-injected control and K7M2 tumour-bearing mice (Supplementary Table 2) have been deposited at Figshare (https://doi.org/10.6084/m9.figshare.22233253). Lipidomics data derived from livers of PBS-injected control and B16F10 tumour-bearing mice (Supplementary Table 3) have been deposited at Figshare (https://doi.org/10.6084/m9.figshare.22233265). Lipidomics data derived from livers of PBS-injected control and K7M2 tumour-bearing mice (Supplementary Table 4) have been deposited at Figshare (https://doi.org/10.6084/m9.figshare.22233274). Metabolomics data derived from livers of PBS- and B16F10-TE-EVP-educated mice (Supplementary Table 8) have been deposited at Figshare (https://doi.org/10.6084/m9.figshare.22233289). Metabolomics data derived from livers of PBS- and K7M2-TE-EVP-educated mice (Supplementary Table 9) have been deposited at Figshare (https://doi.org/10.6084/m9.figshare.22233298). Lipidomics data derived from livers of PBS- and B16F10-TE-EVP-educated mice (Supplementary Table 10) have been deposited at Figshare (https://doi.org/10.6084/m9.figshare.22233307). Lipidomics data derived from livers of PBS- and K7M2-TE-EVP-educated mice (Supplementary Table 11) have been deposited at Figshare (https://doi.org/10.6084/m9.figshare.22233316). Metabolomics data derived from skin-TE-EVPs and B16F10-TE-EVPs (Supplementary Table 14) have been deposited at Figshare (https://doi.org/10.6084/m9.figshare.22233352). Metabolomics data derived from livers of PBS- and B16F10-CL-EVP-educated mice (Supplementary Table 29) have been deposited at Figshare (https://doi.org/10.6084/m9.figshare.22233379). Lipidomics data derived from livers of PBS- and B16F10-CL-EVP-educated mice (Supplementary Table 30) have been deposited at Figshare (https://doi.org/10.6084/m9.figshare.22233403). Metabolomics data derived from livers of PBS- and K7M2-CL-EVP-educated mice (Supplementary Table 31) have been deposited at Figshare (https://doi.org/10.6084/m9.figshare.22233424). Lipidomics data derived from livers of PBS- and K7M2-CL-EVP-educated mice (Supplementary Table 32) have been deposited at Figshare (https://doi.org/10.6084/m9.figshare.22233445). Source data are provided with this paper.

37. Livak, K. J. & Schmittgen, T. D. Analysis of relative gene expression data using real-time quantitative PCR and the $2^{-\Delta\Delta CT}$ method. *Methods* **25**, 402–408 (2001).
38. Chevalier, C. et al. Primary mouse osteoblast and osteoclast culturing and analysis. *STAR Protoc.* **2**, 100452 (2021).
39. Zhang, H. & Lyden, D. Asymmetric-flow field-flow fractionation technology for exomere and small extracellular vesicle separation and characterization. *Nat. Protoc.* **14**, 1027–1053 (2019).
40. Rodrigues, G. et al. Tumour exosomal CEMIP protein promotes cancer cell colonization in brain metastasis. *Nat. Cell Biol.* **21**, 1403–1412 (2019).
41. de Graaf, I. A. et al. Preparation and incubation of precision-cut liver and intestinal slices for application in drug metabolism and toxicity studies. *Nat. Protoc.* **5**, 1540–1551 (2010).
42. Paish, H. L. et al. A bioreactor technology for modeling fibrosis in human and rodent precision-cut liver slices. *Hepatology* **70**, 1377–1391 (2019).
43. Hennessey, R. C. et al. Ultraviolet radiation accelerates NRas-mutant melanomagenesis: A cooperative effect blocked by sunscreen. *Pigment Cell Melanoma Res.* **30**, 477–487 (2017).
44. Bosenberg, M. et al. Characterization of melanocyte-specific inducible Cre recombinase transgenic mice. *Genesis* **44**, 262–267 (2006).
45. Weiss, T. J. et al. Cell-intrinsic melanin fails to protect melanocytes from ultraviolet-mutagenesis in the absence of epidermal melanin. *Pigment Cell Melanoma Res.* **36**, 6–18 (2023).
46. Borgogna, J. C. et al. The association of *Chlamydia trachomatis* and *Mycoplasma genitalium* infection with the vaginal metabolome. *Sci. Rep.* **10**, 3420 (2020).
47. Chong, J., Wishart, D. S. & Xia, J. Using MetaboAnalyst 4.0 for comprehensive and integrative metabolomics data analysis. *Curr. Protoc. Bioinformatics* **68**, e86 (2019).
48. Subramanian, A. et al. Gene set enrichment analysis: a knowledge-based approach for interpreting genome-wide expression profiles. *Proc. Natl Acad. Sci. USA* **102**, 15545–15550 (2005).
49. Liberzon, A. et al. The Molecular Signatures Database (MSigDB) hallmark gene set collection. *Cell Syst.* **1**, 417–425 (2015).

Acknowledgements The authors acknowledge the Genomics Resource Core Facility (Weill Cornell Medicine), Electron Microscopy and Histology Core Facility (Weill Cornell Medicine), Molecular Cytology Core Facility (Memorial Sloan Kettering Cancer Center, MSKCC) and Laboratory of Comparative Pathology (MSKCC) for their high-quality service. The authors also acknowledge technical support from Wyatt Technology. The authors thank members of the Lyden laboratory for insightful discussions. The authors gratefully acknowledge support from the National Cancer Institute (CA232093, CA163117 and CA207983 to D.L. and CA218513 to D.L. and H.Z.), the Thompson Family Foundation (to D.L. and D.K.), the Tortolani Foundation (to D.L. and J.B.), the Pediatric Oncology Experimental Therapeutics Investigator's Consortium, the Malcolm Hewitt Weiner Foundation, the Manning Foundation, the Sohn Foundation, the AHEPA Vth District Cancer Research Foundation, the Children's Cancer and Blood Foundation, the Hartwell Foundation (to D.L.), the National Institutes of Health (R01CA234614, 2R01AI107301, R01CA234614 and R01DK121072 to R.E.S.), the United States Department of Defense (W81XWH-21-1-0978 to R.E.S.), the Paul G. Allen Family Foundation UWSC13448 (to R.E.S.), the National Natural Science Foundation of China (81902730 to J.L.), Guangdong Foundation of Medical Science and Technology (A2019213 to J.L.), China Scholarship Council (CSC No. 202008440567 to J.L.), the Swedish Cancer Society Pancreatic Cancer Fellowship (to L.B.), the Lions International Postdoctoral fellowship (to L.B.), the Sweden-America stipend (to L.B.), and the fellowship from Alan and Sandra Gerry Metastasis and Tumor Ecosystems Center of Memorial Sloan Kettering Cancer Center (to C.P.Z.). The part of the research involved in developing osteosarcoma PDXs and tumour imaging was funded in part through the NIH/NCI Cancer Center Support Grant P30 CA008748 to MSKCC, the National Institutes of Health (R01CA237213 to C.E.B and V.P., and R01CA254036 to S.K.B.). R.E.S. is an Irma Hirschl Trust Research Award Scholar. Schematic models were generated in part using Servier Medical Art, provided by Servier, licensed under a Creative Commons Attribution 3.0 unported license, with further modifications.

Author contributions D.L., H.Z., G.W. and R.E.S conceived the hypothesis. G.W. coordinated the project, designed the experimental approach, performed most of the experiments, analysed and interpreted the data, and wrote the manuscript. J.L. performed experiments and analysed the data. L.B. coordinated the patient sample preparation and data collection. H.C., G.C.T., M.H., S.L., F.Z., M.C., H.S.K., H.W. and P.L. performed experiments. E.A.H. and J.C.L. performed echocardiography on mice. V.P. and C.E.B. provided livers of genetically engineered mouse model of melanoma. P.R.O. provided help with RNA-seq data analysis. Z.L. conducted metabolomic, lipidomic, free fatty acid, drug metabolism and TPA mass spectrometry. V.K.R. and J.H.H. generated osteosarcoma PDX models. J.H., C.P.Z., M.A.H., P.M.G., D.J.D., J.L.G., K.A.K., M.J., S.K.B., D.K. and W.R.J. provided human samples. J.H.Z., G.S.P., T.M.T., M.E., N.B., Z.S., D.P. and J.B. read the manuscript and provided feedback. I.R.M. edited the manuscript, coordinated sourcing of samples and provided feedback. D.L. and H.Z. interpreted the data and wrote the manuscript. R.E.S. interpreted the data. D.L. led the project.

Competing interests D.L. is on the scientific advisory board of Aufbau Holdings. R.E.S. is on the scientific advisory board of Miromatrix and is a speaker and consultant for Alnylam. M.E. is a member of the research advisory board for brensocatib for Insmed, a member of the scientific advisory board for Vividion Therapeutics and a consultant for Protalix BioTherapeutics, and holds shares in Agios. The other authors declare no competing interests.

Additional information

Supplementary information The online version contains supplementary material available at https://doi.org/10.1038/s41586-023-06114-4.

Correspondence and requests for materials should be addressed to Robert E. Schwartz, Haiying Zhang or David Lyden.

Peer review information *Nature* thanks Ekihiro Seki and the other, anonymous, reviewer(s) for their contribution to the peer review of this work. Peer review reports are available.

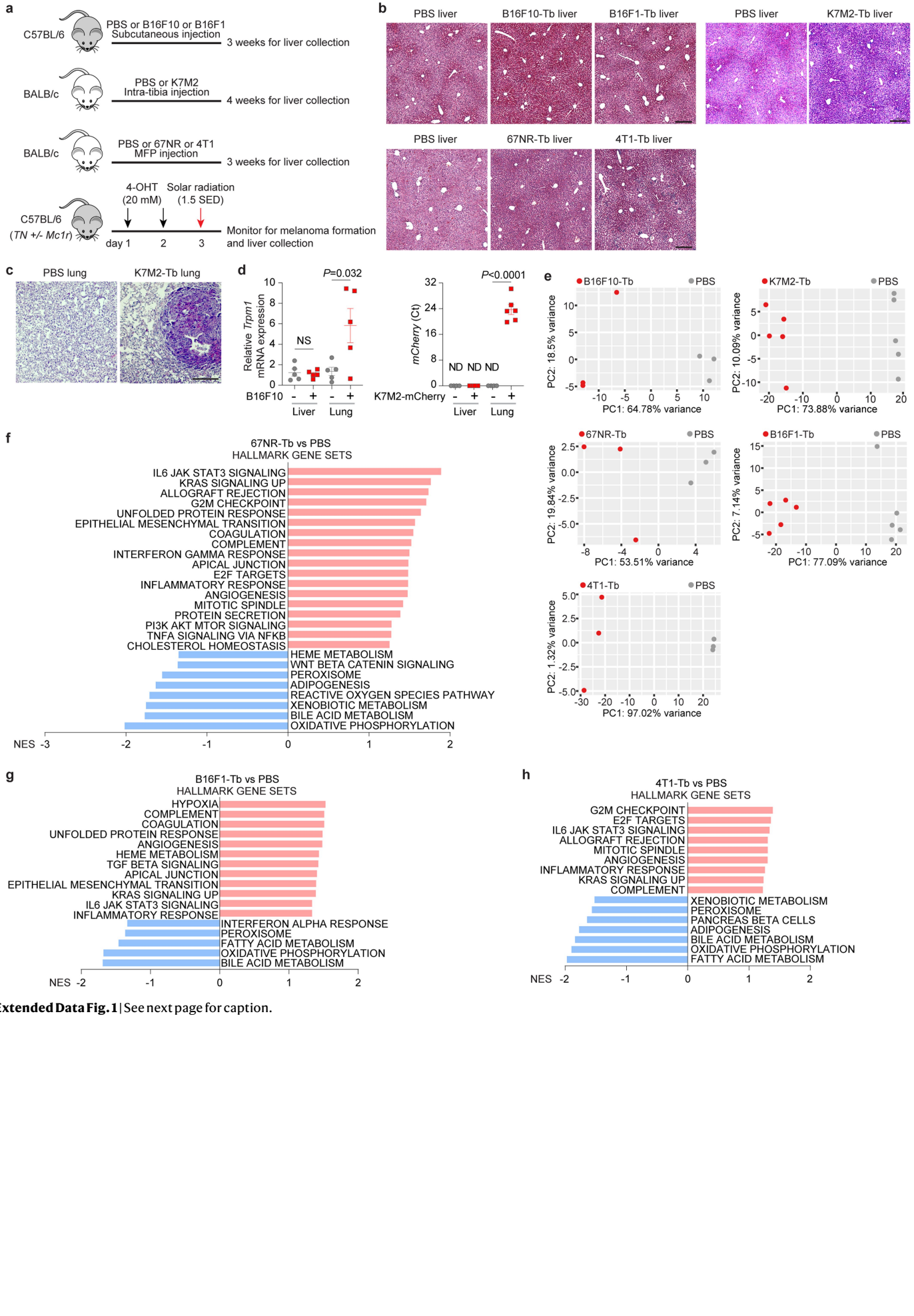

Extended Data Fig. 1 | See next page for caption.

Extended Data Fig. 1 | Primary tumours dysregulate the metabolism of metastasis-free livers. a, Schematic representation of mouse tumour models utilized in this study. B16F10, K7M2, 67NR, B16F1 and 4T1 cells, were orthotopically injected into syngeneic mice. Age and sex-matching mice injected with PBS were used as controls of these experimental mouse models. C57BL/6 *TN* mice carrying a Cre-inducible $Nras^{Q61R}$ oncogene were employed for generating spontaneous melanoma. Non-tumour bearing control mice carried the $Nras^{Q61R}$, $p16^{fl/fl}$ and Tyr-CRE-ER(T2) alleles but were not treated to induce CRE activity or tumour formation. Functionally null *Mc1r* increased melanoma susceptibility. **b**, Representative H&E staining images of the livers from B16F10-Tb and B16F1-Tb mice (top, left), K7M2-Tb mice (top, right), 67NR-Tb and 4T1-Tb mice (bottom), and their respective controls. This experiment was repeated three times independently with similar results. **c**, Representative H&E staining images of lung metastases in the PBS control mice and K7M2-Tb mice. This experiment was repeated three times independently with similar results. **d**, RT-qPCR analysis of *Trpm1* and *mCherry* expression in livers and lungs of mice implanted with B16F10 and mCherry-expressing K7M2 cells, respectively, compared to their controls. $n = 5$ per group for B16F10-Tb model, $n = 4$ control and $n = 6$ K7M2-mCherry-Tb mice. NS, not significant; ND, not detected. **e**, Principal component analysis (PCA) of gene expression in the livers from mice implanted with B16F10, or K7M2, or 67NR, or B16F1, or 4T1 tumour cells, compared to their respective PBS-injected controls. Results showed that the gene expression profiles of livers from tumour-bearing mice independently segregated from their respective controls. $n = 3$ mice per group for B16F10-Tb, 67NR-Tb and 4T1-Tb models; $n = 5$ mice per group for K7M2-Tb and B16F1-Tb models. **f**-**h**, GSEA of the gene expression profiles, which were ranked based on the sign of $\log_2FC * (-\log_{10}P \text{ value})$, in the livers from 67NR-Tb mice (**f**), B16F1-Tb mice (**g**), or 4T1-Tb mice (**h**), compared to their respective PBS-injected controls, using hallmark gene sets, and the significantly changed signaling pathways with FDR<0.2 are shown. $n = 3$ mice per group for 67NR-Tb and 4T1-Tb models; $n = 5$ mice per group for B16F1-Tb model. Gene lists for signaling pathways are shown in Supplementary Tables 19–21. Scale bars for (**b**,**c**), 200 μm. *P* values were determined by two-tailed, unpaired Student's *t*-test (**d**).

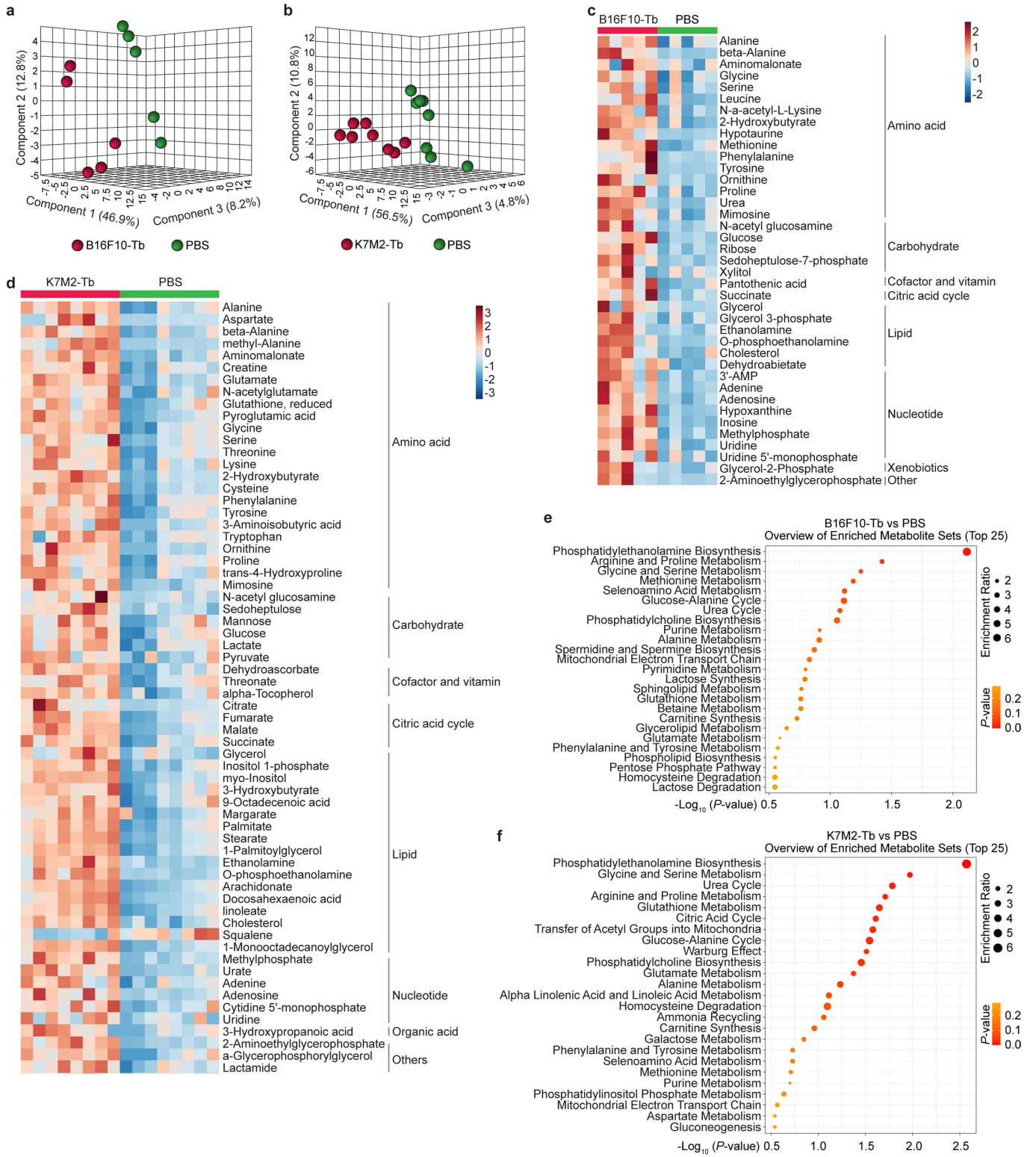

Extended Data Fig. 2 | Primary tumours induce metabolic dysfunction of the metastasis-free livers. a,**b**, PLS-DA plots of metabolites detected in the livers from B16F10-Tb mice (**a**) and K7M2-Tb mice (**b**), compared to their PBS-injected controls. Metabolomic mass spectrometry data are shown in Supplementary Tables 1 and 2. $n = 5$ B16F10-Tb mice and controls; $n = 8$ K7M2-Tb mice and controls. **c**,**d**, Heatmaps showing the significantly changed metabolites, classified into different groups, in the livers from B16F10-Tb mice (**c**) and K7M2-Tb mice (**d**), compared to their PBS-injected controls. $n = 5$ B16F10-Tb mice and controls; $n = 8$ K7M2-Tb mice and controls. **e**,**f**, Metabolite set enrichment analysis of metabolites (shown in **c**,**d**) significantly changed in the livers of B16F10-Tb (**e**) and K7M2-Tb (**f**) mice, compared to their respective PBS-injected controls. $n = 5$ B16F10-Tb mice and controls; $n = 8$ K7M2-Tb mice and controls. *P* values were determined by the hypergeometric test (**e**,**f**).

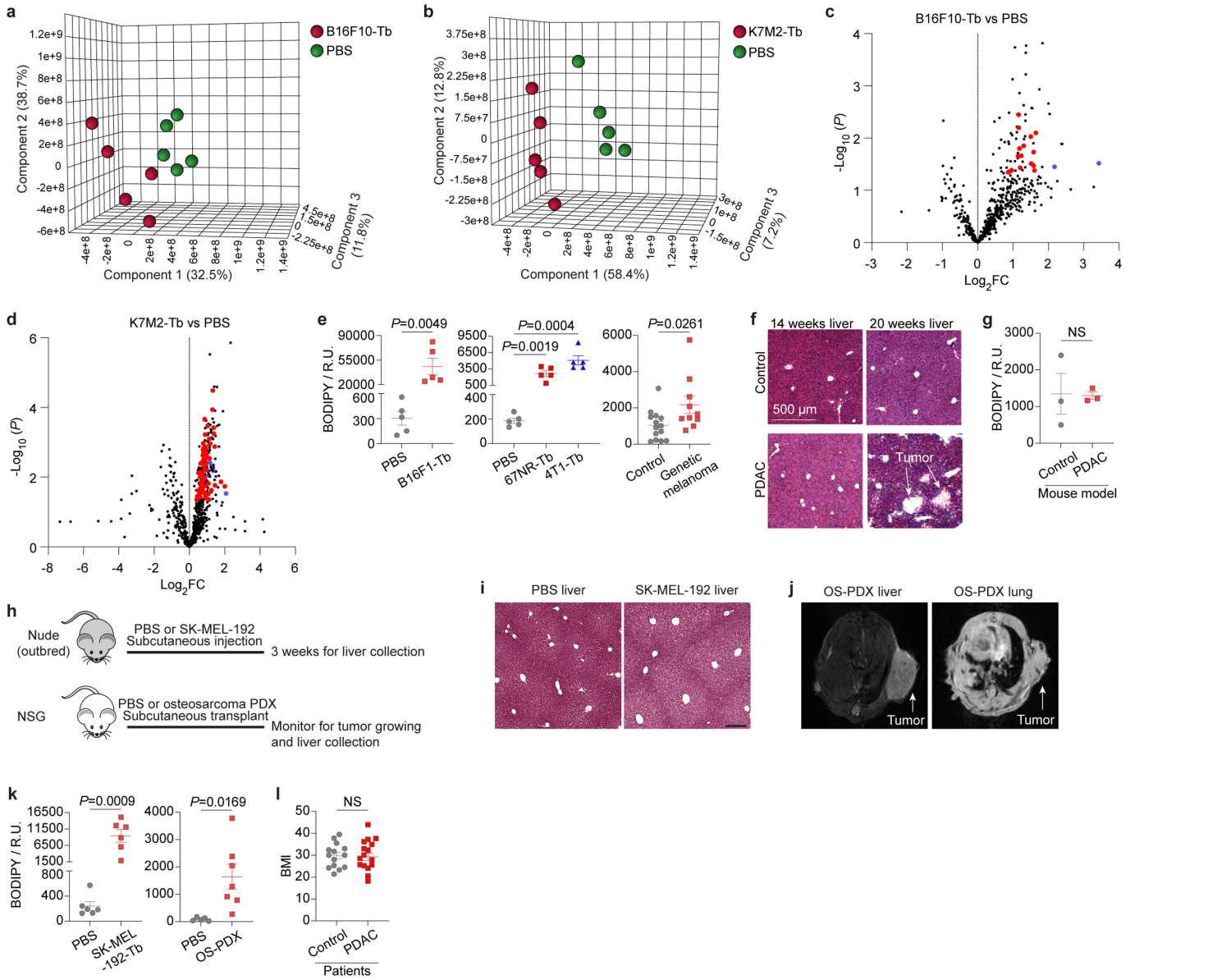

Extended Data Fig. 3 | Primary tumours induce lipid accumulation in metastasis-free livers. a,**b**, PLS-DA plots of the lipid species in the livers from B16F10-Tb mice (**a**) and K7M2-Tb mice (**b**), compared to their PBS-injected controls. Lipidomic mass spectrometry data are shown in Supplementary Tables 3 and 4. $n = 5$ mice per group. **c**,**d**, Volcano plots showing the significantly ($P < 0.05$) enriched triglyceride species (red) and cholesteryl ester species (blue) in the livers from B16F10-Tb mice (**c**) and K7M2-Tb mice (**d**), compared to their PBS-injected controls. $n = 5$ mice per group. **e**, Statistical analysis of BODIPY staining of livers from mouse melanoma B16F1-Tb mice, mouse breast cancer 67NR-Tb and 4T1-Tb mice, genetic melanoma-bearing mice, and their respective controls. $n = 5$ mice per group for B16F1, 67NR and 4T1 models; $n = 14$ control and $n = 10$ tumour-bearing mice for the genetic melanoma model. **f**, Representative H&E staining images of livers from KPC mice. Liver metastasis was observed in 20-week, but not 14-week tumour bearing mice. **g**, Statistical analysis of BODIPY staining of the livers from 14-week PDAC tumour-bearing mice, compared to non-PDAC mouse controls. $n = 3$ mice per group. **h**, Schematic representation of mouse tumour models utilized in this study. SK-MEL-192 cells were subcutaneously injected into nude (outbred) mice. Patient-derived xenograft (PDX) models of osteosarcoma were generated by transplanting surgically excised primary tumour specimens from clinical patients into NOD/SCID/IL2Rγ^{null} (NSG) mice. Age and sex-matching mice injected with PBS were used as controls of these experimental mouse models. **i**, Representative H&E staining images of the livers from SK-MEL-192-Tb and control mice. This experiment was repeated three times independently with similar results. **j**, Representative MRI images showing lung metastasis, but not liver metastasis detected in osteosarcoma-PDX (OS-PDX) mouse models. This experiment was repeated seven times independently with similar results. **k**, Statistical analysis of BODIPY staining of livers from human melanoma SK-MEL-192-Tb mice, osteosarcoma-PDX tumour-bearing mice, and their respective controls. $n = 6$ mice per group for SK-MEL-192 model; $n = 5$ control and $n = 7$ tumour-bearing mice for osteosarcoma-PDX model. **l**, Measurement of body mass index (BMI) of PDAC patients and control subjects with benign lesions. $n = 14$ control subjects and $n = 16$ PDAC patients. Scale bars, 500 μm for (**f**) and 200 μm for (**i**). *P* values were determined by the two-tailed, unpaired Student's *t*-test (**c**-**e**,**g**,**k**,**l**). Data are mean ± s.e.m. NS, not significant.

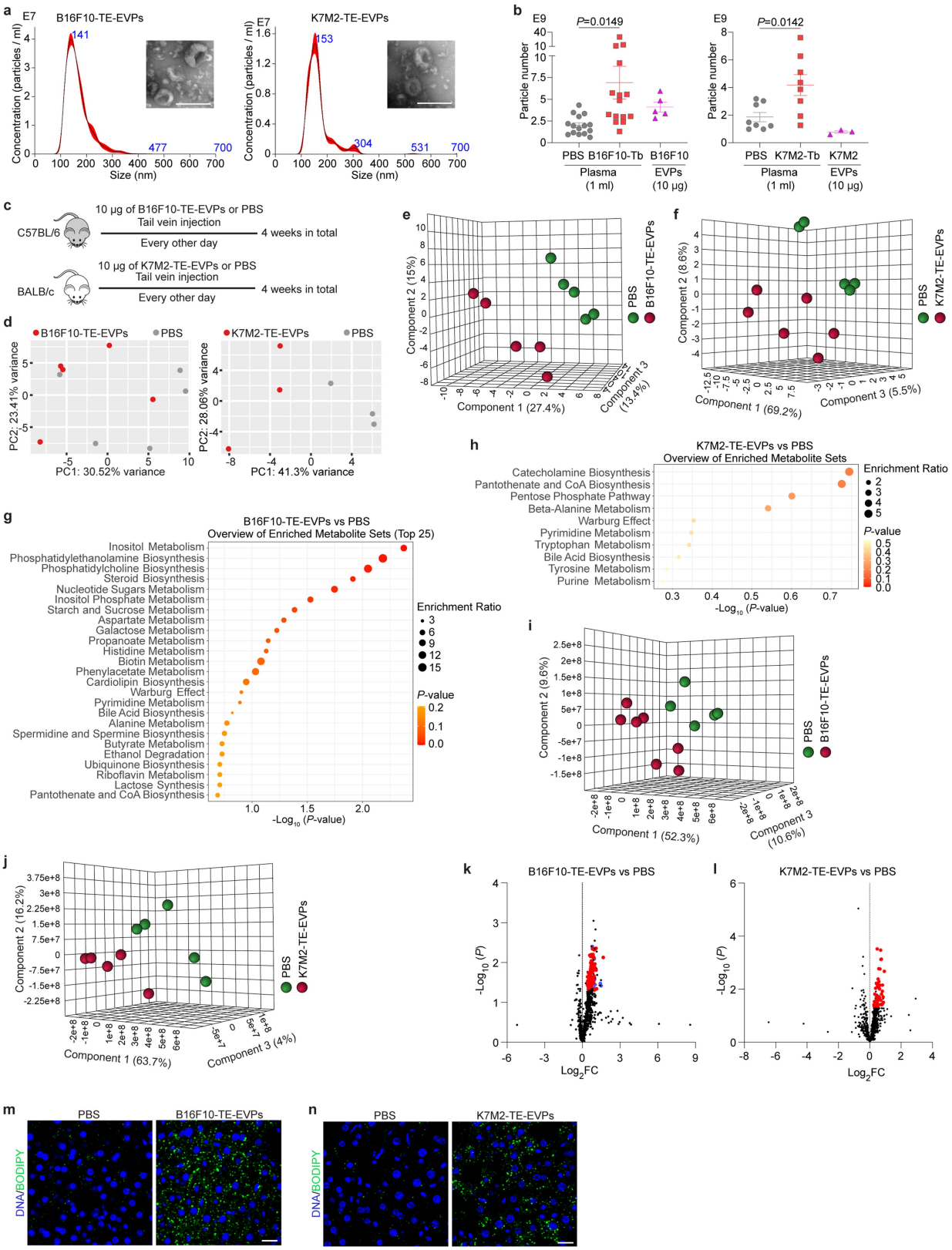

Extended Data Fig. 4 | See next page for caption.

Extended Data Fig. 4 | Tumour explant (TE)-derived EVPs dysregulate liver metabolism. a, Representative nanoparticle tracking analysis (NTA) and TEM images (insertions) of B16F10-TE-EVPs (left) and K7M2-TE-EVPs (right). Shown are graphs and images representative of three independent experiments. **b**, Quantification of the particle numbers in 1 ml of plasma from B16F10-Tb (left) and K7M2-Tb (right) mice, compared to their PBS-injected controls, as well as in 10 μg of EVPs derived from B16F10 (left) and K7M2 (right) cells. $n = 15$ control and B16F10-Tb mice; $n = 8$ control and K7M2-Tb mice; $n = 5$ and $n = 3$ independent experiments for EVPs derived from B16F10 and K7M2 cells, respectively. **c**, Schematic illustration of the procedure of syngeneic mouse education with B16F10-TE-EVPs or K7M2-TE-EVPs, and PBS control. **d**, PCA of gene expression in the livers of mice educated with B16F10-TE-EVPs (left) and K7M2-TE-EVPs (right), compared to PBS-educated controls. $n = 5$ mice per group for B16F10-TE-EVP education model; $n = 3$ mice per group for K7M2-TE-EVP education model. **e**,**f**, PLS-DA plots of metabolites detected in the livers from B16F10-TE-EVP- (**e**) and K7M2-TE-EVP- (**f**) educated mice, compared to PBS-educated controls. Metabolomics data are shown in Supplementary Tables 8 and 9. $n = 5$ B16F10-TE-EVP-educated mice and controls; $n = 6$ K7M2-TE-EVP-educated mice and $n = 5$ controls. **g**,**h**, Metabolite set enrichment analysis of the metabolites significantly changed in the livers from B16F10-TE-EVP- (**g**) and K7M2-TE-EVP- (**h**) educated mice, compared to PBS-educated controls (see lists of metabolites in Fig. 2e, f). $n = 5$ B16F10-TE-EVP-educated mice and controls; $n = 6$ K7M2-TE-EVP-educated mice and $n = 5$ controls. **i**,**j**, PLS-DA plots of the lipid species in the livers from B16F10-TE-EVP- (**i**) and K7M2-TE-EVP- (**j**) educated mice, compared to PBS-educated controls. Lipidomics data are shown in Supplementary Tables 10 and 11. $n = 7$ B16F10-TE-EVP-educated mice and $n = 5$ controls; $n = 5$ K7M2-TE-EVP-educated mice and controls. **k**,**l**, Volcano plots showing the significantly ($P < 0.05$) enriched triglyceride species (red) and cholesteryl ester species (blue) in the livers from B16F10-TE-EVP- (**k**) and K7M2-TE-EVP- (**l**) educated mice, compared to PBS-educated controls. $n = 7$ B16F10-TE-EVP-educated mice and $n = 5$ controls; $n = 5$ K7M2-TE-EVP-educated mice and controls. **m**,**n**, Representative images of BODIPY staining of the livers from B16F10-TE-EVP- (**m**) and K7M2-TE-EVP- (**n**) educated mice, and PBS-educated controls. Associated quantification of BODIPY staining was shown in Fig. 2i, j. Scale bars, 200 nm for (**a**) and 20 μm for (**m**,**n**). *P* values were determined by the two-tailed, unpaired Student's *t*-test (**b**,**k**,**l**), or hypergeometric test (**g**,**h**). Data are mean ± s.e.m.

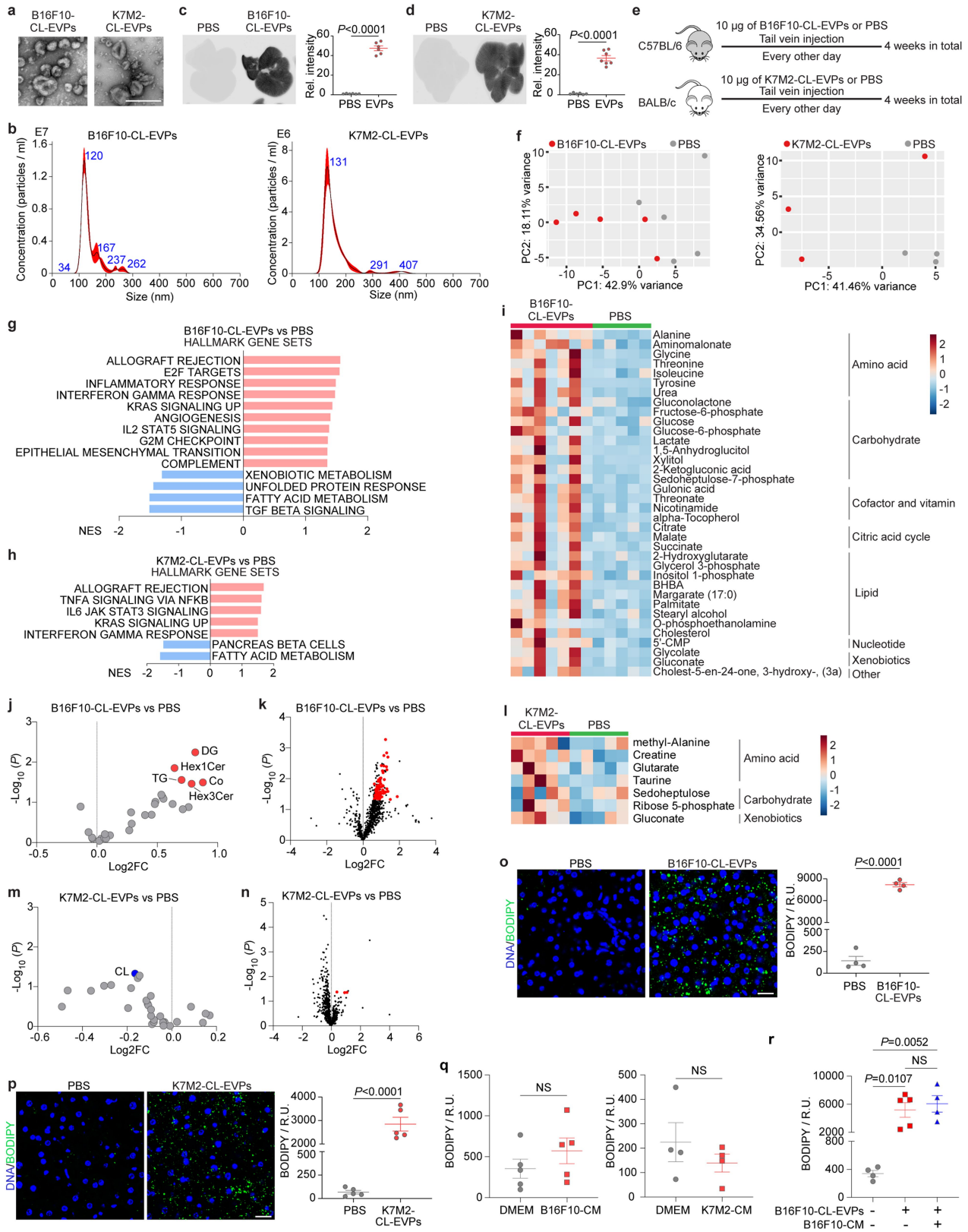

Extended Data Fig. 5 | See next page for caption.

Extended Data Fig. 5 | Tumour cell line (CL)-derived EVPs dysregulate liver metabolism. a, Representative TEM images of B16F10-CL-EVPs (left) and K7M2-CL-EVPs (right). Scale bar, 200 nm. This experiment was repeated three times independently with similar results. **b**, NTA of B16F10-CL-EVPs and K7M2-CL-EVPs. Shown are graphs representative of three independent experiments. **c**,**d**, Representative images (left) and associated statistical analysis of relative signal intensity (right) of the livers from mice 24 h post intravenous injection of 10 μg of CellVue NIR815-labeled B16F10-CL-EVPs (**c**) and K7M2-CL-EVPs (**d**), and their mock PBS-injected controls. $n = 6$ mice injected with B16F10-CL-EVPs or PBS mock reaction; $n = 7$ mice injected with K7M2-CL-EVPs and $n = 6$ mice injected with PBS mock control. **e**, Schematic illustration of syngeneic mouse education with B16F10-CL-EVPs or K7M2-CL-EVPs, and PBS control. **f**, PCA of gene expression in the livers from mice educated with B16F10-CL-EVPs (left) and K7M2-CL-EVPs (right), compared to PBS-educated controls. $n = 5$ mice per group for B16F10-CL-EVP education model; $n = 3$ mice per group for K7M2-CL-EVP education model. **g**,**h**, GSEA of gene expression profiles, ranked based on the sign of $\log_2$FC∗(-$\log_{10}P$ value), in the livers from B16F10-CL-EVP- (**g**) and K7M2-CL-EVP- (**h**) educated mice, compared to PBS-educated controls, using hallmark gene sets. Significantly changed signaling pathways with nominal $P < 0.05$ are shown. $n = 5$ B16F10-CL-EVP-educated mice and controls; $n = 3$ K7M2-CL-EVP-educated mice and controls. Gene lists for signaling pathways are shown in Supplementary Tables 22 and 23. **i**, Heatmap showing the metabolites significantly changed in the livers of B16F10-CL-EVP-educated mice, compared to PBS-educated controls. $n = 5$ control and $n = 7$ B16F10-CL-EVP-educated mice. Metabolomic mass spectrometry data are shown in Supplementary Table 29. **j**,**k**, Volcano plots showing the significantly ($P < 0.05$) enriched lipid classes (red) (**j**) and the significantly ($P < 0.05$) enriched triglyceride species (red) (**k**) in the livers of B16F10-CL-EVP-educated mice, compared to PBS-educated controls. $n = 5$ control and $n = 6$ B16F10-CL-EVPs educated mice. Lipidomic mass spectrometry data are shown in Supplementary Table 30. **l**, Heatmap showing the metabolites significantly changed in the livers of K7M2-CL-EVP-educated mice, compared to PBS-educated controls. $n = 5$ K7M2-CL-EVP-educated mice and controls. Metabolomics MS data are shown in Supplementary Table 31. **m**,**n**, Volcano plots showing the significantly ($P < 0.05$) changed lipid class (blue) (**m**), and the significantly ($P < 0.05$) enriched triglyceride species (red) (**n**) in the livers from K7M2-CL-EVP-educated mice, compared to PBS-educated controls. $n = 5$ control and $n = 4$ K7M2-CL-EVP-educated mice. Lipidomic mass spectrometry data are shown in Supplementary Table 32. **o**,**p**, Representative immunofluorescence (IF) images (left) and associated statistical analysis (right) of BODIPY staining of the livers from B16F10-CL-EVP- (**o**) and K7M2-CL-EVP- (**p**) educated mice, and PBS-educated controls. $n = 4$ mice per group for B16F10-CL-EVP-education model; $n = 5$ mice per group for K7M2-CL-EVP-education model. Scale bars, 20 μm. **q**, Quantification of BODIPY staining of the livers from B16F10- and K7M2-conditioned media -educated mice, compared to blank DMEM media-educated mice. $n = 5$ mice per group for B16F10-conditioned media model and $n = 4$ mice per group for K7M2-conditioned media model. **r**, Quantification of BODIPY staining of the livers from PBS-educated and B16F10-CL-EVP-educated mice, in the absence or presence of B16F10-conditioned media co-education. $n = 4$ mice educated with PBS, $n = 5$ mice educated with B16F10-CL-EVPs alone, and $n = 4$ mice educated with B16F10-CL-EVPs together with B16F10-conditioned media. *P* values were determined by the two-tailed, unpaired Student's *t*-test for (**c**,**d**,**j**,**k**,**m**-**p**) and one-way ANOVA with post hoc Tukey's test for (**r**). Data are mean ± s.e.m. NS, not significant. CM, conditioned media.

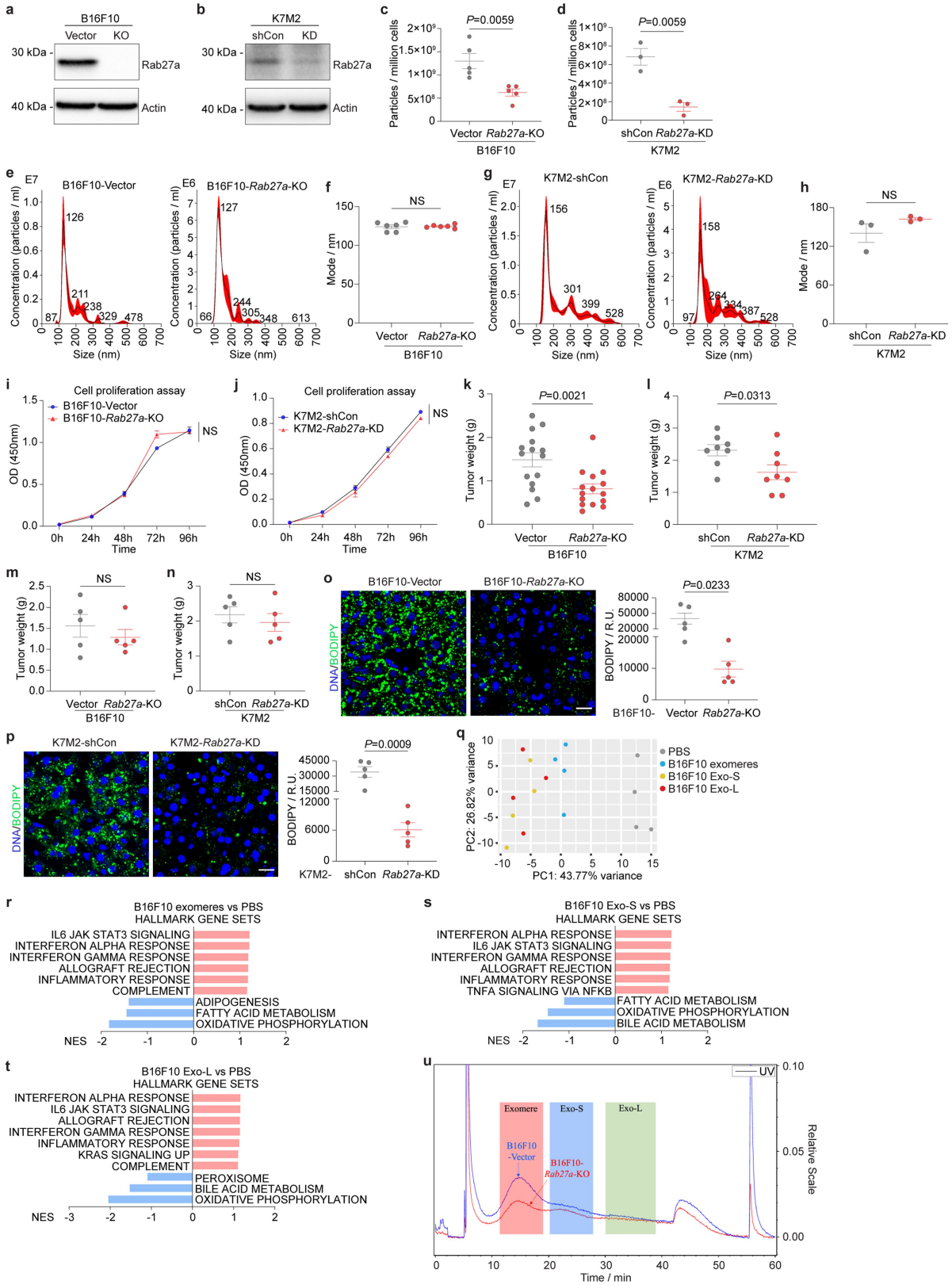

Extended Data Fig. 6 | See next page for caption.

Extended Data Fig. 6 | Ablation of Rab27a expression suppresses EVP secretion from tumour cells. a, Western blot analysis of Rab27a expression in B16F10 cells infected with vector control or *Rab27a*-CRISPR KO virus. Actin was used as a loading control. Shown is representative data from three independent experiments. **b**, Western blot analysis of Rab27a expression in K7M2 cells infected with vector control (shCon) or *Rab27a*-shRNA KD virus. Actin was used as a loading control. Shown is representative data from three independent experiments. **c**, NTA of the numbers of EVPs secreted from B16F10-control (Vector) or B16F10-*Rab27a*-KO cells. $n = 5$ independent experiments per group. **d**, NTA of the numbers of EVPs secreted from K7M2-control (shCon) or K7M2-*Rab27a*-KD cells. $n = 3$ independent experiments per group. **e**,**f**, Representative NTA profiles (**e**) and associated analysis of the diameter mode (**f**) of EVPs isolated from B16F10-control (Vector) or B16F10-*Rab27a*-KO cells. $n = 6$ independent experiments per group. **g**,**h**, Representative NTA profiles (**g**) and associated analysis of the diameter mode (**h**) of EVPs isolated from K7M2-control (shCon) or K7M2-*Rab27a*-KD cells. $n = 3$ independent experiments per group. **i**, Proliferation of B16F10-control (Vector) and B16F10-*Rab27a*-KO cells. $n = 3$ independent experiments. **j**, Proliferation of K7M2-control (shCon) and K7M2-*Rab27a*-KD cells. $n = 4$ independent experiments. **k**, Statistical analysis of the weights of tumours from mice inoculated with B16F10-control (Vector) or B16F10-*Rab27a*-KO cells. $n = 15$ mice per group. **l**, Statistical analysis of the weights of tumours from mice inoculated with K7M2-control (shCon) or K7M2-*Rab27a*-KD cells. $n = 8$ mice per group. **m**,**n**, Statistical analysis showing the similar tumour burden from a subset of mice in **k** and **l** inoculated with B16F10-*Rab27a*-KO cells (**m**), or K7M2-*Rab27a*-KD cells (**n**) subjected to BODIPY staining of their livers as shown in (**o**,**p**). $n = 5$ mice per group. **o**,**p**, Representative images (left) and associated statistical analysis (right) of BODIPY staining of the livers from B16F10-*Rab27a*-KO (**o**) and K7M2-*Rab27a*-KD (**p**) tumour bearing mice, and their respective controls. $n = 5$ mice per group. Scale bars, 20 µm. **q**, PCA of the gene expression profiling in the livers from mice educated with control PBS, B16F10 exomeres, or B16F10 Exo-S, or B16F10 Exo-L for 4 weeks. $n = 4$ mice per group. **r**-**t**, GSEA of gene expression profiles, which were ranked based on the sign of $\log_2$FC∗(-$\log_{10}$*P* value), in the livers from B16F10 exomere- (**r**), Exo-S- (**s**), and Exo-L- (**t**) educated mice, compared to PBS-educated controls. ($n = 4$ each). Signaling pathways significantly changed with nominal $P < 0.05$ are shown. Gene lists for signaling pathways are shown in Supplementary Tables 24–26. **u**, EVPs isolated from equal numbers of B16F10-Vector control and B16F10-*Rab27a*-KO cells were resolved via AF4. Shown are real time measurement of UV on a relative scale (right axis), indicating the abundance of fractionated particles. Shaded areas mark the elution time periods for exomeres (red), Exo-S (blue) and Exo-L (green), respectively. As reflected by the UV signal, the production of exomeres, Exo-S (to a less extent) and Exo-L (to the least extent) were reduced in the B16F10-*Rab27a*-KO cells compared to the B16F10-Vector control cells. *P* values were determined by the two-tailed, unpaired Student's *t*-test (**c**,**d**,**f**,**h**,**k**-**p**), or two-way ANOVA followed with Bonferroni's multiple comparisons test (**i**,**j**). Data are mean ± s.e.m. NS, not significant. KO, knockout. KD, knockdown. For western blotting source data of (**a**,**b**), see Supplementary Fig. 1.

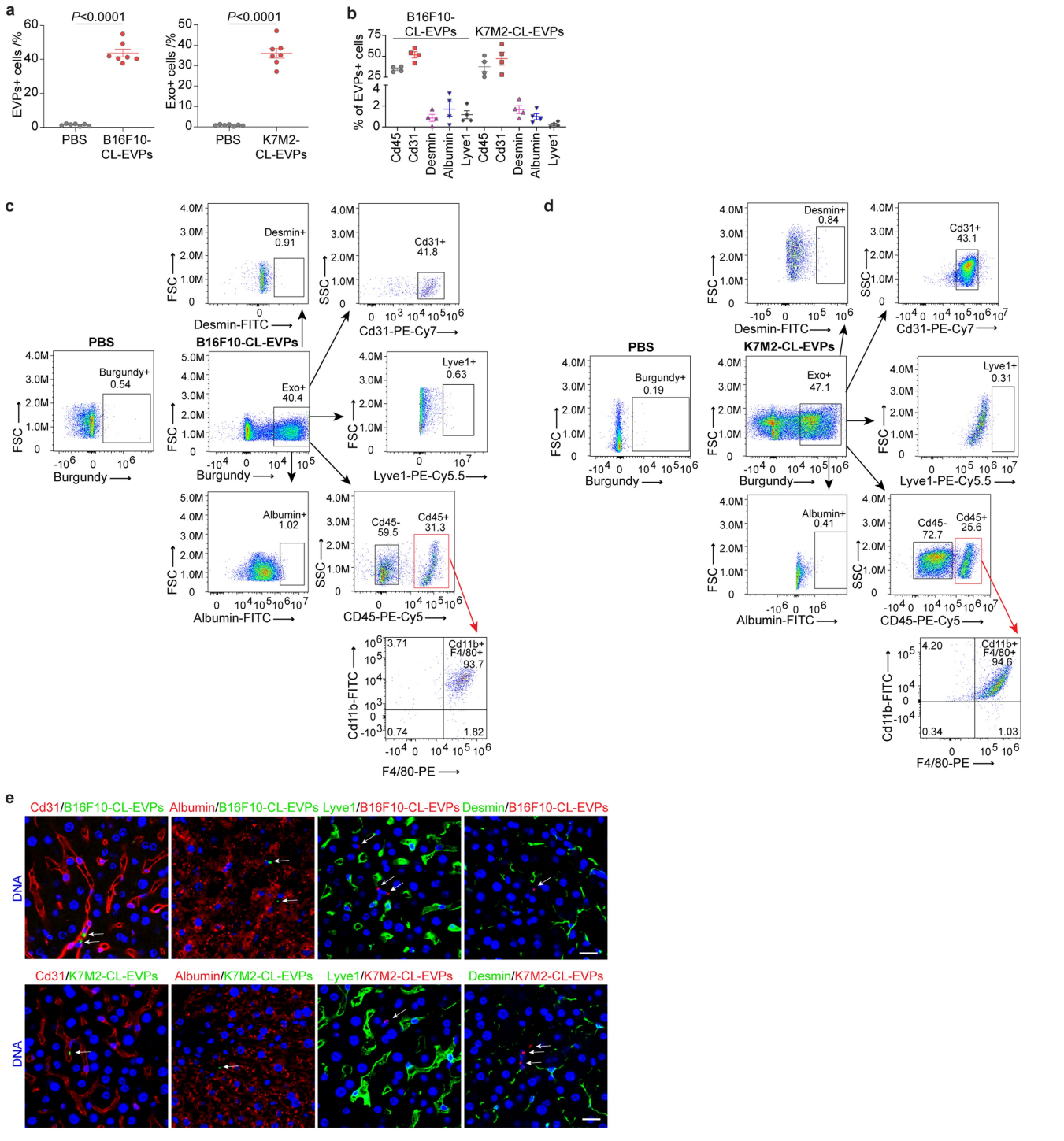

Extended Data Fig. 7 | Tumour-derived EVPs are uptaken by Kupffer cells in the liver. a, Flow cytometry analysis of the percentage of EVP positive cells in the livers from mice 24 h post intravenous injection of 10 μg of CellVue Burgundy-labeled B16F10-CL-EVPs (left) and K7M2-CL-EVPs (right), and PBS controls. $n = 7$ mice per group. **b**, Flow cytometry analysis of the percentage of different cell types, including Cd45$^+$ immune cells, Cd31$^+$ vascular endothelial cells, desmin$^+$ stellate cells, albumin$^+$ hepatocytes, Lyve1$^+$ lymphatic and sinusoidal endothelial cells, among the B16F10-CL-EVP and K7M2-CL-EVP positive cells shown in **a**. $n = 4$ each. **c**,**d**, Representative flow cytometry gating strategy evaluating the percentage of different cell types, including Cd31$^+$ vascular endothelial cells, albumin$^+$ hepatocytes, Lyve1$^+$ lymphatic and sinusoidal endothelial cells, desmin$^+$ stellate cells, Cd45$^+$ immune cells and Cd11b$^+$F4/80$^+$ Kupffer cells in Cd45$^+$ immune cells, among the B16F10-CL-EVP- (**c**) and K7M2-CL-EVP- (**d**) positive cells shown in **a**,**b** and Fig. 3a. **e**, Representative images of the immunofluorescence (IF) co-staining of EVPs (indicated by white arrows) with Cd31$^+$ vascular endothelial cells, albumin$^+$ hepatocytes, Lyve1$^+$ lymphatic and sinusoidal endothelial cells, and desmin$^+$ stellate cells 24 h post intravenous injection of B16F10-CL-EVPs (top) or K7M2-CL-EVPs (bottom). DNA in blue. Scale bars, 20 μm. This experiment was repeated three times independently with similar results. *P* values were determined by the two-tailed, unpaired Student's *t*-test (**a**).

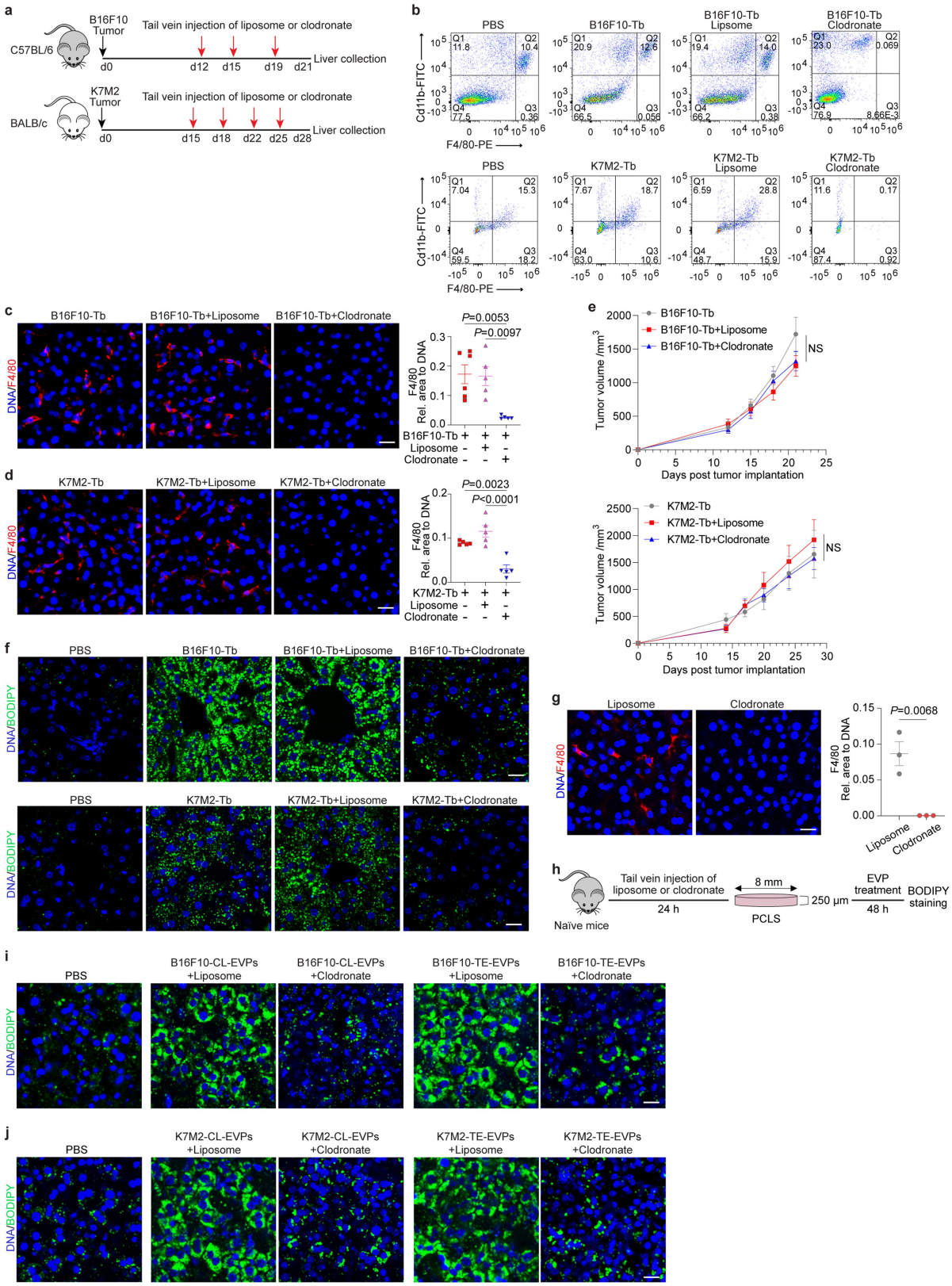

Extended Data Fig. 8 | See next page for caption.

Extended Data Fig. 8 | Depletion of Kupffer cells alleviates tumour EVP-induced fatty liver formation without impairing tumour growth. **a**, Schematic illustration of liposome or clodronate (100 µl of suspension per 10 g of mouse weight) treatment, delivered via intravenous injection to B16F10-Tb and K7M2-Tb mice. The concentration of clodronate in the suspension is 5 mg ml^{-1}. **b**, Representative flow cytometry gating strategy examining the abundance of Kupffer cells (Cd11b^{+}F4/80^{+}) in the livers from PBS-injected control mice, B16F10-Tb (up) or K7M2-Tb (bottom) mice, and tumour-bearing mice treated with liposome or clodronate. Associated quantification of Kupffer cell abundance was shown in Fig. 3c. **c**,**d**, Representative IF images (left) and associated statistical analysis (right) of Kupffer cell staining of the livers from B16F10-Tb (**c**) and K7M2-Tb (**d**) mice, and tumour-bearing mice treated with liposome or clodronate. F4/80 staining for Kupffer cells in red, and DNA in blue. For B16F10-Tb model, $n = 6$ B16F10-Tb mice, $n = 5$ B16F10-Tb mice treated with liposome or clodronate. For K7M2-Tb model, $n = 5$ mice per group. **e**, Measurement of the tumour volumes from B16F10-Tb (left) or K7M2-Tb (right) mice, and tumour-bearing mice treated with liposome or clodronate as shown in (**a**). $n = 5$ B16F10-Tb mice and $n = 7$ B16F10-Tb mice treated with liposome or clodronate; $n = 3$ K7M2-Tb mice and $n = 5$ K7M2-Tb mice treated with liposome or clodronate. **f**, Representative IF images of BODIPY staining of the livers from PBS-injected control mice, B16F10- or K7M2-Tb mice, and the tumour-bearing mice treated with liposome or clodronate as shown in Fig. 3d. **g**, Representative IF images (left) and associated statistical analysis (right) of the precision-cut liver slices (PCLS) stained with F4/80 (red) and DAPI (blue) to show the Kupffer cell depletion in mouse livers 24 h post treatment with liposome or clodronate (100 µl of suspension per 10 g of mouse weight). $n = 3$ mice per group. **h**, Schematic illustration of PCLS from naïve mice 24 h post treatment with liposome or clodronate (100 µl of suspension per 10 g of mouse weight) followed by EVP (10 µg ml^{-1}) treatment ex vivo for 48 h. Liver slices were then subjected to BODIPY staining. **i**,**j**, Representative IF images of BODIPY staining of PCLS sectioned from liposome- or clodronate- (100 µl of suspension per 10 g of mouse weight) treated mice (as shown in **g**) that were further treated with 10 µg ml^{-1} of B16F10-CL-EVPs or B16F10-TE-EVPs (**i**), K7M2-CL-EVPs or K7M2-TE-EVPs (**j**) ex vivo for 48 h (see also Fig. 3e, f). PCLS from naïve mice treated with PBS were used as controls. BODIPY in green and DNA in blue. Scale bars, 20 µm. *P* values were determined by the one-way ANOVA with post hoc Tukey's test (**c**,**d**), or two-way ANOVA followed with Bonferroni's multiple comparisons test (**e**), or two-tailed, unpaired Student's *t*-test (**g**). Data are mean ± s.e.m. NS, not significant.

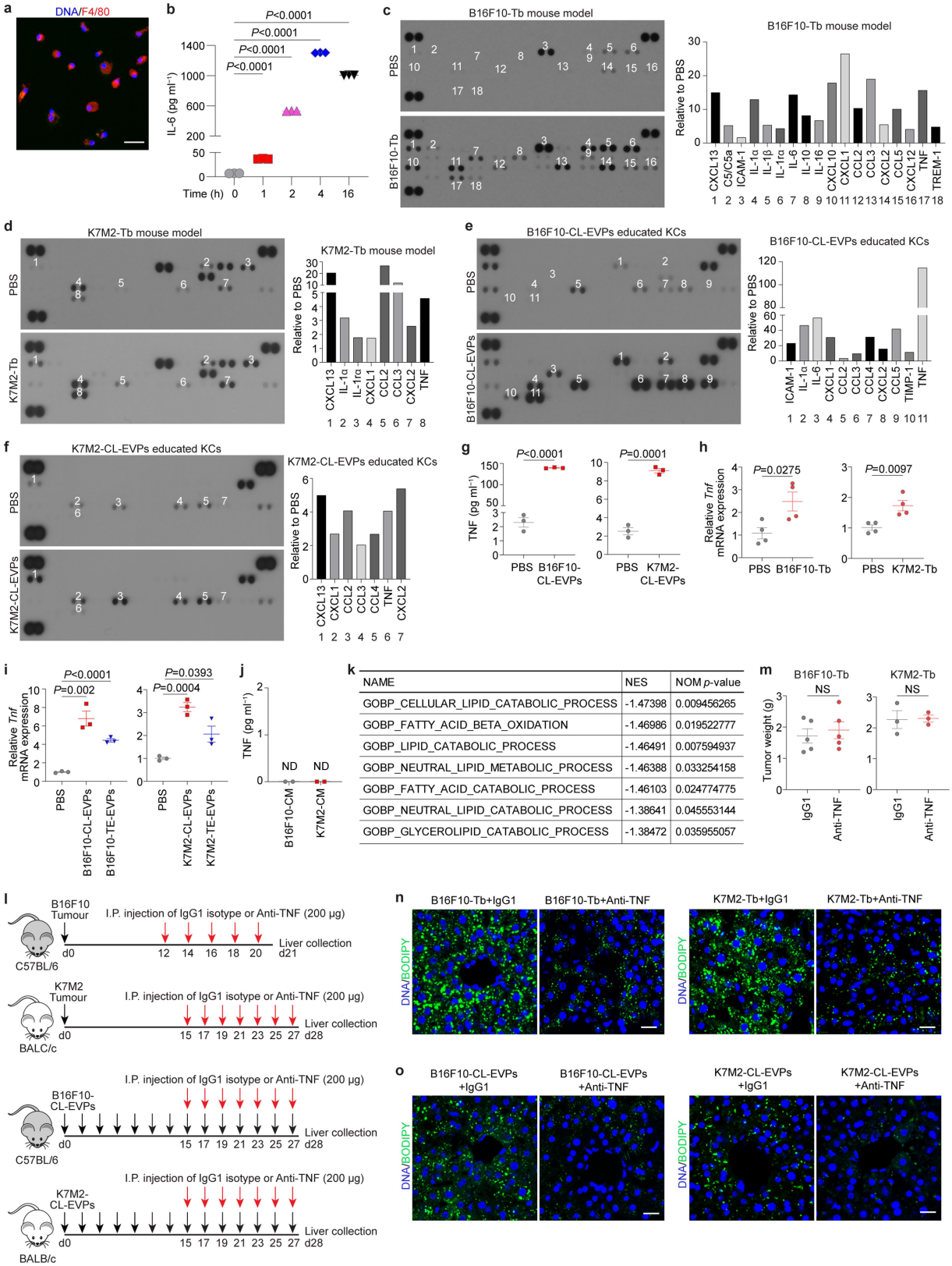

NAME	NES	NOM *p*-value
GOBP_CELLULAR_LIPID_CATABOLIC_PROCESS	-1.47398	0.009456265
GOBP_FATTY_ACID_BETA_OXIDATION	-1.46986	0.019522777
GOBP_LIPID_CATABOLIC_PROCESS	-1.46491	0.007594937
GOBP_NEUTRAL_LIPID_METABOLIC_PROCESS	-1.46388	0.033254158
GOBP_FATTY_ACID_CATABOLIC_PROCESS	-1.46103	0.024774775
GOBP_NEUTRAL_LIPID_CATABOLIC_PROCESS	-1.38641	0.045553144
GOBP_GLYCEROLIPID_CATABOLIC_PROCESS	-1.38472	0.035955057

Extended Data Fig. 9 | See next page for caption.

Extended Data Fig. 9 | Tumour EVPs promote TNF secretion from Kupffer cells. a, Representative IF image of the primary Kupffer cells isolated from naïve mice. F4/80 in red and DAPI in blue. Shown is a representative image from three independent experiments. Scale bar, 20 μm. **b**, ELISA analysis of IL-6 secretion from naïve mice-derived Kupffer cells after treatment with LPS (1 μg ml^{-1}). $n = 3$ independent experiments per group. **c**,**d**, Representative cytokine array blots and associated quantification charts for the cytokines and chemokines in the whole cell lysates of Kupffer cells isolated from B16F10-Tb mice (**c**) and K7M2-Tb mice (**d**), and their respective PBS-injected controls. **e**,**f**, Representative cytokine array blots and associated quantification charts for the cytokines and chemokines in the conditioned media of Kupffer cells isolated from naïve mice and educated with 10 μg ml^{-1} of B16F10-CL-EVPs (**e**) or K7M2-CL-EVPs (**f**) in vitro for 3 days, and their respective PBS-educated controls. **g**, TNF ELISA on the conditioned medium of Kupffer cells educated with 10 μg ml^{-1} of B16F10-CL-EVP- (left), or K7M2-CL-EVP- (right), and their respective PBS controls for 3 days. $n = 3$ independent experiments per group. **h**, RT-qPCR analysis of *Tnf* expression in Kupffer cells isolated from B16F10-Tb (left), or K7M2-Tb (right) mice, and their respective PBS-injected controls. n = 4 mice per group. **i**, RT-qPCR analysis of *Tnf* expression in Kupffer cells treated with control PBS, EVPs derived from B16F10 cells or B16F10 tumour explants (left), or EVPs derived from K7M2 cells or K7M2 tumour explants (right) for 4 h. $n = 3$ independent experiments per group. **j**, TNF ELISA on EVP-depleted conditioned media from B16F10 and K7M2 cells. $n = 2$ independent experiments. ND, not detected. CM, conditioned medium. **k**, GSEA of gene expression profiles, ranked based on the sign of $\log_2$FC$*$(-$\log_{10}P$ value), in hepatocytes 24 h post treatment with recombinant mouse TNF protein (25 ng ml^{-1}), compared to PBS control, using Gene Ontology gene sets. Shown are downregulated lipid catabolism-associated gene sets. NES, normalized enrichment score. NOM p-value, nominal p-value. **l**, Schematic Illustration of anti-TNF antibody (200 μg per mouse) or IgG1 isotype control (200 μg per mouse) treatment of tumour-bearing mice or tumour EVP-educated mice. I.P., intraperitoneal. **m**, Weights of tumours from mice inoculated with B16F10 (left) or K7M2 (right) cells and treated with anti-TNF antibody or IgG1 isotype control as shown in (**l**). $n = 5$ mice per group for B16F10-Tb model and $n = 3$ per group for K7M2-Tb model. **n**,**o**, Representative images of BODIPY staining of the livers from B16F10- and K7M2-Tb mice (**n**), and B16F10-CL-EVP- and K7M2-CL-EVP-educated mice (**o**), treated with anti-TNF antibody or IgG1 isotype control (see also Fig. 4d, e). Scale bars, 20 μm. P values were determined by the one-way ANOVA with post hoc Tukey's test (**b**), or two-tailed, unpaired Student's t-test (**g**-**i**,**m**). Data are mean ± s.e.m. NS, not significant. For cytokine array blot source data of (**c**-**f**), see Supplementary Fig. 2.

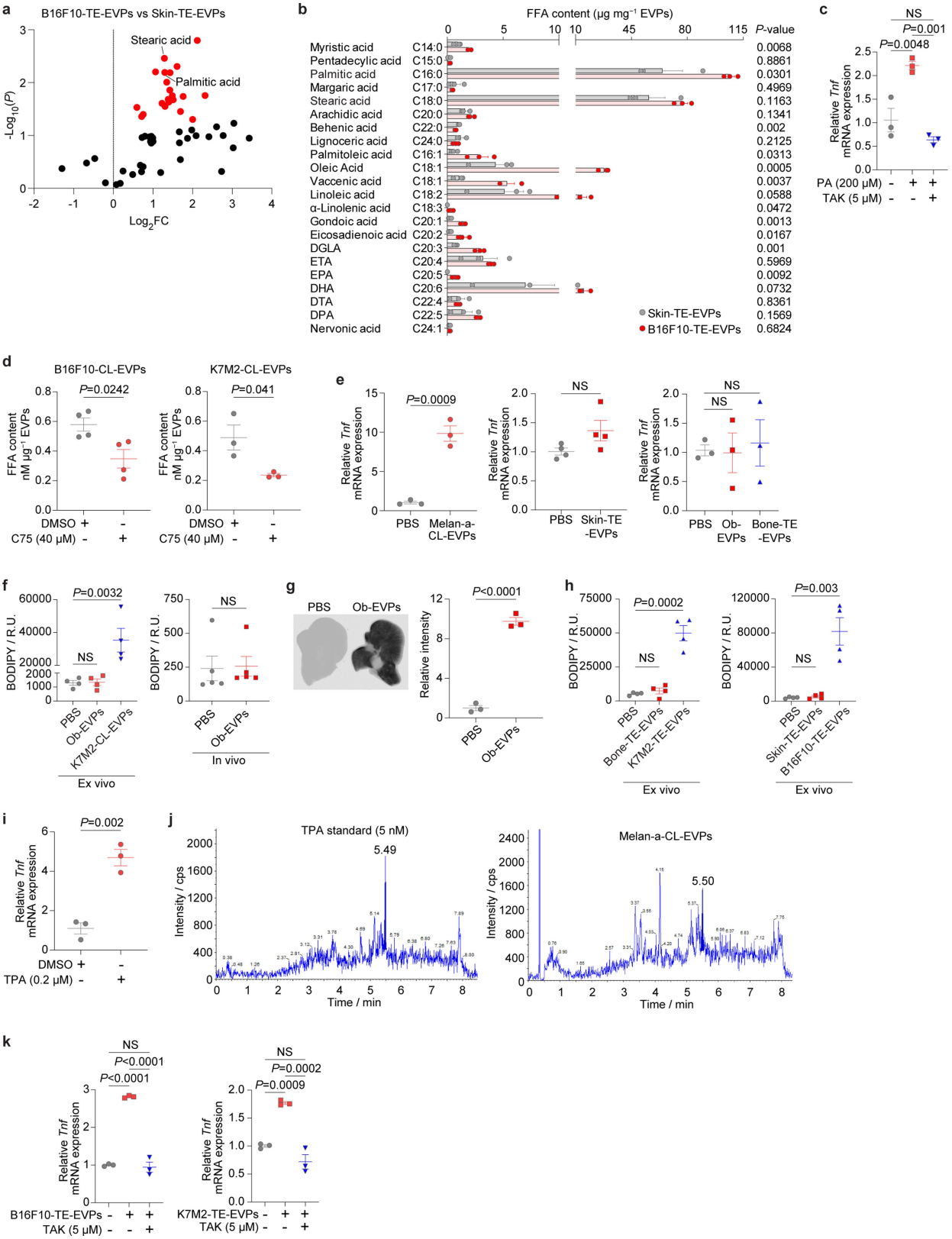

Extended Data Fig. 10 | See next page for caption.

Extended Data Fig. 10 | Tumour EVP-packaged palmitic acid (PA) induces TNF secretion from Kupffer cells. a, Volcano plot of metabolites significantly changed (highlighted in red, $P < 0.05$) in B16F10-TE-EVPs versus skin tissue explant-derived EVPs (skin-TE-EVPs). $n = 5$ B16F10-TE-EVPs and $n = 4$ skin tissue explant-derived EVPs. **b**, Quantitative mass spectrometry analysis of the long-chain free fatty acids, including saturated and unsaturated fatty acids, in the B16F10-TE-EVPs and skin tissue explant-derived EVPs (skin-TE-EVPs). $n = 3$ per EVP group. **c**, RT-qPCR analysis of *Tnf* expression in Kupffer cells from naïve C57BL/6 mice treated with DMSO or the TLR4 inhibitor TAK (5 μM) for 1 h followed by vehicle (100% ethanol diluted into PA-carrier medium at 1:1000 dilution) or 200 μM of PA with or without TAK (5 μM) for 4 h. $n = 3$ mice per group. **d**, FFA content in the EVPs isolated from B16F10 (left) or K7M2 (right) cells treated with DMSO or C75 (40 μM) for 48 h. $n = 4$ independent experiments for DMSO- or C75-treated B16F10 cells; $n = 3$ independent experiments for DMSO- or C75-treated K7M2 cells. **e**, RT-qPCR analysis of *Tnf* expression in Kupffer cells isolated from naïve C57BL/6 (left and middle) or BALB/c (right) mice then treated with control PBS, Melan-a-CL-EVPs (left), skin tissue explant-derived EVPs (skin-TE-EVPs, middle), osteoblast-EVPs (Ob-EVPs, right), or bone tissue explant-derived EVPs (bone-TE-EVPs, right) in vitro for 4 h. $n = 3$ independent experiments per group for treatment with Melan-a-CL-EVPs, Ob-EVPs, bone-TE-EVPs, and their PBS controls. $n = 4$ independent experiments for treatment with skin-TE-EVPs and PBS. **f**, Quantification of BODIPY staining of precision-cut liver slices treated with Ob-EVPs or K7M2-CL-EVPs ex vivo for 48 h, or livers educated with Ob-EVPs in vivo for 4 weeks, compared to PBS-treated or PBS-educated controls, respectively. $n = 4$ mice per group for ex vivo EVP treatment and $n = 5$ mice per group for in vivo EVP education. **g**, Representative LI-COR Odyssey images (left) and associated statistical analysis of relative signal intensity (right) of the livers from mice 24 h post intravenously injection of 10 μg of CellVue NIR815-labeled Ob-EVPs and mock PBS control. $n = 3$ mice per group. **h**, Quantification of BODIPY staining of the PCLS treated with control PBS, bone tissue explant-derived EVPs (bone-TE-EVPs) or K7M2-TE-EVPs (left), skin tissue explant-derived (skin-TE-EVPs) or B16F10-TE-EVPs (right) ex vivo for 48 h. $n = 4$ mice per group. **i**, RT-qPCR analysis of *Tnf* expression in the Kupffer cells isolated from C57BL/6 mice and treated with DMSO or 12-*O*-tetradecanoylphorbol-13-acetate (TPA) (0.2 μM) in vitro for 4 h. TPA induced Kupffer cell *Tnf* expression, compared to DMSO control. $n = 3$ independent experiments. **j**, Representative LC-MS/MS chromatograms of TPA standard (5 nM, left) and TPA detected in the Mela-a-CL-EVPs (right). The concentration of TPA detected in Mela-a-CL-EVPs was 6.5 nM per 100 μg of EVPs. **k**, RT-qPCR analysis of *Tnf* expression in Kupffer cells which were pre-treated with DMSO or TAK (5 μM) for 1 h, and subsequently treated with PBS, 10 μg of B16F10-TE-EVPs or K7M2-TE-EVPs with or without TAK (5 μM) for 4 h. $n = 3$ independent experiments. *P* values were determined by the two-tailed, unpaired Student's *t*-test (**a**,**b**,**d**-**i**,**k**), or one-way ANOVA with post hoc Tukey's test (**c**), or Data are mean ± s.e.m. NS, not significant.

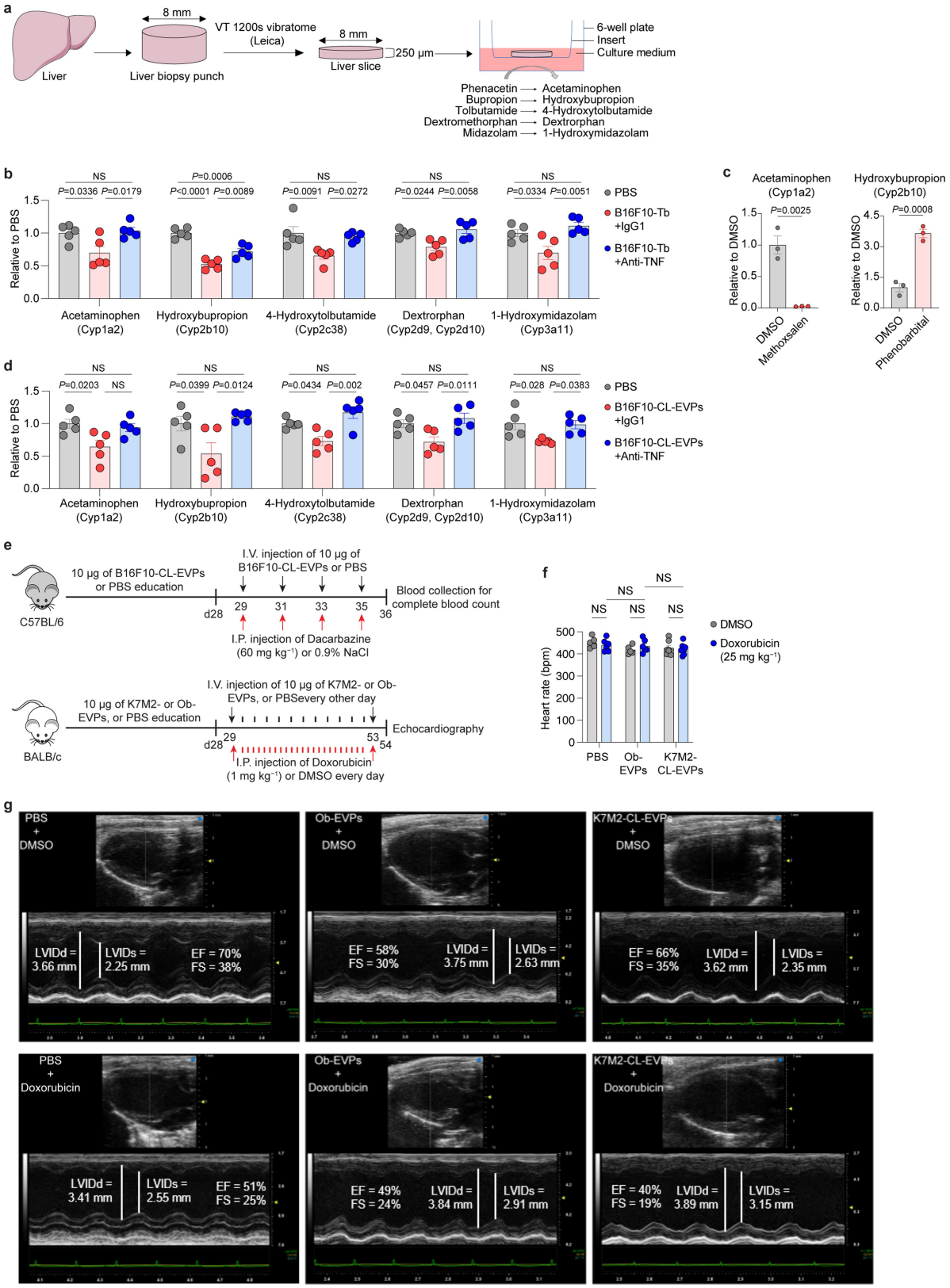

Extended Data Fig. 11 | See next page for caption.

Extended Data Fig. 11 | Tumour EVPs suppress liver drug metabolism and enhance chemotoxicity. a, Schematic illustration of the procedure of drug-metabolizing activity analysis of the PCLS. Substrates of Cytochrome P450 enzymes (including phenacetin, bupropion, tolbutamide, dextromethorphan and midazolam) were added to the media, and their corresponding metabolites (including acetaminophen, hydroxybupropion, 4-hydroxytolbutamide, dextrorphan and 1-hydroxymidazolam) were analyzed by LC-MS/MS. **b**, Drug-metabolizing activity of the core CYP enzymes in the PCLS sectioned from PBS-injected mice, and B16F10-Tb mice treated with anti-TNF antibody or IgG1 isotype control. $n = 5$ mice per group. **c**, Drug-metabolizing activity of Cyp1a2 (left) or Cyp2b10 (right) in the PCLS pre-treated with DMSO control or mathoxsalen (5 μM), or phenobarbital (0.1 mM) for 24 h. $n = 3$ mice per group. **d**, Drug-metabolizing activity of the core CYP enzymes in the PCLS sectioned from naïve mice pre-treated with PBS or 10 μg ml^{-1} of B16F10-CL-EVPs with co-treatment of anti-TNF antibody (20 μg ml^{-1}) or IgG1 isotype (20 μg ml^{-1}) control for 24 h. $n = 5$ mice per group. **e**, Schematic illustration of the procedure of chemotoxicity analysis using EVP-educated mice. For melanoma model (top), C57BL/6 mice were intravenously injected with PBS or 10 μg of B16F10-CL-EVPs every other day for 4 weeks, and then intraperitoneally injected with dacarbazine (60 mg kg^{-1}) or 0.9% NaCl together with intravenous injection of PBS or 10 μg of B16F10-CL-EVPs every other day for 4 times. Retroorbital blood of the mice was then collected for complete blood count. For osteosarcoma model (bottom), BALB/c mice were intravenously injected with PBS, 10 μg of osteoblast-EVPs (Ob-EVPs) or K7M2-CL-EVPs every other day for 4 weeks, and then intraperitoneally injected with doxorubicin (1 mg kg^{-1}) or DMSO every 24 h together with intravenous injection of PBS, 10 μg of Ob-EVPs or K7M2-CL-EVPs every other day for 25 days, and mice were then subjected to echocardiography. **f**, Statistical analysis of the heart rates of PBS-, Ob-EVP- or K7M2-CL-EVP-educated mice after treatment of DMSO or doxorubicin (cumulative dose of 25 mg kg^{-1}). No difference of heart rates was observed in different groups. $n = 6$ mice for PBS groups and $n = 7$ mice for K7M2-CL-EVP groups, $n = 5$ and $n = 6$ for DMSO and doxorubicin treated Ob-EVP-educated mice, respectively. **g**, Representative M-mode images of echocardiography for PBS-, Ob-EVP- or K7M2-CL-EVP-educated mice after treatment of DMSO or doxorubicin as described in (**e**). LVIDd, left ventricular internal dimension at end diastole. LVIDs, left ventricular internal dimension at end systole. EF, ejection fraction. FS, fractional shortening. *P* values were determined by the one-way ANOVA with post hoc Tukey's test (**b**,**d**), or two-tailed, unpaired Student's *t*-test (**c**), or two-way ANOVA followed with Fisher's LSD test (**f**). Data are mean ± s.e.m. NS, not significant. Ob, osteoblast. I.V., intravenours. I.P., intraperitoneal.

nature portfolio

Corresponding author(s): Robert E. Schwartz
Haiying Zhang
David Lyden

Last updated by author(s): Mar 8, 2023

Reporting Summary

Nature Portfolio wishes to improve the reproducibility of the work that we publish. This form provides structure for consistency and transparency in reporting. For further information on Nature Portfolio policies, see our Editorial Policies and the Editorial Policy Checklist.

Statistics

For all statistical analyses, confirm that the following items are present in the figure legend, table legend, main text, or Methods section.

n/a	Confirmed	
☐	☒	The exact sample size (*n*) for each experimental group/condition, given as a discrete number and unit of measurement
☐	☒	A statement on whether measurements were taken from distinct samples or whether the same sample was measured repeatedly
☐	☒	The statistical test(s) used AND whether they are one- or two-sided *Only common tests should be described solely by name; describe more complex techniques in the Methods section.*
☒	☐	A description of all covariates tested
☐	☒	A description of any assumptions or corrections, such as tests of normality and adjustment for multiple comparisons
☐	☒	A full description of the statistical parameters including central tendency (e.g. means) or other basic estimates (e.g. regression coefficient) AND variation (e.g. standard deviation) or associated estimates of uncertainty (e.g. confidence intervals)
☐	☒	For null hypothesis testing, the test statistic (e.g. *F*, *t*, *r*) with confidence intervals, effect sizes, degrees of freedom and *P* value noted *Give P values as exact values whenever suitable.*
☒	☐	For Bayesian analysis, information on the choice of priors and Markov chain Monte Carlo settings
☒	☐	For hierarchical and complex designs, identification of the appropriate level for tests and full reporting of outcomes
☒	☐	Estimates of effect sizes (e.g. Cohen's *d*, Pearson's *r*), indicating how they were calculated

Our web collection on statistics for biologists contains articles on many of the points above.

Software and code

Policy information about availability of computer code

Data collection	No software was used
Data analysis	Statistical analysis: GraphPad Prism 9 Image Quantification: Image J (version 1.53i); Image Studio (version 5.2) BODIPY staining images: Zeiss 880 Laser Scanning Confocal Microscope Extracellular vesicle and particle (EVP) images: JEOL JSM 1400 (JEOL, USA, Ltd, Peabody, MA) transmission electron microscope Quantitative real-time PCR: Bio-Rad CFX Manager (Version 3.1) RNA sequencing analysis: bcl2fastq (Version 2.19, Illumina); TopHat2 (Version 2.0.11); Cufflinks (Version 2.1.1); DESeq2 package Gene Set Enrichment Analysis: GSEA (Version 4.1.0 & version 4.3.2) Asymmetric-flow field-flow fractionation (AF4): Chemstation software (Version 4.0, Agilent Technologies) with integrated Eclipse module (Wyatt Technology); Astra (Version 6.1, Wyatt Technology) EVP size and particle number analysis: NanoSight NTA (Version 3.3) In vivo EVP biodistribution assessment: ImageStudio software (Version 5.2, LI-COR) GC/MS metabolomics: GC-MS system (Agilent Inc, CA, USA) consisting of an Agilent 7890 gas chromatograph, an Agilent 5975 MSD and 7683B autosampler; AMDIS (Version 2.71) (NIST, MD, USA) Lipidomics MS: Thermo Q-Exactive MS system; Xcalibur (Version 3.0.63); LipidSearch (Version 4.1.30, Thermo) Metabolomics and lipidomics data analysis: MetaboAnalyst (Version 4.0) Free fatty acids analysis: Agilent 7890B GC with 5977A/Extractor XL MS system Drug-metabolizing activity analysis: Triple 6500+ LC-MS/MS system (Sciex, Framingham, MA); Analyst Software (Version 1.7.1, Sciex) LC-MS/MS analysis of TPA in EVP samples: 6500+ QTRAP LC-MS/MS system (Sciex, Framingham, MA) ; Analyst Software (Version 1.7.1, Sciex) Flow cytometry: FlowJo (version 10)

Metastasis monitoring of patient-derived xenograft model of osteosarcoma: The 400 MHz Bruker 9.4T Biospec scanner equipped with a 530 mT/m ID 114 mm gradient (Bruker Biospin MRI GmbH, Ettlingen, Germany)
Echocardiography: VisualSonics Vevo 3100 system equipped with MX400 transducer (Visual Sonics); VisualSonics Vevo LAB image analysis software
Details are described in Materials and Methods section.

For manuscripts utilizing custom algorithms or software that are central to the research but not yet described in published literature, software must be made available to editors and reviewers. We strongly encourage code deposition in a community repository (e.g. GitHub). See the Nature Portfolio guidelines for submitting code & software for further information.

Data

Policy information about availability of data

All manuscripts must include a data availability statement. This statement should provide the following information, where applicable:

- Accession codes, unique identifiers, or web links for publicly available datasets
- A description of any restrictions on data availability
- For clinical datasets or third party data, please ensure that the statement adheres to our policy

RNA-seq raw data and associated processed data files that support the findings of this study have been deposited in the Gene Expression Omnibus under accession codes GSE199863 and GSE220446. Metabolomics data derived from livers of PBS-injected control and B16F10-Tb mice (Supplementary Table 1) have been deposited at Figshare (DOI: 10.6084/m9.figshare.22233187). Metabolomics data derived from livers of PBS-injected control and K7M2-Tb mice (Supplementary Table 2) have been deposited at Figshare (DOI: 10.6084/m9.figshare.22233253). Lipidomics data derived from livers of PBS-injected control and B16F10-Tb mice (Supplementary Table 3) have been deposited at Figshare (DOI: 10.6084/m9.figshare.22233265). Lipidomics data derived from livers of PBS-injected control and K7M2-Tb mice (Supplementary Table 4) have been deposited at Figshare (DOI: 10.6084/m9.figshare.22233274). Metabolomics data derived from livers of PBS- and B16F10-TE-EVP-educated mice (Supplementary Table 8) have been deposited at Figshare (DOI: 10.6084/m9.figshare.22233289). Metabolomics data derived from livers of PBS- and K7M2-TE-EVP-educated mice (Supplementary Table 9) have been deposited at Figshare (DOI: 10.6084/m9.figshare.22233298). Lipidomics data derived from livers of PBS- and B16F10-TE-EVP-educated mice (Supplementary Table 10) have been deposited at Figshare (DOI: 10.6084/m9.figshare.22233307). Lipidomics data derived from livers of PBS- and K7M2-TE-EVP-educated mice (Supplementary Table 11) have been deposited at Figshare (DOI: 10.6084/m9.figshare.22233316). Metabolomics data derived from skin-TE-EVPs and B16F10-TE-EVPs (Supplementary Table 14) have been deposited at Figshare (DOI: 10.6084/m9.figshare.22233352). Metabolomics data derived from livers of PBS- and B16F10-CL-EVP-educated mice (Supplementary Table 29) have been deposited at Figshare (DOI: 10.6084/m9.figshare.22233379). Lipidomics data derived from livers of PBS- and B16F10-CL-EVP-educated mice (Supplementary Table 30) have been deposited at Figshare (DOI: 10.6084/m9.figshare.22233403). Metabolomics data derived from livers of PBS- and K7M2-CL-EVP-educated mice (Supplementary Table 31) have been deposited at Figshare (DOI: 10.6084/m9.figshare.22233424). Lipidomics data derived from livers of PBS- and K7M2-CL-EVP-educated mice (Supplementary Table 32) have been deposited at Figshare (DOI: 10.6084/m9.figshare.22233445). Metabolomics data were analyzed using MetaboAnalyst 4.0 (https://www.metaboanalyst.ca/home.xhtml), and metabolite set enrichment analysis was performed based on the Small Molecule Pathway Database (SMPDB) (http://www.smpdb.ca/).

Human research participants

Policy information about studies involving human research participants and Sex and Gender in Research.

Reporting on sex and gender	Sex (female and male) were collected from the medical record and included in the Supplementary Table 5 for each participant. The numbers of female and male participants are also indicated in the Supplementary 5. Sex was not used as a variable in data analysis and our findings do not apply to only one sex.
Population characteristics	Fresh human liver tissues were obtained intraoperatively at Memorial Sloan Kettering Cancer Center (MSKCC, IRB #15-015) from patients undergoing pancreatectomy for either localized resectable pancreatic cancer or non-cancerous pancreatic/peri-pancreatic lesions (details of included pathologies are shown in Supplementary Table 5). None of the patients had any evidence of distant metastasis at the time of surgery. Patients with pancreatic cancer were followed for at least 21 months (up to 8 years) after surgery and site(s) of initial recurrence was identified. In addition, fresh, grossly normal liver tissues were obtained from patients undergoing hepatectomy for hepatic adenomas at MSKCC (IRB #06-107). Intraoperative liver biopsies were collected from patients with germline CDH1 mutations undergoing risk-reducing gastrectomy at the NIH (IRB #13-C-0076). Although these patients had very early-stage incidental gastric cancer in the stomach specimens, none had evidence of metastasis on imaging or by pathologic examination of sampled tissues (lymph nodes, skin, spleen, liver and jejunum). Lastly, unaffected liver specimens from decedents who have previously been diagnosed with pancreatic ductal adenocarcinoma were obtained from the University of Nebraska Medical Center (UNMC)'s Tissue Bank through the Rapid Autopsy Program (RAP) in compliance with IRB 091-01. To ensure specimen quality, organs were harvested within three hours post-mortem. For patient-derived xenograft model of osteosarcoma, the primary osteosarcoma tumors were surgically removed from patients at MSKCC according to the IRB approved protocol (MSKCC IRB #06-107 and #17-067). Deidentified patient information with relevant population characteristics and clinical annotation is available in Supplementary Table 5.
Recruitment	Patients undergoing pancreatectomy for either localized resectable pancreatic cancer or non-cancerous pancreatic/peri-pancreatic lesions who did not receive any neoadjuvant therapy and had no other synchronous malignancies or contraindication to liver biopsy (e.g. coagulopathy), were approached at the MSKCC hepatopancreatobiliary clinic and offered to participate (MSKCC IRB # 15-015). Patients undergoing hepatectomy for hepatic adenomas at MSKCC were also offered to participate (MSKCC IRB #06-107). Patients who agreed and signed informed consent were included. Patients with germline CDH1 mutations undergoing risk-reducing gastrectomy at the NIH were offered to participate, and intraoperative liver biopsies were collected from patients who signed informed consent (IRB #13-C-0076). Autopsies (unaffected liver specimens) from decedents who have previously been diagnosed with pancreatic ductal adenocarcinoma were obtained from the UNMC's Tissue Bank through the Rapid Autopsy Program (RAP) in compliance with IRB 091-01. Osteosarcoma patients

without liver metastasis were offered to participate, and primary tumors were surgically removed from patients who signed informed consent (MSKCC IRB #06-107 and #17-067) for establishing patient-derived xenograft.

Ethics oversight

The collection and use of human liver tissues and primary osteosarcoma tumors have been approved by the Institutional Review Boards of MSKCC (IRB #15-015, #06-107 and #17-067), NIH (IRB #13-C-0076), UNMC (IRB #091-01) and WCM (IRB #0604008488). All individuals provided informed consent for tissue donation. The study is compliant with all relevant ethical regulations regarding research involving human participants.

Note that full information on the approval of the study protocol must also be provided in the manuscript.

Field-specific reporting

Please select the one below that is the best fit for your research. If you are not sure, read the appropriate sections before making your selection.

☒ Life sciences ☐ Behavioural & social sciences ☐ Ecological, evolutionary & environmental sciences

For a reference copy of the document with all sections, see nature.com/documents/nr-reporting-summary-flat.pdf

Life sciences study design

All studies must disclose on these points even when the disclosure is negative.

Sample size	No statistical method was used to predetermine sample size. The sizes of samples and animals were chosen based on previous studies (PMID: 29875463 and 26524530) to provide a sufficient level of statistical power for revealing the indicated biological effects. A minimum of 3 independent biological samples and animals are used for detecting statistical significance between groups. For human studies, data were collected from as many individuals as were available to give sufficient sample size for conducting statistical analysis of the indicated biological effects. The precise number of independent experiments, animals and human samples used in this study were indicated in the Figure and Extended Data Figure legends.
Data exclusions	No data was excluded from the analyses.
Replication	All attempts at replication were successful with similar results. The replication number or mouse number for each experiment was indicated in the figure legends.
Randomization	Age and sex matched groups of mice were randomly allocated to the experimental groups, and housed in the same conditions. For all other experiments, samples or animals were randomly allocated to experimental groups and processed.
Blinding	For human studies, the samples were collected by clinical staff who were not blinded since they need to get the biopsies and autopsies and determine the experimental group allocation of those samples after pathological evaluation. However, for lipid droplet staining on human liver samples using BODIPY, the investigators were blinded to group allocation during data collection and analysis. For mouse echocardiography, the echocardiographer was blinded to treatment conditions of different mouse groups. For cell line and animal related studies, the investigators were not blinded since different treatments were required for separate groups.

Reporting for specific materials, systems and methods

We require information from authors about some types of materials, experimental systems and methods used in many studies. Here, indicate whether each material, system or method listed is relevant to your study. If you are not sure if a list item applies to your research, read the appropriate section before selecting a response.

Materials & experimental systems

n/a	Involved in the study
☐	☒ Antibodies
☐	☒ Eukaryotic cell lines
☒	☐ Palaeontology and archaeology
☐	☒ Animals and other organisms
☒	☐ Clinical data
☒	☐ Dual use research of concern

Methods

n/a	Involved in the study
☒	☐ ChIP-seq
☐	☒ Flow cytometry
☒	☐ MRI-based neuroimaging

Antibodies

Antibodies used

For flow cytometry:
TruStain FcX™ PLUS (anti-mouse CD16/32) Antibody (clone S17011E), Biolegend, Cat#156603
Brilliant Violet 421™ anti-mouse CD45 Antibody (clone 30-F11), Biolegend, Cat#103133
FITC anti-mouse/human CD11b Antibody (clone M1/70), Biolegend, Cat#101205

PE anti-mouse F4/80 Antibody (clone BM8), Biolegend, Cat#123109
PE/Cyanine7 anti-mouse CD31 Antibody (clone 390), Biolegend, Cat#102417
LYVE-1 Antibody [PE/Cy5.5], NOVUS Biological, Cat#NB100-725PECY55
Polyclonal Rabbit anti Mouse ALB / Serum Albumin Antibody (FITC, IF), LSBio, Cat#LS C348036
Desmin antibody (FITC), Biorbyt, Cat#orb15501

For western blot:
Mouse monoclonal anti-β-Actin (clone 13E5), Cell Signaling Technology, Cat#4970
Mouse monoclonal anti-Rab27A (clone D7Z9Q), Cell Signaling Technology, Cat#69295
Anti-rabbit IgG, HRP-linked Antibody, Cell Signaling Technology, Cat#7074

For immunofluorescence staining:
Mouse/Rat CD31/PECAM-1 Antibody, R&D Systems, Cat#AF3628-SP
Albumin Antibody, Novus Biologicals, Cat#NB600-41532
F4/80 antibody, clone Cl:A3-1, Bio-Rad, Cat#MCA497GA
Anti-LYVE1 antibody, Abcam, Cat#ab14917
Anti-Desmin antibody, Abcam, Cat#ab15200
Donkey anti-Goat IgG (H+L) Cross-Adsorbed Secondary Antibody, Alexa Fluor 555, ThermoFisher, Cat#A-21432
Goat anti-Rat IgG (H+L) Cross-Adsorbed Secondary Antibody, Alexa Fluor 488, ThermoFisher, Cat#A-11006
Goat anti-Rabbit IgG (H+L) Highly Cross-Adsorbed Secondary Antibody, Alexa Fluor 488, ThermoFisher, Cat#A-11034

For in vivo neutralization:
InVivoPlus anti-mouse TNFα, BioXCell, Cat#BP0058
InVivoPlus IgG1 isotype control, BioXCell, Cat#BP0290

Validation

All antibodies used in this study are commercially available, and have been validated by the manufacturer. The validation data of the antibodies are stated on the manufacturer's websites as shown below:
TruStain FcX™ PLUS (anti-mouse CD16/32) Antibody (clone S17011E), Biolegend, Cat#156603 (https://www.biolegend.com/en-us/products/trustain-fcx-plus-anti-mouse-cd16-32-antibody-17085)
Brilliant Violet 421™ anti-mouse CD45 Antibody (clone 30-F11), Biolegend, Cat#103133 (https://www.biolegend.com/en-us/products/brilliant-violet-421-anti-mouse-cd45-antibody-7253)
FITC anti-mouse/human CD11b Antibody (clone M1/70), Biolegend, Cat#101205 (https://www.biolegend.com/en-us/products/fitc-anti-mouse-human-cd11b-antibody-347)
PE anti-mouse F4/80 Antibody (clone BM8), Biolegend, Cat#123109 (https://www.biolegend.com/en-us/products/pe-anti-mouse-f4-80-antibody-4068)
PE/Cyanine7 anti-mouse CD31 Antibody (clone 390), Biolegend, Cat#102417 (https://www.biolegend.com/en-us/products/pe-cyanine7-anti-mouse-cd31-antibody-3942)
LYVE-1 Antibody [PE/Cy5.5], NOVUS Biological, Cat#NB100-725PECY55 (https://www.novusbio.com/products/lyve-1-antibody_nb100-725pecy55#datasheet)
Polyclonal Rabbit anti Mouse ALB / Serum Albumin Antibody (FITC, IF), LSBio, Cat#LS C348036 (https://www.lsbio.com/antibodies/alb-antibody-serum-albumin-antibody-fitc-flow-if-immunofluorescence-ls-c348036/358993#sds-msds-section)
Desmin antibody (FITC), Biorbyt, Cat#orb15501 (https://www.biorbyt.com/desmin-antibody-fitc-orb15501.html)
Mouse monoclonal anti-β-Actin (clone 13E5), Cell Signaling Technology, Cat#4970 (https://www.cellsignal.com/products/primary-antibodies/b-actin-13e5-rabbit-mab/4970)
Mouse monoclonal anti-Rab27A (clone D7Z9Q), Cell Signaling Technology, Cat#69295 (https://www.cellsignal.com/products/primary-antibodies/rab27a-d7z9q-rabbit-mab/69295)
Anti-rabbit IgG, HRP-linked Antibody, Cell Signaling Technology, Cat#7074 (https://www.cellsignal.com/products/secondary-antibodies/anti-rabbit-igg-hrp-linked-antibody/7074)
Mouse/Rat CD31/PECAM-1 Antibody, R&D Systems, Cat#AF3628-SP (https://www.rndsystems.com/products/mouse-rat-cd31-pecam-1-antibody_af3628)
Albumin Antibody, Novus Biologicals, Cat#NB600-41532 (https://www.novusbio.com/products/albumin-antibody_nb600-41532)
F4/80 antibody, clone Cl:A3-1, Bio-Rad, Cat#MCA497GA (https://www.bio-rad-antibodies.com/monoclonal/mouse-f4-80-antibody-cl-a3-1-mca497.html?f=purified&JSESSIONID_STERLING=842F78BC9E779924660A7E4C800BB2EF.ecommerce1&evCntryLang=US-en&cntry=US&thirdPartyCookieEnabled=true)
Anti-LYVE1 antibody, Abcam, Cat#ab14917 (https://www.abcam.com/products/primary-antibodies/lyve1-antibody-bsa-and-azide-free-ab14917.html)
Anti-Desmin antibody, Abcam, Cat#ab15200 (https://www.abcam.com/products/primary-antibodies/desmin-antibody-cytoskeleton-marker-ab15200.html)
Donkey anti-Goat IgG (H+L) Cross-Adsorbed Secondary Antibody, Alexa Fluor 555, ThermoFisher, Cat#A-21432 (https://www.thermofisher.com/antibody/product/Donkey-anti-Goat-IgG-H-L-Cross-Adsorbed-Secondary-Antibody-Polyclonal/A-21432)
Goat anti-Rat IgG (H+L) Cross-Adsorbed Secondary Antibody, Alexa Fluor 488, ThermoFisher, Cat#A-11006 (https://www.thermofisher.com/antibody/product/Goat-anti-Rat-IgG-H-L-Cross-Adsorbed-Secondary-Antibody-Polyclonal/A-11006)
Goat anti-Rabbit IgG (H+L) Highly Cross-Adsorbed Secondary Antibody, Alexa Fluor 488, ThermoFisher, Cat#A-11034 (https://www.thermofisher.com/antibody/product/Goat-anti-Rabbit-IgG-H-L-Highly-Cross-Adsorbed-Secondary-Antibody-Polyclonal/A-11034)
InVivoPlus anti-mouse TNFα, BioXCell, Cat#BP0058 (https://bioxcell.com/invivoplus-anti-mouse-tnfa)
InVivoPlus IgG1 isotype control, BioXCell, Cat#BP0290 (https://bioxcell.com/invivoplus-rat-igg1-isotype-control-anti-trinitrophenol-bp0290)

Eukaryotic cell lines

Policy information about cell lines and Sex and Gender in Research

Cell line source(s)

B16-F10, K7M2, B16-F1, 4T1 and 293T cells were purchased from American Type Culture Collection (ATCC). 67NR cell line was obtained from Dr. Fred Miller (Karmanos Cancer Institute, PMID: 1540948). SK-MEL-192 was obtained from MSKCC. The

	murine melanocyte Melan-a was obtained from The Wellcome Trust Functional Genomics Cell Bank. Primary osteoblasts were isolated from mouse bones, and primary hepatocytes and Kupffer cells were isolated from mouse livers.
Authentication	No further authentication was conducted for B16-F10, K7M2, B16-F1, 4T1, and 293T cells purchased from ATCC, as well as murine melanocyte Melan-a obtained from The Wellcome Trust Functional Genomics Cell Bank due to their clear provenance. B16F1, B16F10, and Melan-a cell lines showed melanin secretion upon culturing. 67NR has been widely used in published literature (PMID: 35122036; PMID: 27974799; PMID: 31451770; PMID: 15210113), and no further authentication was performed. SK-MEL-192 cell line harboring BRAF(V600E) mutation was confirmed by allele-specific polymerase chain reaction (PMID: 24710597). Primary osteoblasts were isolated from mouse bones using a published protocol (PMID: 33912848), and their differentiation was confirmed by Alizarin Red-S staining to assess mineralization after culturing in stimulation medium for 14–21 days. Primary Kupffer cells were confirmed by F4/80 immunofluorescence staining and release of IL-6 after lipopolysaccharide (LPS) treatment. Primary hepatocytes were isolated following the widely used protocol (PMID: 22105762 and PMID: 20204628).
Mycoplasma contamination	Cell lines are routinely tested and confirmed to be negative for mycoplasma.
Commonly misidentified lines (See ICLAC register)	No commonly misidentified cell lines were used in this study.

Animals and other research organisms

Policy information about studies involving animals; ARRIVE guidelines recommended for reporting animal research, and Sex and Gender in Research

Laboratory animals	Female C57BL/6, BALB/c, Nude (outbred) and NOD/SCID/IL2Rynull (NSG) mice aged 6-8 weeks were obtained from The Jackson Laboratory, and were euthanized 3-8 weeks post experiments for downstream analysis depending on the experimental design and tumor progression. KPC mice (Krastm4Tyj Trp53tm1Brn Tg[Pdx1-cre/Esr1*]#Dam/J) were obtained from The Jackson Laboratory (JAX: 032429), both male and female KPC mice were euthanized for downstream analysis within 14-20 weeks after tamoxifen treatment. Male and female C57BL/6 TN mice with or without null Mc1r mutation were provided by Dr. Christin Burd laboratory at The Ohio State University (PMID: 28544727), mice aged 10-20 weeks were euthanized for downstream analysis depending on tumor progression. All mice were housed in the animal facility under conventional conditions with a light (12 hours dark/light circle)-, humidity (30%-70%)- and temperature (70 °F -74 °F)-controlled environment.
Wild animals	No wild animals were used in this study.
Reporting on sex	Sex-associated phenotypes or mechanisms were not the focus for designing experiments in our study. Our study included both female and male mice, and our conclusions from experiments in vivo were not affected by the sex of mice. The sex of animals used in the study was reported in the Materials and Methods section.
Field-collected samples	No field-collected samples were used in this study.
Ethics oversight	Treatment of mice was performed in accordance with institutional, IACUC and AAALAS guidelines (Weill Cornell Medicine animal protocols #0709-666A and #2016-0057; The Ohio State University animal protocol #2012A00000134; MSKCC animal protocol #14-02-002) and all animal experiments were conducted in compliance with relevant ethical regulations regarding animal research.

Note that full information on the approval of the study protocol must also be provided in the manuscript.

Flow Cytometry

Plots

Confirm that:

☒ The axis labels state the marker and fluorochrome used (e.g. CD4-FITC).

☒ The axis scales are clearly visible. Include numbers along axes only for bottom left plot of group (a 'group' is an analysis of identical markers).

☒ All plots are contour plots with outliers or pseudocolor plots.

☒ A numerical value for number of cells or percentage (with statistics) is provided.

Methodology

Sample preparation	To identify the recipient cells of tumor-derived EVPs in the livers, mice were intravenously injected 10 μg of CellVue Burgundy-labeled EVPs in 100 μL of PBS, or an equivalent volume of mock reaction mixture. At 24 h post injection, a small lobe of murine liver was digested with Dispase/collagenase/DNase (Roche; 1.5 mg/mL of Dispase II [cat# 4942078001] and collagenase A [cat# 10103586001], 0.1 mg/mL of DNase I [cat# 10104159001]) for 30 min at 37 °C with gentle shaking (40 r.p.m.). Single-cell suspension was obtained by pipetting and filtering through a 70 μm cell strainer. Cells were washed with FC buffer (PBS [Ca2+/Mg2+-free] containing 2% BSA and 2 mM of EDTA) and collected by centrifugation at 300g for 5 min. Cell pellets were incubated with ACK Lysing buffer (Gibco, A10492-01) at room temperature for 5 min to remove red blood cells. Cells were resuspended in FC buffer and one million of cells were incubated with TruStain FcX™ PLUS (anti-mouse CD16/32) antibody (Biolegend, clone S17011E) for 10 min on ice. Subsequently, the cell suspensions were incubated with antibodies (see Supplementary table 28) for 25 min on ice. For labeling the intracellular molecules, cell suspensions were treated with 0.01% PFA for 10 min and 0.5% Tween20 for 15 min before incubating with antibodies. After antibody labeling, cells were

	washed with FC buffer and stained with 0.1 ng/ml of DAPI solution (Thermo Scientific, #62248). To analyze the abundance of Kupffer cells in the livers from mice treated with Liposome (Liposoma BV) or Clodronate (Liposoma BV), livers were subjected to flow cytometry analyses of Cd45, Cd11b and F4/80-expressing cells following the method described above.
Instrument	Cytek Aurora
Software	FlowJo (version 10)
Cell population abundance	In total one million of cells were stained per experiment, and the percentage of different subpopulation of cells was analyzed using the gating strategy as described below.
Gating strategy	Single cells were gated according to FSC and SSC to exclude doublets. Different cell populations were analyzed by gating live (DAPI-negative) and Burgundy-positive cells and then the expression of Cd45, Cd11b, F4/80, Cd31, albumin, Lyve1, and desmin.

☒ Tick this box to confirm that a figure exemplifying the gating strategy is provided in the Supplementary Information.